Solid State Reactions of Barium Carbonate with Tetravalent Metal Oxides

A Thesis Presented for the Degree of

Doctor of Philosophy

by

John Douglas Hancock, B.Sc.

Department of Ceramics with Refractories Technology,

Faculty of Materials Technology,

University of Sheffield.

August 1970

ACKNOWLEDGMENTS

The author wishes to express his thanks to his supervisor, Dr. J. H. Sharp, for his advice and encouragement throughout the course of this work and preparation of the thesis. He would also like to thank Professor J. White, Mr. C. Richmond and Dr. D. M. Tinsley for many useful discussions.

The author also acknowledges his indebtedness to the Science Research Council for the provision of a research bursary which made this work possible.

He would also like to acknowledge the assistance of:

Mr. J. M. DeVine of the Metallurgy Department for assistance on Scanning Electron Microscopy;

Mr. C. M. Wilson for the Electron Probe Micro-Analysis; and the technical staff of the Department of Ceramics with Refractories Technology.

SUMMARY

The thermal decomposition of barium carbonate and the solid state reactions between barium carbonate and tetravalent metal oxides, namely TiO_2, ZrO_2, SiO_2, GeO_2 and SnO_2, have been investigated.

The kinetics of decomposition of barium carbonate in nitrogen and in vacuo have been established using isothermal weight loss measurements. Particle morphology and sample compaction effect the kinetic behaviour, which is further complicated by a polymorphic transformation and liquid formation within the temperature range studied. Meaningful kinetic data cannot be obtained when the rate of reaction is relatively fast because the endothermic nature of the reaction leads to departures from true isothermal conditions within the sample so that heat transfer becomes the rate-determining step. The observed activation energy for the decomposition of barium carbonate was ~ 60 kcal/mole in the temperature range from 800°C to 1000°C.

Mixtures of $BaCO_3$-MO_2 prepared in water were appreciably more reactive than those prepared in acetone. The geometry of the particle contacts was examined by scanning electron microscopy, which showed that the oxide particles were better dispersed in aqueous mixtures. The SEM was subsequently used to assess the suitability of various preparations for kinetic studies. Products of these reactions were examined by x-ray diffraction and electron probe micro-analysis.

SUMMARY CONTD.

The kinetics of decomposition of $BaCO_3$-MO_2 mixtures have been investigated using a vacuum thermobalance. A method of kinetic analysis combining a reduced time scale method with the classical nuclei growth analysis has been used to observe changes in reaction mechanism with temperature. The observed activation energies were always similar in value to the heats of formation of the Ba_2MO_4 products, regardless of the composition of the initial mixture.

CONTENTS

CONTENTS CONTD.

CONTENTS CONTD.

CONTENTS CONTD.

CONTENTS CONTD.

NOMENCLATURE

α: fraction reacted

$D_2\alpha$: a two dimensional diffusion controlled reaction into a cylinder of radius r and the product volume is assumed to equal that of the starting material.

$R_2\alpha$: a phase boundary controlled reaction of a circular disc reacting from the edge inward or for a cylinder.

$R_3\alpha$: a phase boundary controlled reaction for a sphere reacting from the surface inward.

$F_1\alpha$: a reaction controlled by classical first order kinetics.

t_α method: the activation energy E is given by $\log t_\alpha = \frac{C}{2.303} + \frac{E}{4.576T}$ where t_α is the time from the beginning of a reaction to attain a chosen value of the fraction reacted α, (usually 0.50 and hence $t_{0.5}$).

LnLn analysis: a plot of $\text{Ln}\left[-\text{Ln}(1-\alpha)\right]$ against Ln Time resulting in a value of the slope m which may be non-integral.

Isokinetic: a process is isokinetic when the reaction mechanism does not change with temperature i.e. when the LnLn analysis curves are of the same shape and can be brought into identity merely

by lateral shift along the Ln Time axis.

Austin-Rickett analysis: a plot of $\mathrm{Ln}\left[\frac{\alpha}{1-\alpha}\right]$ against Ln Time resulting in a slope n.

Z Factor: the volume of reaction product formed per unit volume of reactant consumed.

SEM: scanning electron microscopy

B:BaO Z:ZrO_2 S:SiO_2 G:GeO_2 T:TiO_2 Sn:SnO_2 Sr:SrO.

CHAPTER 1

Introduction

When the pressure, temperature or composition of a system is changed, new equilibrium states are fixed by the thermodynamics of the system. However, the attainment of the new equilibrium state will depend on the kinetics of the processes involved and, since in many systems equilibrium is never reached, the rate at which equilibrium is approached is just as important as knowledge of the equilibrium state. Carbonates and oxides are widely used as raw materials in the ceramics industry, and some of the particular compositions used in this investigation are already used in the field of electrical ceramics. Unlike the barium carbonate-iron oxide[1,2,3] system, which has been studied in detail, due to the use of barium ferrites in soft and hard ceramic magnets, only a relatively small amount of work has been done on the systems considered in this investigation and the recent literature is limited to studies of carbonate-titania mixtures of importance in ferroelectric applications. The strontium carbonate and strontium carbonate-titania systems have been investigated by Wanamaker[4], and Harris and Cook[5] respectively. Hulbert and Popowich[6] found that the kinetics of strontium carbonate-titania were best described by the Ginstling-Brounshtein equation when stoichiometric rutile was used, but nuclei growth models were applicable when non-stoichiometric rutile was used.

The early work of Jander[7] on the decomposition kinetics of barium carbonate-silica does not appear to have been followed up with further studies of similar systems and the literature is limited to studies of other carbonates. The extensive work of Centnerszwer, Huttig and Zawadski on the decomposition of carbonates has been reported by Garner[8]. Centnerszwer found that after the maximum rate of reaction, the rate obeyed a first order law, but found an inherent difficulty in carbonate systems in the occurrence of 'false equilibria'. Zawadski and Breitsznayder found that annealing crystals of carbonates in carbon dioxide gas above the dissociation pressure diminished the rate of formation of the oxide phase in vacuo. They concluded that the rate of nucleation in carbonates depends on the pressure of carbon dioxide and is expecially slow near to the dissociation pressure. They also stated that dissociation of carbonates could only be determined accurately when the reaction was studied in high vacuum or allowances made for the recombination reaction.

Templeton and Pask[9] studied the reaction between barium carbonate and rutile (TiO_2) and concluded that a small amount of $BaTiO_3$ was initially formed at contact surfaces, and the reaction then became diffusion controlled, with all the compounds indicated by the

phase diagram at a certain temperature appearing in varying amounts, depending on the rates of diffusion. On this basis, Ba_2TiO_4 should appear between $BaTiO_3$ and $BaCO_3$ and occur in increasing amounts until all the carbonate is consumed. Swann[10] also studied the reaction between barium carbonate and titania (anatase) and suggested that Ba_2TiO_4 is always the first compound formed when the reaction is carried out in a nitrogen atmosphere; but $BaTiO_3$ is formed first of all when an atmosphere of carbon dioxide is used. This suggestion is in agreement with the thermodynamics of the barium carbonate-titania system (Figure 2) which indicates that $BaTiO_3$ is formed at temperatures less than 1060°C when 1 atmos. pressure of carbon dioxide is used according to the equation:

$$Ba_2TiO_4 + CO_2 \longrightarrow BaTiO_3 + BaCO_3$$

Although the work of Hills[11] was limited to the decomposition of calcium carbonate, it has implications for all endothermic decompositions. It had been assumed for some time that decomposition of calcium carbonate was phase boundary controlled, (sometimes called the advancing interface mechanism), and yet the data of Hills proved almost without doubt that a heat-mass transfer mechanism controlled the rate of decomposition of single spheres of calcium carbonate. However, the experimental conditions of Hills' work were widely different from the normal approach to

determining kinetic mechanisms as he used very large sample weights (~ 2g.) and very fast reaction rates (~ 70 minutes for complete decomposition), whereas the emphasis in most kinetic model studies should be towards small samples and slow reaction rates. Hills' results indicate that a change in mechanism is to be expected when reaction rates and sample sizes are in excess of some maximum tolerable values, but with slow reaction rates and small samples, (100 mg. and 700 minutes for complete decomposition), his results may not be in conflict with the generally accepted model for the decomposition of calcium carbonate.

A possible explanation of the absence of detailed studies on the kinetics of decomposition of barium carbonate-metal oxide systems lies in the necessary control and understanding of the mixing geometry of powder mixtures required before realistic kinetic measurements and interpretations can be attempted. It is only since the innovation of the scanning electron microscope that the geometry of loose powder mixtures could be realistically examined before, during, and after reaction. De Vine et al[12] have suggested that SEM will be applied more and more to ceramic systems in the future, and one might expect a renewed interest in the kinetic aspects of carbonate-oxide reactions. Indeed the barium carbonate-iron

oxide system has recently been examined using SEM as a major technique to compare the relationship between the texture and reactivity of commercial iron oxides in barium carbonate mixtures.

CHAPTER 2

Thermodynamics

At equilibrium a system is in its lowest energy state for the composition, temperature and pressure conditions imposed on it. The kinetics of the processes involved in attaining this equilibrium state from any arbitrary starting point are frequently more important than knowledge of the final state, which is obtained from thermodynamics. However, it is useful to be able to define the final state, and to evaluate the possible reaction mechanisms by examination of the free energy diagram.

2.1. Decomposition of a Carbonate

The criterion of whether a reaction is possible is that the standard free energy change is negative. The free energy, G, of any single substance or mixture at a temperature T, is defined by the relation:

$$G = H - TS$$

where H is the heat content, and S is the entropy of the substance or mixture.

For a thermal decomposition of the type,

$$AB\ (s) = A\ (s) + B\ (g)$$

the standard free energy change ΔG° is defined by the relation:

$$\Delta G^\circ = \Delta H^\circ - T\Delta S^\circ = - RT \ln \phi_B$$

The free energy of the reactant AB is essentially unchanged when the pressure of the gas phase ϕ_B is

altered. However, the free energy of the products is increased when ρ_B is increased, and lowered when ρ_B is lowered. At ρ_B = 1 atmos., the free energy curves intersect at T_1 (Figure 1) and this is therefore the decomposition temperature for this pressure. At ρ_B < 1 atmos., the free energy curve of the products is lowered, and the decomposition temperature is lowered to T_2 (Figure 1). T_1 and T_2 are theoretical decomposition temperatures, but the reaction may be so slow at both these temperatures that no reaction is observed, and the experimental decomposition temperature occurs at a higher temperature than predicted by thermodynamics.

To illustrate this a thermodynamic decomposition temperature for barium carbonate can be calculated for the partial pressure of carbon dioxide in dry air, i.e. 3×10^{-4} atmos., as follows:

$$\Delta G^\circ = \Delta H^\circ - T\Delta S^\circ = -4.575 \log_{10} \rho_{CO_2}$$

$$= 64{,}330 - T.\ 40.6$$

$$\therefore T = 1134^\circ K \text{ or } 861^\circ C.$$

However, decomposition of barium carbonate is not observed experimentally until ~ 950°C, and even at this temperature is very slow (of the order of days). Some thermodynamic and experimental decomposition temperatures (for calcium carbonate and barium carbonate) are shown in Table 1.

TABLE 1 - Thermodynamic and Experimental Decomposition Temperatures of $CaCO_3$ and $BaCO_3$.

		1 Atmos CO_2	50% CO_2	10% CO_2
$CaCO_3$	Theoretical	897°C	852°C	760°C
	Experimental	910°C	870°C	780°C
		1 Atmos CO_2	3×10^{-4} Atmos	10% CO_2
$BaCO_3$	Theoretical	-	861°C	1151°C
	Experimental	melts	950°C	1200°C

2.2. The Effect of a Second Solid Phase on the Decomposition of a Carbonate

The second phase may have no effect on the reaction and merely act as a diluent, but consider the reaction:

$$AB\ (s) + C\ (s) = AC\ (s) + B\ (g)$$

When C forms a stable compound with A, then the effect of adding C to AB is to lower the decomposition temperature of the latter. This is best illustrated by an example, such as the reaction between calcium carbonate and silica considered by White[14]. For the reactions:

$$CaCO_3 = CaO + CO_2,\ \Delta G^\circ = 40{,}250 - 34.4T \qquad (1)$$

$$CaO + SiO_2 = CaSiO_3,\ \Delta G^\circ = -21{,}300 + 0.12T \qquad (2)$$

Adding (1) + (2) leads to the overall reaction:

$$CaCO_3 + SiO_2 = CaSiO_3 + CO_2, \quad \Delta G^\circ = 18{,}950 - 34.3T$$

The condition for equilibrium at 1 atmos. pressure of carbon dioxide is for $\Delta G^\circ = 0$, which corresponds to a temperature of 553°K or 280°C. The addition of silica to calcium carbonate lowers the thermodynamic decomposition temperature at 1 atmos. pressure of CO_2 from 897°C to 280°C. It is very unlikely that any appreciable reaction could be observed at this temperature, and the reaction would occur at some higher temperature determined by the kinetics of the processes involved. The thermodynamic calculation does not give any information regarding the intermediate stages in the reaction, nor does it require reactions (1) and (2) to occur consecutively.

2.2.1. Barium carbonate-titania system

This system has been considered in detail by Templeton and Pask[9] using the thermodynamic data of Lander[15] and Kelley[16]. A specimen calculation used in the construction of the free energy diagram, Figure 2, for this system is outlined below:

At 1100°K

$$BaCO_3 = BaO + CO_2, \quad \Delta G^\circ = + 21.23$$

$$BaO + TiO_2 = BaTiO_3, \quad \Delta G^\circ = - 35.10$$

Adding for the overall reaction:

$$BaCO_3 + TiO_2 = BaTiO_3 + CO_2, \quad \Delta G^\circ = - 13.87$$

$$2BaCO_3 = 2BaO + 2CO_2, \quad \Delta G^\circ = + 42.46$$

$$2BaO + TiO_2 = Ba_2TiO_4, \quad \Delta G^\circ = -46.90$$

Adding for the overall reaction:

$$2BaCO_3 + TiO_2 = Ba_2TiO_4 + 2CO_2, \quad \Delta G^\circ = -4.44$$

$$BaCO_3 + TiO_2 = BaTiO_3 + CO_2, \quad \Delta G^\circ = -13.87$$

$$2BaCO_3 + TiO_2 = Ba_2TiO_4 + 2CO_2, \quad \Delta G^\circ = -4.44$$

Subtracting

$$BaCO_3 + BaTiO_3 = Ba_2TiO_4 + CO_2, \quad \Delta G^\circ = +9.43$$

Free energy data for this system under a reduced p_{CO_2} can be obtained directly from the diagram for $p_{CO_2} = 1$ atmos. using the following method

$$\Delta G^\circ p_{CO_2 = 1 \text{ atmos.}} = -RT \ln \frac{p_{CO_2}}{p^\circ_{CO_2}}$$

and $$\Delta G^\circ p_{CO_2 = a} = -RT \ln \frac{p_{CO_2}}{p_{CO_2 = a}}$$

Subtracting we obtain the relationship

$$\Delta G^\circ p_{CO_2 = a} = \Delta G^\circ p_{CO_2 = 1} + RT \ln p_a$$

Hence free energy data can be corrected to different partial pressures of carbon dioxide when the data for $p_{CO_2} = 1$ atmos. is already established.

2.3. Interpreting Phase Equilibrium Diagrams

When examining the free energy diagram, Figure 2, three clarifying statements should be remembered; the process tends to proceed spontaneously left to right when ΔG° is negative, at $\Delta G^\circ = 0$ the system is at equilibrium, and when ΔG° is positive, the processs tends to proceed spontaneously in the opposite direction, right to left. Figure 2 shows that $BaTiO_3$

should always be the first product of reaction for all compositions of the carbonate-titania mixture at all temperatures below the decomposition temperature of barium carbonate alone. However, the diagram also shows that the $BaTiO_3$ initially formed, may immediately react with the carbonate, to form Ba_2TiO_4, when the temperature is above 1060°C and P_{CO_2} = 1 atmos. One interesting aspect of this system concerns the formation of Ba_2TiO_4; the thermodynamics indicate that when Ba_2TiO_4 is present in a quenched sample then it must have been present at the firing temperature. However, the presence of $BaTiO_3$ in a quenched sample does not prove its presence at the firing temperature as it can be formed on cooling by the reaction:

$$Ba_2TiO_4 + CO_2 \longrightarrow BaCO_3 + BaTiO_3$$

A similar argument can be developed for the strontium carbonate-titania system.

The thermodynamic decomposition temperatures of barium carbonate and strontium carbonate under different gas phase pressures can be predicted from the diagram. These calculated temperatures are the theoretical maximum temperatures for isothermal decomposition studies of carbonate-oxide mixtures, i.e. the maximum temperatures below which the carbonate cannot decompose without directly forming a product with the oxide. In practice, this maximum is determined

experimentally as that temperature at which the rate of decomposition of the carbonate to its oxide is no longer negligible, compared to the rate of the carbonate decomposition, due to the presence of the added oxide.

2.4. Stability of Metal Oxides

The oxide used to lower the decomposition temperature of the carbonate may be unstable under the conditions of temperature and pressure operating during the decomposition. When temperature and pressure conditions are known, the stability of the oxide can be determined, but in this investigation the effective partial pressure of oxygen operating during a decomposition could not be established, and only the relative stabilities of the five oxides could be compared. This is discussed in detail in Chapter 13, the decomposition of barium carbonate-stonnic oxide mixtures, as stannic oxide is reduced under the conditions of temperature and pressure operating in the vacuum thermobalance.

FIGURE 1: Free energy curves showing the change in the theoretical decomposition temperature as the pressure of the gas phase F_B is lowered.

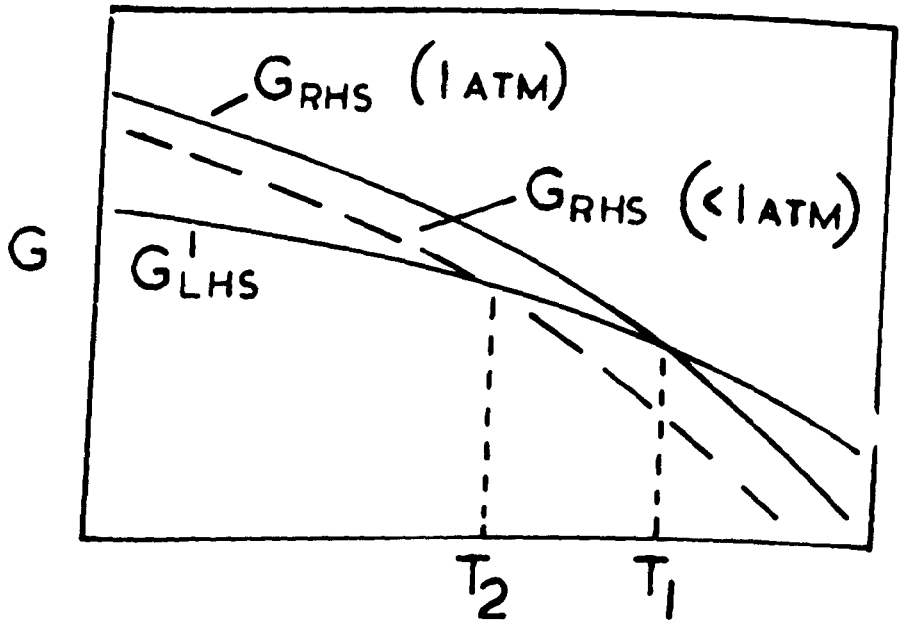
G
G_{RHS} (1 ATM)
G_{RHS} (<1 ATM)
G'_{LHS}
T_2
T_1

FIGURE 2: Free energy data for barium carbonate-titania system and strontium carbonate-titania system.

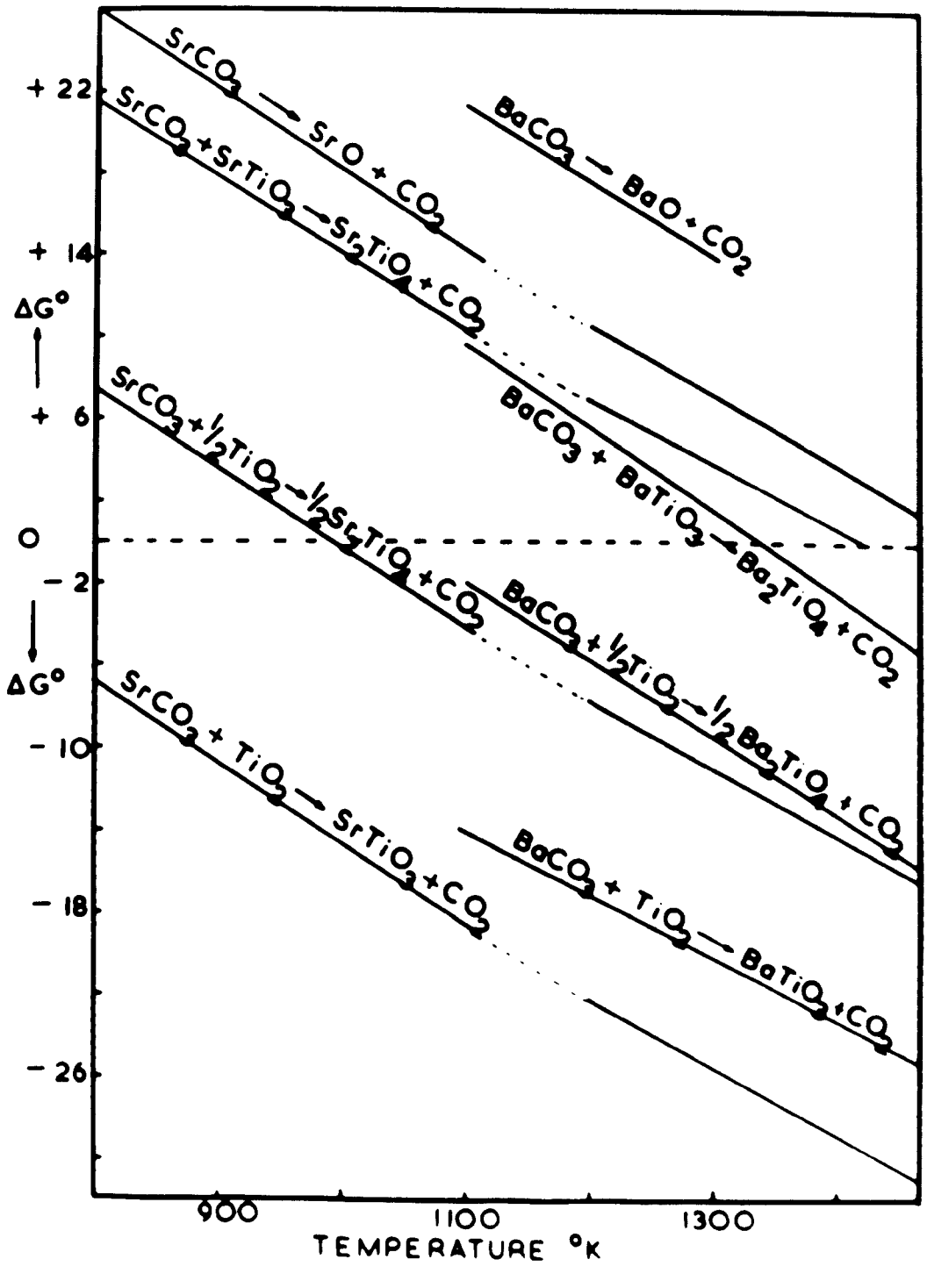
+ 22
+ 14
ΔG°
+ 6
0
- 2
ΔG°
- 10
- 18
- 26
SrCO3 → SrO + CO2
BaCO3 → BaO + CO2
SrCO3 + SrTiO3 → Sr2TiO4 + CO2
BaCO3 + BaTiO3 → Ba2TiO4 + CO2
SrCO3 + ½TiO2 → ½Sr2TiO4 + CO2
BaCO3 + ½TiO2 → ½Ba2TiO4 + CO2
SrCO3 + TiO2 → SrTiO3 + CO2
BaCO3 + TiO2 → BaTiO3 + CO2
900
1100
1300
TEMPERATURE °K

CHAPTER 3

Kinetic Models and Analysis

Phase equilibrium diagrams are used to represent the ranges of temperature, pressure and composition in which different phases are stable. When the pressure, temperature or composition is changed, new equilibrium states are fixed, but the attainment of these new conditions depends on the kinetics of the processes involved. In many systems, equilibrium is never reached, and the rate at which equilibrium is approached, is just as important as knowledge of the equilibrium state.

In reactions involving solids, the reactants cannot be mixed on an atomic level, and this is one of the factors that makes it difficult to apply the classical concepts of order and molecularity, which are used extensively in studies of the kinetics of gas phase and liquid phase reactions. For heterogeneous reactions, the nucleus and matrix or the crystal and melt, are separated by a reaction interface and two steps must occur for the reaction to proceed; material transport to the interface and reaction at the phase boundary. In some cases, a third requisite is the transport of reaction products away from the interface. The reaction at the phase boundary liberates or absorbs heat and changes the boundary temperature. Any of these steps may limit

the overall rate of reaction, since the rate is determined by the slowest step.

3.1. Diffusion Models

The most widely studied system of a transport rate controlled process is the parabolic rate law obtained for certain oxidation reactions. The rate of diffusion of any atomic species A across a plane at right angles to the diffusion direction, is given by Fick's Law.

$$J_A = - D_A \frac{\partial C_A}{\partial Z}$$

where J_A is the flux of A through the plane, D_A is the diffusion coefficient of A and $\frac{\partial C_A}{\partial Z}$ is the concentration gradient, (chemical activity gradient), of A across the plane in the direction of diffusion.

A simple case is where a layer of new phase is formed and diffusion occurs through it, while the concentration of the diffusion species at the boundaries of the layer remain constant. When the diffusion is one of interstitial atoms through the product layer then:

$$J_{Ai} = - D_{Ai} \frac{(C_1 - C_2)}{Z}$$

C_1 and C_2 are the concentrations of interstitial atoms at interface 1 and 2 respectively and Z is the product layer thickness.

When Λ is the volume of product per interstitial atom, and C is the concentration of interstitial atoms:

$$\Lambda = \frac{1}{C}$$

$$\frac{dZ}{dt} = J_{Ai}\Lambda = D_{Ai}\ \frac{(C_1 - C_2)}{Z}\ .\ \Lambda$$

$$\frac{dZ}{dt} = D_{Ai}\frac{(C_1 - C_2)}{C}\ .\ \frac{1}{Z}$$

$$= D\ \frac{1}{Z}$$

Integration gives $Z^2 = 2Dt$, the parabolic law of diffusion, which applies only to one-dimensional diffusion when the geometry of the interface does not alter during the reaction.

3.1.1. Jander's model

Jander[7] applied the parabolic law to powdered compacts, and it is worth considering in detail the assumptions necessary in deriving his formula:

(a) the reaction can be classed as an additive reaction with compound formation i.e. solid solution does not occur,

(b) nucleation, followed by surface diffusion, occurs at a temperature below that required for bulk diffusion, i.e. a coherent product layer is present before bulk diffusion commences,

(c) the solid state reaction is bulk diffusion controlled, i.e. the chemical reaction at the phase boundary is considerably faster than the transport process,

(d) bulk diffusion is uni-directional,

(e) the reacting particles are all spheres of uniform radii,

(f) the ratio of the volume of product layer to the volume of reacted material is unity,

(g) the increase in thickness of the product layer follows the parabolic rate law,

(h) the diffusion coefficent of the transport species is independent of time,

(i) the activity of the reactants remains constant on both sides of the reaction interface,

(j) the surface of the component in which the reaction takes place is completely coated with particles of the other component as though the former particles were immersed in a melt of the latter.

Let V be the volume of unreacted material at time t.

Then $V = \frac{4}{3}\pi (r_o - y)^3$ where r_o is the initial radius

and $V = \frac{4}{3}\pi r_o^3 (1 - \alpha)$ where α is the fraction reacted completed at time t

Equating we have $y = r_o \left[1 - (1 - \alpha)^{1/3} \right]$

$$K_J t = \frac{2KDt}{r_o^2} = \left[1 - (1 - \alpha)^{1/3} \right]^2 = D_3(\alpha)$$

where K_J is the rate constant.

It is often found, and not suprisingly, considering the number of requirements stated in the Jander theory, that the above equation does not adequately represent solid-solid reaction data, and a more complicated situation actually exists. There have been many attempts to develop equations for simple geometric systems, using different assumptions concerning the formation of the product layer, and these have been reviewed by Hulbert[17].

3.1.2. Ginstling and Brounshtein model

Ginstling and Brounshtein[18] discarded the parabolic law in favour of an equation relating the growth of the product layer to Barrer's equation[19] for steady state heat transfer through a spherical shell. The parabolic law is not applicable for spherical particles, since the area of the interface changes during reaction and hence the amount of material transport to the interface decreases as the reaction proceeds.

Let r_t be the radius of sphere of unreacted material at any time t and V_t the volume of this sphere.

Then $V_t = \frac{4}{3} \pi r_t^3$

Assuming tha rate of change of V_t is analagous to Barrer's equation for the flux of heat diffusing through a spherical shell of radius $r_o - r_t$ under steady state conditions, then

$$\frac{dV_t}{dt} = - \frac{4 \pi K D r_o r_t}{r_o - r_t}$$

where D is the diffusion coefficient of the migrating species.

Let α be the fraction reacted then

$$V_t = \frac{4}{3} \pi r_o^3 (1 - \alpha)$$

Equating

$$r_t = r_o (1 - \alpha)^{1/3}$$

Differentiating

$$\frac{dV_t}{dt} = 4 \pi r_t^2 \frac{dr_t}{dt}$$

Equating

$$r_t \, dr_t - \frac{r_t^2}{r_o} dr_t = - K D \, dt$$

Integrating and using the boundary conditions

$r_t = r_o$ at $t = 0$

$$\frac{r_t^2}{2} - \frac{r_t^3}{3r_o} = - K D t + \frac{r_o^2}{6}$$

Substituting $K_G - B^t = \frac{2KDt}{r_o^2} = 1 - \frac{2}{3} \alpha - (1 - \alpha)^{2/3} = D_4(\alpha)$

3.1.3. Carter-Valensi model

Carter[20] improved the above equation by accounting for differences in the volume of the product layer with respect to that of the volume of reactant consumed, and concluded that his additional consideration scarcely altered the Ginstling and Brounshtein equation until the ratio was greater than 2:1. Valensi[21] also developed the same solid state reaction model, but

from a different starting point, and the equation is referred to as the Valensi-Carter equation, where Z represents the volume of the reaction product formed per unit volume of reactant consumed.

$$K_{C-V}t = \frac{Z - \left[1 + (Z-1)\alpha\right]^{2/3} - (Z-1)(1-\alpha)^{2/3}}{Z - 1}$$

However, this equation is rarely used, due to the lack of high temperature density data for calculating the Z value.

3.1.4. Summary

In the solid state reaction models discussed so far, K is proportional to $\frac{1}{r^2}$ and r has been assumed constant. Hence control of the particle size of the reactants is very important-when diffusion controlled mechanisms are likely to be rate controlling.

3.2. Phase-Boundary Models

A solid state reaction is phase boundary controlled when diffusion through the product layer is so rapid that the reactants cannot combine fast enough at the reaction interface to reach an equilibrium. The reaction is then controlled by the movement of an interface at a constant velocity u.

Assuming (a) the reaction rate is proportional to the surface area of the fraction of unreacted material, and (b) nucleation occurs instantaneously,

so that the surface of each particle is covered with a layer of product.

Then, for spheres of uniform radii:

$$-\frac{dV_t}{dt} = K S_t$$

where V_t is the unreacted volume at time t and S_t is the surface area of unreacted particles.

When V_o is the original volume and α the fraction reacted

$$1 - \alpha = \frac{V_t}{V_o} = \frac{\frac{4}{3}\pi r_t^3}{\frac{4}{3}\pi r_o^3}$$

$$r_t^2 = (1 - \alpha)^{2/3} r_o^2$$

The rate of change of fraction reacted is given by:

$$-\frac{d(1 - \alpha)}{dt} = \frac{d\left(\frac{V_t}{V_o}\right)}{dt} = K \frac{S_t}{V_o}$$

Hence $$\frac{d\alpha}{dt} = \frac{K\, 4\pi r_t^2}{\frac{4}{3}\pi r_o^3}$$

Substituting for r_t^2

$$\frac{d\alpha}{dt} = \frac{3K(1-\alpha)^{2/3}}{r_o}$$

Integrating and choosing the boundary conditions $x = 0$ at $t = 0$.

$$K_p - b^t = \frac{Kt}{r_o} = \left[1 - (1 - \alpha)^{1/3}\right]$$

Similarly for a circular disc reacting from the edge or for a contracting cylinder

$$K_p - b^t = \frac{K t}{r_o} = \left[1 - (1 - \alpha)^{\frac{1}{2}} \right]$$

The mechanism which leads to a phase boundary controlled reaction assumes that the nucleation step occurs instantaneously, so that the surface of each particle is covered with a layer of product. However, nucleation of the reactant may not necessarily be followed by rapid surface growth, and another approach to solid state reactions is to consider the nucleation of products at active sites, and the rate at which these nucleated particles grow.

3.3. Nuclei Growth Models

Nucleation and growth of crystals from a solid matrix is fundamentally the same as growth from a vapour or liquid, with the added complication that the volume change accompanying the phase transformation requires an additional term to be considered in determining the free energy change for nucleation and growth. This strain energy, which must be overcome for a nucleus to form and grow, does not alter the overall characteristics of the transformation.

The decomposition of powder samples of carbonates etc. introduces two other factors; a very large surface area is available for heterogeneous nucleation, and the

size of the crystals that can be grown is limited by the particle size of the material. The rate of nucleation may then be slow, compared with the amount of crystal growth required to exhaust the volume of small particles. Hence, the overall rate of reaction is largely determined by the rate of nucleation which is proportional to the volume of matrix material available. Therefore the reaction rate is proportional to the amount of material remaining, and in classical reaction kinetics nomenclature this is then a first order reaction.

3.3.1. Simple theory

If N_o preferred nucleation sites per unit volume of reactant become nuclei according to a classical first order rate process, then the number of active sites remaining at time t is given by:

$$N_t = N_o \exp.^{(-ft)}$$

where f is the nucleation frequency.

The nucleation rate per unit volume I is given by:

$$I = f N_t = f N_o \exp.^{(-ft)}$$

There are two limiting forms of this equation corresponding to very small or very large values of (ft). Small values of (ft) imply that I is effectively constant (case A). Large values of (ft) effectively mean that nucleation occurs so rapidly that the nucleation time may be neglected, i.e. all nucleation sites are

exhausted at an early stage in the reaction (case B).

The equations that can be developed for nuclei growth and empirical solutions for metallic systems are of the general form:

$$\ln \frac{1}{1 - \alpha} = (Kt)^m$$

Examples of this equation are those of Avrami-Erofe'ev[22,23] where m is any integer and the Johnson-Mehl equation where m = 4. Hulbert[17] has tabulated the theoretical m values for various boundary conditions using three cases of nucleation rate Table 2.

3.4. Heat-Mass Transfer Models

A heat-mass transfer mechanism occurs when the reaction is controlled by the transfer of heat to the reaction boundary and the transfer of gaseous products away from the boundary. This approach has been used successfully by Hills[11] in an investigation of the decomposition of single spheres of calcium carbonate. One interesting result of Hills' investigation, and an earlier one by Warner, is that the reaction rate is proportional to the interfacial area for a reaction controlled by heat and mass transfer. Previously it had been thought that only a diffusion and mass transfer mechanism would result in a reaction rate proportional to the interface area.

One would expect heat transfer effects to become more pronounced and possibly eventually rate controlling

as the sample weight is increased. Since the experimental conditions in this investigation have been chosen so as to minimise heat transfer effects as far as possible, it would be difficult, if not impossible, to derive a heat-mass transfer model for these conditions. However, the qualitative aspects of a heat transfer rate controlling step can be deduced and applied to the decomposition of barium carbonate in a nitrogen atmosphere.

3.5. Kinetic Analysis

Sharp et al[24] have shown that reduced time master curves can be used as a first step in the determination of a reaction mechanism. Their tables show that when the main types of mechanism are compared, a broad classification into three groups is possible; the first group containing the diffusion models, the second the phase boundary controlled and first order reactions, and the third the Arrami-Erofe'ev equations. They also show that differentiation within each group requires very careful and precise experimental data beyond a fraction reacted of 0.7. The normal forms of the equations are listed below, together with the reduced time scale forms. Table 3 contains reduced time scale values for the nine equations considered.

D1(α): one-dimensional diffusion process with constant diffusion coefficent.

$$D1(\alpha) = \alpha^2 = \left(\frac{K}{x^2}\right) t = 0.2500 \; t/t_{0.5}$$

where 2x is the thickness of the reacting layer.

D2(α): two-dimensional diffusion controlled reaction into a cylinder of radius r. The product volume is assumed to be that of the original material

$$D2(\alpha) = (1 - \alpha)\ln(1 - \alpha) + \alpha = (K/r^2)$$

$$= 0.1534\ t/t_{0.5}$$

D3(α): three-dimensional diffusion controlled reaction according to Jander.

$$D3(\alpha) = \left[1 - (1 - \alpha)^{1/3}\right]^2 = (K/r^2)\ t$$

$$= 0.0426\ t/t_{0.5}$$

D4(α): three dimensional diffusion controlled reaction according to Ginstling and Brounshtein.

$$D4(\alpha) = (1 - \tfrac{2\alpha}{3}) - (1 - \alpha)^{2/3} = (K/r^2)\ t$$

$$= 0.0367\ t/t_{0.5}$$

R2(α): phase boundary controlled reaction for a circular disc reacting from the edge inward, or for a cylinder, where u is the interface velocity.

$$R2(\alpha) = 1 - (1 - \alpha)^{\frac{1}{2}} = (\tfrac{u}{r})\ t$$

$$= 0.2929\ t/t_{0.5}$$

R3(α): phase boundary controlled reaction for a sphere of radius r reading from the surface inward.

$$R3(\alpha) = 1 - (1 - \alpha)^{1/3} = (\tfrac{u}{r})\ t$$

$$= 0.2063\ t/t_{0.5}.$$

F1(α): a reaction obeying classical first order kinetics

$$F1(\alpha) = \ln(1 - \alpha) = - kt$$
$$= - 0.6931\ t/t_{0.5}$$

A2(α): Avrami-Erofe'ev equation for nucleation.

$$A2(\alpha) = 2\sqrt{- \ln(1 - \alpha)} = kt$$
$$= 0.8326\ t/t_{0.5}$$

A3(α): Avrami-Erofe'ev equation for nucleation.

$$A3(\alpha) = 3\sqrt{- \ln(1 - \alpha)} = kt.$$
$$= 0.8850\ t/t_{0.5}$$

3.5.1. LnLn analysis

The classical method of nuclei growth analysis can be combined with reduced-time scale tables to produce a method of reaction mechanism analysis that is universally applicable to solid state reactions. Since the method uses a slope as diagnostic of the mechanism involved, the common difficulties of "zero time errors", and the time period required to obtain the operating conditions, can be observed in the analysis, but do not prohibit the use of this method as they do for reduced-time scale methods.

Any method of reaction mechanism analysis that produces a linear function whereby a single value can be determined and used as diagnostic of the process involved, is always preferable to one involving comparison with theoretical curves and numerical tables. This is

particularly true for isothermal data where there is always difficulty in arranging for a sample to attain instantaneously the experimental conditions of temperature and pressure and hence establishing the zero time. The time period required to attain the experimental conditions and the zero time error may be negligible, compared with the time for complete reaction, but using the method of Sharp et al[24] these time factors must be negligible compared with the time required for 50% reaction for a meaningful comparison of the data with their numerical tables.

The classical method of reaction mechanism analysis used in phase transformation studies, and reactions involving concepts of order and molecularity involves plotting the function Ln $[- \text{Ln}(1 - \alpha)]$ against Ln Time to obtain a linear fraction with slope m. Examples of this are the Avrami-Erofe'ev equations and the Johnson-Mehl equation, and the analysis is only meaningful when integral values of m are obtained. Diffusion controlled and phase boundary controlled reactions, which are of possible interest in ceramic systems, cannot be mathematically juggled to yield linear functions on a nuclei growth analysis. However, in the range $\alpha = 0.15$ to $\alpha = 0.50$, all the commonly used equations can be considered as linear functions, and the m values are shown in Figure 3. The data was obtained from the tables of Sharp et al by choosing

100 min. as the time for 50% reaction and, as would be expected, it is difficult to distinguish solely on this analysis the individual diffusion models and within the group comprising first order and phase boundary models. However, the two major groups are so widely separated in m values that they can be immediately differentiated, and the particular model within the group found by trial and error. When the zero time error is constant, the method cannot be used to determine the reaction mechanism by comparison with the theoretical m values, but the concepts of isokinetic processes can be introduced so that an interpretation of the process in terms of a physical model is not required. A process is isokinetic when the reaction mechanism does not change with temperature i.e. when the LnLn analysis curves at different temperatures are of the same shape, and can be brought into identity merely by lateral shift along the Ln Time axis. The concept of isokinetic processes can always be used to interpret decomposition data, even when the mechanism does change with temperature. Two situations are likely to occur; firstly the LnLn analysis may show a progressive change in the process mechanism indicated by a change in the shape of the LnLn analysis curves, or secondly, the analysis curves may change dramatically, indicating a complete change in the reaction mechanism.

All the diffusion controlled and phase boundary models considered so far exhibit positive deviation from linearity at high values of fraction reacted However, a negative deviation may occur, and it has been found[25] empirically that linear functions can be obtained in such systems when Ln $(\frac{\alpha}{1-\alpha})$ is plotted against Ln Time. When the slope is unity, the Prout-Tempkins equation is obtained but this has never been derived theoretically and, in fact, there is no mathematical justification of any equations of this form. However, this analysis can also be used to interpret decomposition data when the concept of isokinetic processes is introduced.

3.5.2. Activation energy determination

The classical method of determining the temperature dependence of any reaction mechanism is the $t\alpha$ method, and the basic requirement of the method is that the overall process can be represented by:

$\frac{d\alpha}{dt} = K\ f(\alpha)$ where $f(\alpha)$ is solely determined by the single variable α. When $t\alpha$ is the time from the start of the reaction,then:

$$\int_0^{\alpha} \frac{d\alpha}{f(\alpha)} = K\ t\alpha$$

For a thermally activated process $K = Ae^{\frac{-E}{RT}}$

The temperature dependence is then given by

$$\ln t\alpha = \ln C + \frac{E}{RT}$$

When a discontinuity is obtained in the graph of $\ln t\alpha$ against $\frac{1}{T}$, this method gives no indication of the type of mechanism change. Since one requirement of this method is that $t\alpha$ is the time from the beginning of the reaction, this method cannot be used when temperature variations occur at the start of an isothermal process or there is some doubt concerning the zero time.

For systems where the reaction mechanism is known, an Arrhenius plot can be obtained, on rates taken from the mechanism function versus time graph. If the reaction mechanism is not known, and the $t\alpha$ method is not applicable, an Arrhenius Plot can be constructed by utilising the m value or values obtained from the LnLn analysis, when a system is isokinetic over some temperature range and some range of the fraction reacted α is linear with slope p on a LnLn analysis, rate constants can be calculated by computing values of the function $\sqrt[p]{-\ln(1-\alpha)}$ against time over the range of linearity.

FIGURE 3: Application of LnLn analysis to some commonly used solid state reaction models.

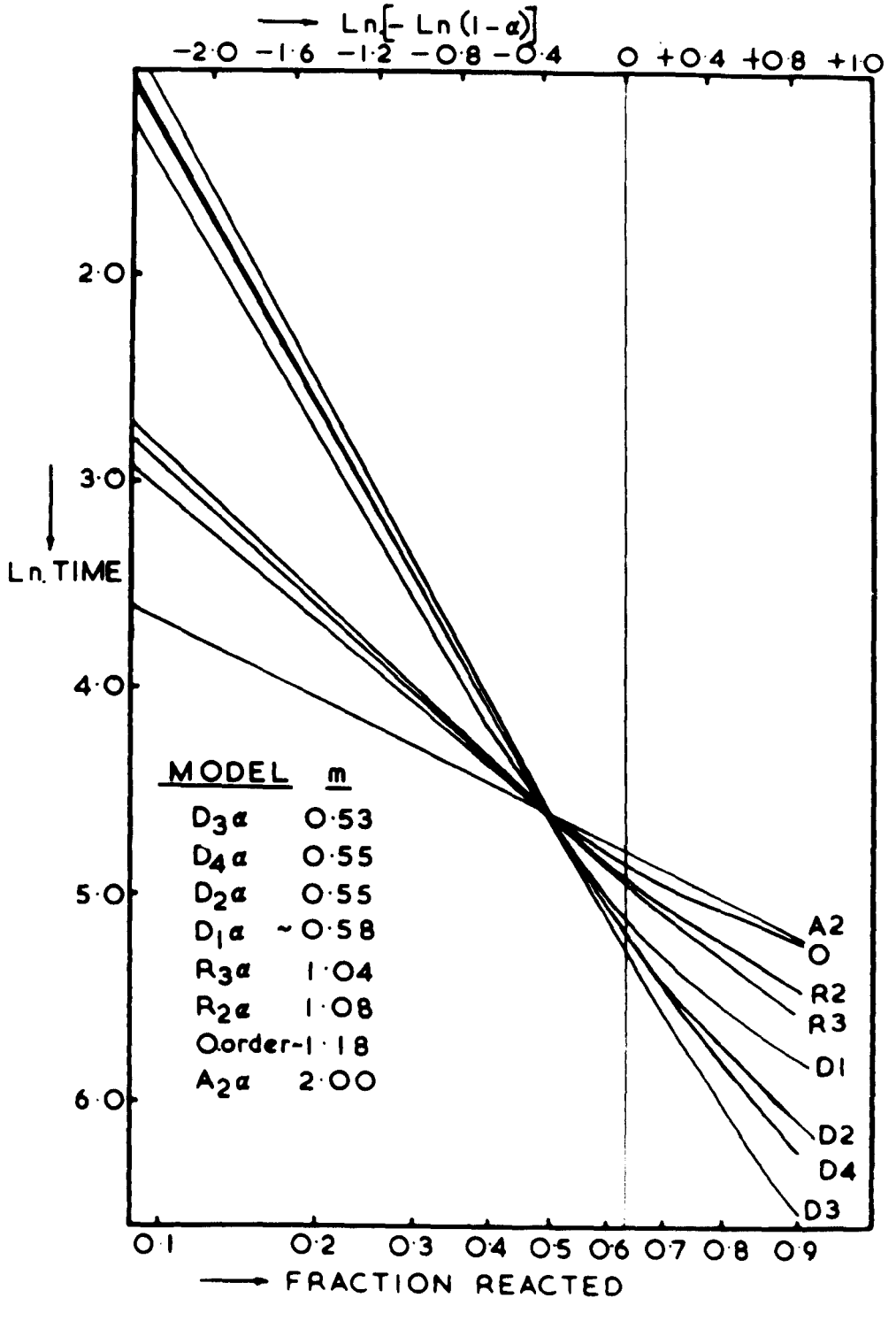
Ln[- Ln (1 - α)]
-2·0 -1·6 -1·2 -0·8 -0·4 0 +0·4 +0·8 +1·0
2·0
3·0
4·0
5·0
6·0
Ln. TIME
MODEL m
D3α 0·53
D4α 0·55
D2α 0·55
D1α ~0·58
R3α 1·04
R2α 1·08
Oorder-1·18
A2α 2·00
A2
O
R2
R3
D1
D2
D4
D3
0·1 0·2 0·3 0·4 0·5 0·6 0·7 0·8 0·9
FRACTION REACTED

TABLE 2 - Summary of Nuclei Growth Models for Solid-Solid Interaction[17]

('m' values listed for the appropriate boundary conditions)

Three-Dimensional Growth (i.e. Spheres)	Phase Boundary controlled	Diffusion controlled
Case (A) Constant Nucleation Rate	4	2.5
Case (B) Zero Nucleation Rate (saturation of point sites)	3	1.5
Case (C) Decreasing Nucleation Rate	3-4	1.5-2.5
Two-Dimensional Growth (i.e. Plates)		
Case (A) Constant Nucleation Rate	3	2
Case (B) Zero Nucleation Rate	2	1
Case (C) Decreasing Nucleation Rate	2-3	1-2
One-Dimensional Growth (i.e. Rods)		
Case (A) Constant Nucleation Rate	2	1.5
Case (B) Zero Nucleation Rate	1	0.5
Case (C) Decreasing Nucleation Rate	1-2	0.5-1.5

TABLE 3 - Values of α and t/t0.5 (Sharp et al[24])

α	D1(α)	D2(α)	D3(α)	D4(α)	F1(α)	R2(α)	R3(α)	A2(α)	A3(α)
0.1	0.040	0.033	0.028	0.032	0.152	0.174	0.165	0.390	0.533
0.2	0.160	0.140	0.121	0.135	0.322	0.362	0.349	0.567	0.685
0.3	0.360	0.328	0.295	0.324	0.515	0.556	0.554	0.717	0.801
0.4	0.640	0.609	0.576	0.595	0.737	0.768	0.762	0.858	0.903
0.5	1.000	1.000	1.000	1.000	1.000	1.000	1.000	1.000	1.000
0.6	1.440	1.521	1.628	1.541	1.322	1.253	1.277	1.150	1.097
0.7	1.960	2.207	2.568	2.297	1.737	1.543	1.607	1.318	1.198
0.8	2.560	3.115	4.051	3.378	2.322	1.887	2.014	1.524	1.322
0.9	3.240	4.363	6.747	5.028	3.322	2.334	2.602	1.822	1.492

CHAPTER 4

Experimental Techniques

Introduction

A study was made of several techniques that might be potentially useful in investigations of solid state reactions. Of the techniques investigated, differential thermal analysis, thermogravimetric analysis, transmission electron microscopy, infrared spectroscopy and electron probe micro-analysis were found to be useful to a limited extent, and the instruments used, and the operating techniques, are shown in Table 4. The two techniques that were found to be particularly successful were - scanning electron microscopy and x-ray diffraction analysis, and these were adopted to be used in conjunction with the vacuum thermobalance studies.

4.1. Materials and Mixing Procedure

The purity and particle sizes of all the materials used in this investigation are shown in Table 5. All the carbonate-metal oxide samples were prepared by mixing the weighed constituents in an ultrasonic bath, in the presence of the chosen media for five minutes, followed by shaking in a glass bottle by hand, for a further five minutes. Analar acetone and distilled water were the two mixing media used throughout the investigation.

4.2. Thermal Analysis

4.2.1. Thermogravimetry

The effects of mixing techniques, crucible materials, particle sizes and sample weights were investigated, using a Stanton TR-1 thermobalance, giving a linear temperature rise of ~ 4°C/min. up to a maximum temperature of 1000°C, and the results of this study are discussed in Chapter 5.

4.2.2. Vacuum thermobalance

A photograph of the thermobalance and a front elevation are shown in Figures 4 and 5. A copper-beryllium spring was used to determine the weight changes of the sample, and the sensitivity of the spring was 0.760 mm./mg. The sample was contained in a crucible suspended by a fine platinum wire, which was connected to the spring with a fine nickel wire. This particular arrangement allowed a maximum loading capacity of 350mg. of the sample and its crucible. The extension of the spring was determined with a cathetometer, measuring to $\pm$ 0.02mm. movement of the nylon crosswires glued to the nickel supporting wire.

The thermobalance had been partially constructed before this present investigation had started, and its original design had assumed that the furnace would be raised around the silica tube containing the sample, at the beginning of an experiment. However, preliminary experiments showed that this design was unsuitable for

accurate kinetic studies, as twenty minutes elapsed before the sample reached an equilibrium temperature after the furnace had been raised around the silica tube. This temperature lag led to induction periods on the graphs used for kinetic analysis and these periods were not reproducible. Therefore, the design of the thermobalance was modified, to allow the sample to be lowered into the silica tube with the furnace already in position, and at an equilibrium control temperature. The large size of the glass column needed to contain the spring and sample made it impractical to use a rigid supporting wire for the spring, as this would have increased the height even further. The desired effect was achieved by supporting the spring with a nylon thread fastened to a rotating wheel at the top of the column. The top of the column consisted of a rotary shaft vacuum seal, screwed and sealed into a machined duralium head. The rotar was connected to a crown wheel and pinion to transmit the rotation to a driving wheel near the cathetometer. Preliminary experiments showed that there was no detectable movement of the sping, due to slackness in the transmission system, even though a locking device was not incorporated into the system. Hence the furnace could be raised on its four vertical runners around the silica tube and allowed to reach a controlling

temperature while the column was being evacuated and the sample held outside the furnace. This arrangement had one disadvantage in that the cathetometer reading at time zero could not be measured accurately, as the lowering of the sample into the furnace caused the spring to oscillate for about twenty minutes. However, this oscillation period was reduced by lowering the crucible until it just touched the thermocouple insert tube, damping the oscillation and allowing an accurate cathetometer reading to be taken after about ten minutes.

The spring was calibrated with known weights at its normal operating position in the column i.e. after lowering the crucible into the cold furnace. This was done to allow for any effects the nylon supporting thread may have had under normal operating conditions. The cathetometer reading at time zero was calculated from the reading at complete decomposition, assuming the theoretical weight loss. A comparison of this calculated reading, with one obtained by extrapolation from experimental values obtained during the early stages of a run, gave very good agreement.

The furnace tube was wound with Nichrome wire to give a uniform temperature zone five inches long and the temperature control unit, built in the department, gave $\pm$ 2°C variation at the furnace wall. The sample temperature was measured with a chromel-alumel thermocouple fitting into an insert tube at the base of the

silica tube. In a preliminary experiment, a thermocouple was fastened to a crucible and supported from the column head. The sample temperature measured in this way was within $\pm$2°C of the insert temperature and hence the insert temperature was used as the true sample temperature in all the calculations. An attempt was made to measure the time taken by the sample to reach an equilibrium temperature when once lowered into the furnace. Unfortunately, this was found to be impossible to measure, as the geometry of the column prevented the thermocouple from moving more than three inches inside the column. However, a combination of thermocouple movement and raising the furnace around the silica tube to approximate to the normal experimental conditions, indicated that the time taken for the sample to reach temperature was very small and negligible, when compared with the time required to achieve total decomposition of the sample.

The water jacket around the spring was lagged, and fed with a recirculating water supply from a thermostat bath controlling to better than $\pm$ 0.5°C. This was necessary, as the extension of a spring under a given load has a notable temperature coefficient. A Genevac vacuum unit, combining a rotary and an oil diffusion pump with a maximum capacity of 270 litres/min., was used to give a vacuum of $\leq 10^{-4}$ torr in the column at the start of a run. The pressure during a

run, was observed with a Penning gauge inserted just above the pumping line, and a liquid nitrogen trap was used between the column and pumping unit. The apparent pressure in the column during an isothermal run, was about 10^{-3} torr, reaching 5×10^{-6} torr at the completion of the run. Mercury manometers were connected into the pumping line for measuring the pressure in a closed system when this was required.

FIGURE 4: The Vacuum Thermobalance

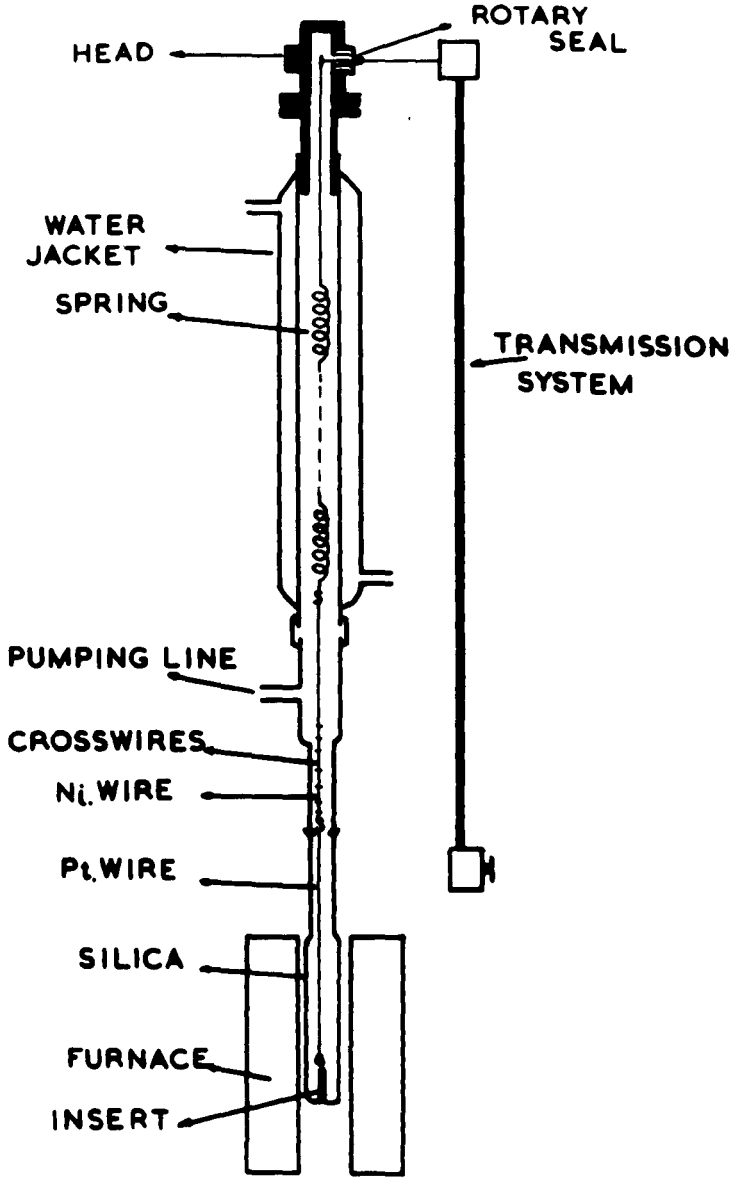
HEAD
ROTARY SEAL
WATER JACKET
SPRING
TRANSMISSION SYSTEM
PUMPING LINE
CROSSWIRES
Ni. WIRE
Pt. WIRE
SILICA
FURNACE
INSERT

FIGURE 5: The Vacuum Thermobalance.

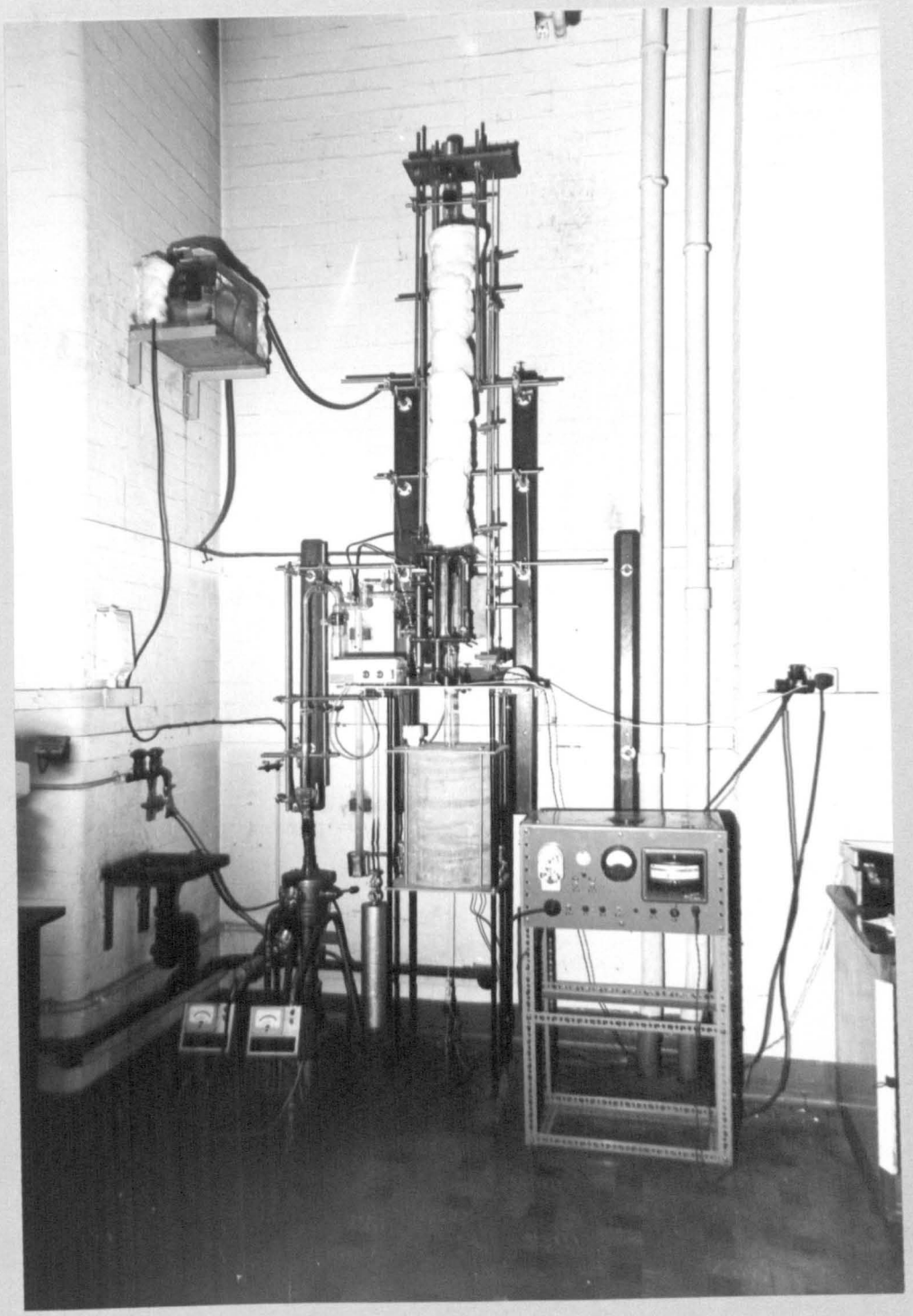

TABLE 4 - Experimental Techniques and Apparatus

TECHNIQUE	APPARATUS	COMMENTS
Differential Thermal Analysis (DTA)	Netzsch	Standard technique generally but some use of carbonate as the inert material
Electron Microscopy (EM)	Philips (EM100)	Standard Technique
Stereo-scanning Electron Microscopy (SEM)	CAMBRIDGE	see DeVine et al[12]
Infrared Spectroscopy	Perkin Elmer 337	Standard Technique using KBr discs
Electron Probe Micro-Analysis (EPMA)	A.E.I.	Standard Technique
Thermogravimetry	Stanton TR-1	Dynamic to 1000°C and then isothermal. No atmosphere control.
Mass Spectrometer	A.E.I. (MS10)	Standard Technique

TABLE 5: Purity and Morphology of Raw Materials

	Purity	Nomenclature	Comments
Carbonates			
Barium	Analar	$BaCO_3$ I	Spherical particles Surface Area $1.3 m^2 g$
Carbonate	Analar	$BaCO_3(\ell)$	laths 10μ x1μx1μ (Fig. 17)
	Analar	$BaCO_3(s)$	0.5μ spherical particles and ~2μ discs (Fig. 18a)
	Spec. Pure	$BaCO_3(sp)$	spheres, laths and plates (Fig. 19a)
Strontium	Commercial	$SrCO_3$	less 300 mesh
Carbonate	Grade Spec. Pure	$SrCO_3(sp)$	less 300 mesh(Fig19b)
Oxides			
Zirconia (baddeleyite)	Analar	ZrO_2	spherical(Fig.35) less 300 mesh
Stannic Oxide	Analar	SnO_2 II	less 300 mesh(Fig49)
	Commercial grade	SnO_2 I	less 300 mesh
Titania (ANATASE)	Commercial grade	TiO_2	less 300 mesh(Fig40)
Silica	99.85% Quartz	SiO_2 I	greater than 300mesh
		SiO_2 II	less 300 mesh(Fig54a)
	Analar	SiO_2 III	less than 300 mesh (Fig 54b)
Germania	Spec. Pure	GeO_2	less than 300 mesh (Fig. 46)

CHAPTER 5

Preliminary Results

An investigation was made into the general factors affecting the thermal decomposition in air of barium and strontium carbonates when heated alone, and in the presence of oxides of tetravalent cations. It was hoped that this study would assist in identifying the important factors in solid state reactions involving these materials, before a detailed kinetic model study was commenced.

5.1. Thermogravimetry

The general results of this investigation are given in Tables 6, 7, 8 and 9. The temperature at which the fraction reacted completed, was 0.1 is represented as $T_{0.1}$, α_{1000} is the fraction reacted completed at 1000°C and t_{1000} is the time required at 1000°C to achieve complete decomposition.

5.1.2. Particle size

The decomposition data for the mixtures $BaCO_3$I: SiO_2I, $BaCO_3$I: SiO_2II and the corresponding strontium carbonate-silica mixtures, are shown in Tables 6 and 7. In both the barium and strontium carbonate mixtures, a large increase in the reactivity of a mixture was observed when the coarse silica (SiO_2I) was replaced with a silica of particle sizes less than 300 mesh (SiO_2II). These results were not unexpected, and illustrate the dangers in constructing a table for the

comparison of the reactivities of barium and strontium carbonate with the chosen oxides, when the oxides do not have similar particle size distributions. However, in the systems in which the particle size of the oxide was comparable with that of the carbonate, the sequence of reactivity of the oxides studied is,

$$GeO_2 > TiO_2 \sim SnO_2 \sim SiO_2 > ZrO_2$$

germonia being clearly the most reactive, and zirconia the least.

5.1.3. Composition effects

The reactivity of a 2:1 carbonate-oxide mixture was always less than that of the corresponding 1:1 mixture. This is due to two factors:

a) dilution effect - a 2:1 mixture contains less mg. of carbonate per 1g mixture than a 1:1 mixture.

b) increasing the percentage of oxide at a fixed sample weight increases the number of point contacts between particles of barium carbonate and particles of the oxide. (See 5.1.5).

5.1.4. Crucible effects

There was no apparent difference in the reactivities of barium carbonate-metal oxide mixtures when decomposed in alumina and platinum crucibles. Such a comparison is not possible in the case of the decomposition of barium carbonate alone, as in this system the platinum crucible is completely destroyed during the decomposition, and the alumina crucible is stained green-brown at its

base. In both the decomposition of strontium carbonate alone, and strontium carbonate-metal oxide mixtures, the crucible material alters the reactivity of the sample, Table 9. All the mixtures decomposed in platinum crucibles were more reactive than the corresponding samples decomposed in alumina crucibles.

5.1.5. Mixing effects

Analar acetone and distilled water were used as mixing media and for all the samples investigated the decomposition temperature of a water prepared sample was lower than the corresponding acetone prepared sample. (Table 8).

These results were supported by the isothermal decomposition data obtained in conjunction with the x-ray analysis experiments (Chapter 6). Scanning electron microscopy showed that the differences in reactivity were due to aggregation effects in the two mixing media; a water mixture resulting in increased contacts between the carbonate particles and the particles of the oxide.

5.1.6. Reaction products

X-ray powder photographs, using the Debye-Scherrer method, were obtained for all the decomposed samples. Some difficulty was encountered in identifying every phase present in the reaction products, but two general results were obtained; a strontium hydroxide phase was found to be present in all the reaction products of the

strontium carbonate systems, and the reaction products in the 1:1 barium carbonate-metal oxide systems were generally the same as those found in the corresponding 2:1 mixtures, e.g. Ba_2GeO_4 was the major reaction product for both 1:1 and 2:1 barium carbonate-germonia mixtures. These results were used as background information for the more detailed x-ray analysis study of reaction products using a diffractometer (Chapter 6).

Infrared spectroscopy was also used as a qualitative technique to determine the products of reaction. This technique was used in conjunction with the x-ray diffraction experiments on the partial products of reaction, and was especially useful in determining the presence of hydroxide phases, and small amounts of unreacted carbonate.

5.2. Differential Thermal Analysis

The phase changes of the individual materials were determined and a study of all the barium-carbonate-metal oxide systems was completed. However, this technique appeared to be more suitable as a minor technique when thermogravimetry was being used, and not really suitable as an aid to isothermal weight change experiments.

5.3. Strontium Carbonate

Thermogravimetry of three samples of strontium carbonate showed that all these materials experienced some loss of weight below 850°C, Figure 6. This was thought to be due to the presence of strontium hydroxide

in the samples, and this was in agreement with the data obtained for strontium carbonate samples that had been heated to 950°C, and then cooled to room temperature, in an atmosphere of carbon dioxide. The decomposition curve of spec. pure strontium carbonate after this treatment, shows no weight loss below 850°C, and the total weight loss coincides with the theoretical value for strontium carbonate, Figure 7. In contrast, none of the other strontium carbonate samples, even after this treatment, gave theoretical weight loss, and all showed loss of weight below 850°C.

5.3.1. Decomposition of Strontium Carbonate in Vacuo

The spec. pure carbonate and its carbonated form were examined by SEM, and were found to be unsuitable for isothermal studies involving analysis of the reaction mechanism, due to the large variations in particle size and shape within each sample. However, the decomposition of two carbonate samples was investigated, so that experience in operating the vacuum thermobalance could be gained. A LnLn analysis of the isothermal data yielded m values in the range 1.00 to 1.30, indicating that the mechanism was not diffusion controlled, but the true reaction mechanism could not be evaluated as predicted by the SEM investigation. Activation energies were calculated using the t_α method, where t_α was the time to reach 50% reaction.

The data are listed in Table 10 and the results are in good agreement with those of Wanamaker[4].

TABLE 10 - Vacuum Kinetic Data for Strontium Carbonate samples.

	Reaction Mechanism	Activation Energy Kcal/mole.
$SrCO_3$ I (containing $Sr(OH)_2$)	zero order	47
$SrCO_3$ spec. pure	unknown	55 ± 4
Carbonated $SrCO_3$ (Wanamaker[4])	unknown	53 ± 3

5.3.2. Strontium carbonate - metal oxide systems

All the partial reaction mixtures of all the strontium carbonate-metal oxide systems at 1000°C, contained a strontium hydroxide phase. An isothermal kinetic investigation of such systems is of dubious significance, as meaningful data can only be obtained when the carbonate decomposes to form a product with the mixed oxide without the intermediate formation of strontium oxide. In addition, a vacuum investigation of strontium carbonate-metal oxide systems would require temperatures less than 580°C, and the furnace used in the thermobalance is not suitable for radiation heating at such low temperatures. Hence, none of the

strontium carbonate-metal oxide mixtures were investigated in the vacuum thermobalance.

5.4. Discussion

The general results of the preliminary investigations are as follows:

a) a vacuum kinetic study of strontium carbonate-metal oxide systems is not worthwhile,

b) the degree of aggregation of the metal oxide in carbonate mixtures depends on the mixing media, and hence the mixing geometry of a particular mixture can be altered by changing the mixing media,

c) the 2:1 compound is usually the major product of reaction in both 1:1 and 2:1 carbonate-metal oxide mixtures during the decomposition of the carbonate.

These results indicate that further information is required on the possible compounds that may be formed during reaction, and that it would be worthwhile attempting to relate the formation of the product phase to the decomposition of the carbonate. (See Chapters 6 and 7).

FIGURE 6: Thermogravimetric curves of strontium carbonate samples.

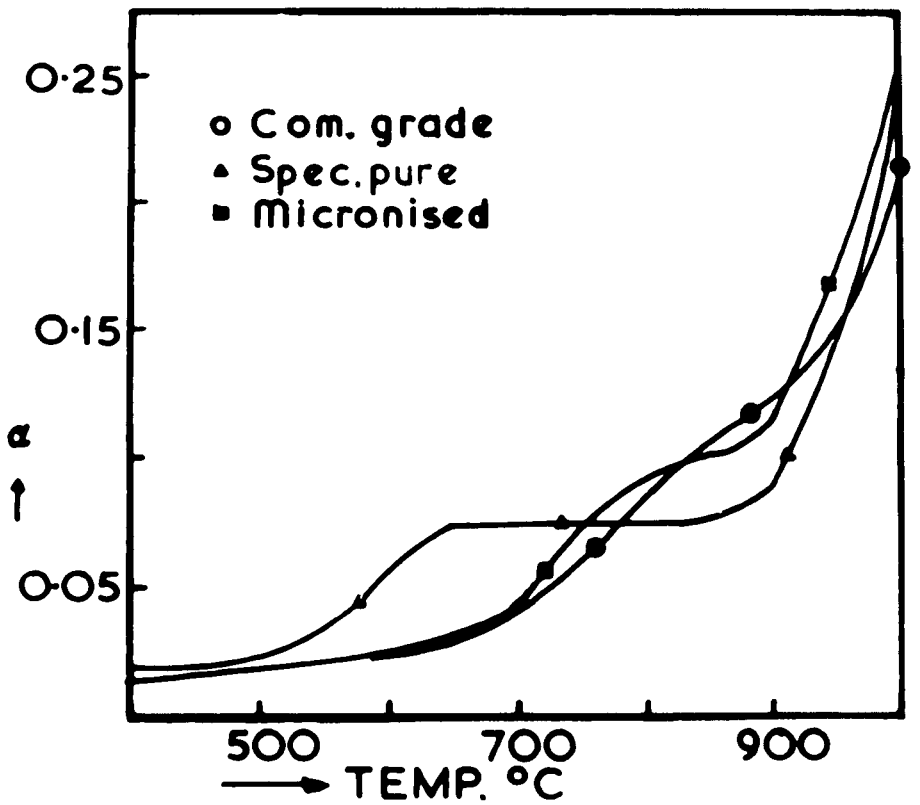
0·25
0·15
0·05
α
o Com. grade
▲ Spec. pure
■ Micronised
500
700
900
TEMP. °C

FIGURE 7: Thermogravimetric curves of strontium carbonate samples.

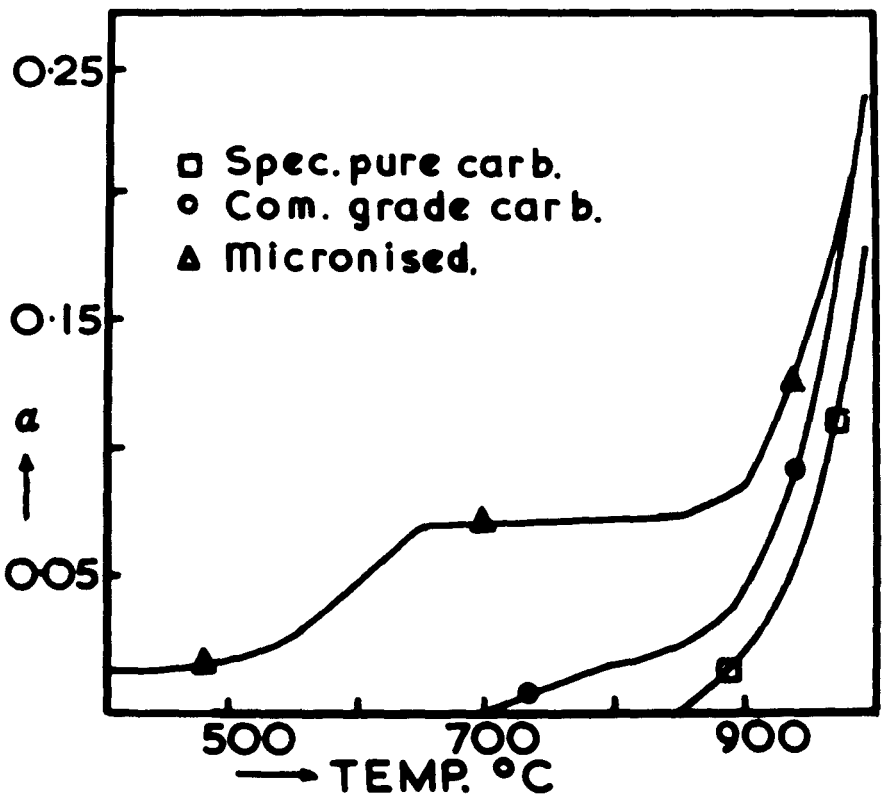
0·25
0·15
a
005
Spec. pure carb.
Com. grade carb.
Micronised.
500
700
900
TEMP. °C

TABLE 6: Thermogravimetric Data of $BaCO_3$-MO_2 Mixtures

SAMPLE	$T_{0.1}$	$T_{0.2}$	$T_{0.4}$	$T_{0.9}$	α at 1000°C	t_{1000} mins
$BaCO_3$I:ZrO_2	>1000	>1000	>1000	>1000	0.00	510
$BaCO_3$I:TiO_2	875	890	975	1000	0.46	210
$BaCO_3$I:SnO_2I	900	960	1000	1000	0.34	240
$BaCO_3$I:SiO_2I	>1000	>1000	>1000	>1000	0.09	690
$BaCO_3$I:SiO_2II	870	940	>1000	>1000	0.36	150
$BaCO_3$I:GeC_2	750	820	915	>1000	0.66	45
2$BaCO_3$I:ZrO_2	>1000	>1000	>1000	>1000	0.00	510
2$BaCO_3$I:TiO_2	935	990	>1000	>1000	0.25	360
2$BaCO_3$I:SnO_2I	930	985	>1000	>1000	0.27	255
2$BaCO_3$I:SiO_2I	>1000	>1000	>1000	>1000	0.09	540
2$BaCO_3$I:SiO_2II	920	968	>1000	>1000	0.33	270
2$BaCO_3$I:GeO_2	-	918	>1000	>1000	0.39	80

TABLE 7: Thermogravimetric Data of $SrCO_3$-MO_2 Mixtures

SAMPLE	$T_{0.1}$	$T_{0.2}$	$T_{0.4}$	$T_{0.9}$	α at 1000°C	t_{1000} mins
$SrCO_3:ZrO_2$	900	985	>1000	>1000	0.31	60
$SrCO_3:TiO_2$	820	920	>1000	>1000	0.41	75
$SrCO_3:SnO_2$ I	875	960	>1000	>1000	0.35	50
$SrCO_3:SiO_2$ I	880	960	>1000	>1000	0.32	60
$SrCO_3:SiO_2$ II	825	925	980	>1000	0.49	30
$SrCO_3:GeO_2$	635	830	875	980	1.00	0
$2SrCO_3:ZrO_2$	900	970	>1000	>1000	0.27	90
$2SrCO_3:TiO_2$	825	950	>1000	>1000	0.37	90
$2SrCO_3:SnO_2$ I	900	960	>1000	>1000	0.33	60
$2SrCO_3:SiO_2$ I	890	960	>1000	>1000	0.32	55
$2SrCO_3:SiO_2$ II	850	935	>1000	>1000	0.38	45

TABLE 8: Thermogravimetric Data of Water and Acetone Mixtures

SAMPLE	PREPARATION	$T_{0.1}$	$T_{0.3}$	$T_{0.4}$	$T_{0.9}$	α at 1000°C	t_{1000} min
$BaCO_3I:ZrO_2$	Acetone	>1000	>1000	>1000	>1000	0.00	510
$BaCO_3I:ZrO_2$	Water	>1000	>1000	>1000	>1000	0.01	480
$BaCO_3I:SnO_2I$	Acetone	900	960	>1000	>1000	0.34	240
$BaCO_3I:SnO_2I$	Water	875	940	995	>1000	0.44	30
$BaCO_3I:TiO_2$	Acetone	875	890	975	>1000	0.46	210
$BaCO_3I:TiO_2$	Water	820	865	915	985	1.00	0
$SrCO_3:SnO_2I$	Acetone	875	960	>1000	>1000	0.35	50
$SrCO_3:SnO_2I$	Water	780	900	985	1000	0.48	30
$SrCO_3:TiO_2$	Acetone	820	920	>1000	>1000	0.41	75
$SrCO_3:TiO_2$	Water	750	860	960	>1000	0.55	30

TABLE 9: Thermogravimetric Data for Samples in Platinum and Alumina Crucibles

SAMPLE	CRUCIBLE	$T_{0.1}$	$T_{0.2}$	$T_{0.4}$	$T_{0.9}$	α at 1000	t_{1000} min
$SrCO_3:ZrO_2$	Platinum	830	925	990	>1000	0.50	30
$SrCO_3:ZrO_2$	Alumina	900	985	>1000	>1000	0.31	60
$BaCO_3(1):ZrO_2$	Platinum	>1000	>1000	>1000	>1000	0.06	300
$BaCO_3(1):ZrO_2$	Alumina	>1000	>1000	>1000	>1000	0.04	300
$SrCO_3$	Alumina	850	980	>1000	>1000	0.02	150
$SrCO_3$	Platinum	830	950	>1000	>1000	0.30	90

CHAPTER 6

X-Ray Analysis of Partial Reaction Products

The purpose of this investigation was to gather general qualitative data on the reactions occurring in carbonate-metal oxide mixtures during and after the decomposition of the carbonate, and to relate these results to isothermal weight loss studies. No attempt was made to determine the composition of partially reacted samples quantitatively, as this would require either, a prepared calibration curve from mixtures of known composition, or the use of an internal standard. In this investigation, the amount of a phase was related to the peak height of one of its characteristic lines, and absorption effects were ignored.

6.1. Technique and Nomenclature

A Philips diffractometer with a scanning speed of 1° per minute was used, and the scale factor chosen so that the same scale could be used throughout each series of partial reaction products.

The amount of a phase was calculated in terms of the peak height, I_t recorded for a particular mixture, and the maximum peak height I_m recorded for that phase in the series of partial products. The amount of a phase present in a reaction mixture was defined as $I_r = \frac{I_t}{I_m} \times 100$.

I_m for the carbonates and oxides was determined on unreacted mixtures, and the maximum peak heights of the final products of reaction were determined from samples soaked at 1000°C for ≥ 70 hours.

Approximately ½g samples were fired in alumina crucibles at 1000°C in an electric furnace. The samples were air quenched immediately on removal from the furnace, except in the case of strontium carbonate-metal oxide mixtures, which were cooled to room temperature in an atmosphere of carbon dioxide (6.3.6.). All the partial reaction mixtures of a particular system were analysed consecutively, so that day-to-day variations in the operation of the diffractometer were avoided.

6.2. Theoretical Predictions

Each reaction is considered as two individual steps; the reactions occurring during the evolution of carbon dioxide, and the reactions that commence after the complete decomposition of the carbonate.

6.2.1. Stage 1: reactions occurring during the decomposition of the carbonate.

Four possible situations are considered:

A No 1:1 compound is formed

B Some 1:1 compound is formed and reacts slowly or rapidly to form a 2:1 compound

C No 2:1 compound is formed

D Some 2:1 compound is formed and reacts slowly or rapidly to form a 1:1 compound.

6.2.1.1. Case A No 1:1 compound is formed

$$2BaCO_3 + 2MO_2 = Ba_2MO_4 + MO_2 + 2CO_2\uparrow$$

The predicted curves for this reaction are shown in Figure 8(a); barium carbonate decreases from 100% to zero, the metal oxide decreases from 100% to 50%, and Ba_2MO_4 increases from zero to 100%. The formation of the 2:1 product, Ba_2MO_4, and the disappearance of the carbonate, are directly proportional with the point of intersection at 50% of each phase.

6.2.1.2. Case B Some 1:1 compound is formed

$$BaCO_3 + MO_2 = BaMO_3 + CO_2\uparrow \quad (1)$$

Followed by,

$$BaMO_3 + BaCO_3 = Ba_2MO_4 + CO_2\uparrow \quad (2)$$

Consider reaction (2) occurring rapidly so that the $BaMO_3$ remains effectively constant at some arbitrary amount (say 10%), until all the barium carbonate has decomposed. Since the 10% of $BaMO_3$ is an arbitrary value, it may or may not be possible to detect this compound under the experimental conditions used in this investigation. Figure 8(b) shows the predicted curves for this situation; barium carbonate decreases from 100% to zero, the metal oxide decreases from 100% to about 50%, Ba_2MO_4 increases from zero to 100%, and $BaMO_3$ increases from zero to 10%.

Now consider reaction (2) occurring slowly, and note that the nomenclature requires a maximum amount

to be shown as 100%. Figure 8(c). The barium carbonate decreases from 100% to zero, the metal oxide decreases from 100% to y% ($50 > y > 0$), Ba_2MO_4 increases from zero to 100%, and $BaMO_3$ increases from zero to z% ($50 > z > 0$).

6.2.1.3. Case C: No 2:1 compound is formed.

$$BaCO_3 + MO_2 = BaMO_3 + CO_2\uparrow$$

Figure 8(d) shows the predicted curves for this ideal case where only one compound is formed, and the rate of formation is directly proportional to the evolution of carbon dioxide.

6.2.1.4. Case D: Some 2:1 compound is formed.

$$BaCO_3 + MO_2 = Ba_2MO_4 + CO_2\uparrow \qquad (3)$$

Followed by,

$$Ba_2MO_4 + MO_2 = 2BaMO_3 \qquad (4)$$

Consider reaction (4) occurring rapidly so that the Ba_2MO_4 remains effectively constant at some arbitrary value (say 10%), but this has to be represented as 100%, according to the nomenclature system employed. The amount of Ba_2MO_4 may be so small as not to be detected in the x-ray analysis, and the system may appear to fit Figure 8(d). Figure 8(e) shows the predicted curves for the case where Ba_2MO_4 is detectable. Now consider reaction (4) occurring slowly, and this situation is shown in Figure 8(f). However, reaction (4) may occur so slowly and therefore the amount of $BaMO_3$ be so small, that it is not detected in the x-ray analysis,

and the results will appear indentical to Figure 8(a).

6.2.2. Stage II: reactions occurring after the complete decomposition of the carbonate in a 1:1 mole mixture.

If some Ba_2MO_4 is formed during the decomposition of the carbonate, this must eventually break down as equilibrium is approached. This may occur by a diffusion controlled solid state reaction:

$$Ba_2MO_4 + MO_2 \longrightarrow 2BaMO_3$$

A second possible mechanism requires the disproportionation of Ba_2MO_4:

$$Ba_2MO_4 \longrightarrow 2\ BaO + MO_2$$

or $$Ba_2MO_4 \longrightarrow BaO + BaMO_3$$

In theory, it should be possible to distinguish between the two mechanisms, since barium oxide is formed as an intermediate step in one case only. However, barium carbonate may be reformed in air from the barium oxide, therefore it may not be possible to evaluate the true mechanism.

6.3. Experimental Results

6.3.1. Barium carbonate-zirconia system

The total interval of 2θ scanned was from 23° to 31°. This range covered the lines used for analysis:

Compound	2θ	ASTM Index No.
$BaCO_3$	24.0	-
ZrO_2	28.2	-
$BaZrO_3$	30.1	8:277

The relative amounts of zirconia could not be determined accurately, as the recorded intensities were not reproducible. This may be due in part to the clustering of oxide particles observed in this system with SEM (Chapter 10). At this time, there is no literature data available for the compound Ba_2ZrO_4, and its existence has not been proved. The results obtained in this investigation have suggested that this compound, if it does exist, is not formed below 1500°C. However, it should be noted that this compound would probably have a structure very similar to $BaZrO_3$, an ideal cubic perovskite, and be analogous to Ba_2SnO_4.

During the decomposition of both the 1:1 and 2:1 mole mixtures, only one compound is formed. This system is ideal for kinetic studies, since only one compound is formed, and the rate of formation is directly proportional to the loss of carbon dioxide, Figures 9(a) and 9(b). However, this is only true when barium zirconate is formed during the decomposition, and, because this occurs under these experimental conditions, it does not necessarily follow that this situation will always occur (See Chapter 10).

6.3.2. Barium carbonate - Germania system

The total interval of 2θ scanned, 23° to 31°, covered the lines used for analysis:

Compound	2θ	ASTM Index No.
$BaCO_3$	24.0	-
GeO_2	26.1	-
$BaGeO_3$	28.8	12:355
Ba_2GeO_4	29.3	10:261
$BaGe_2O_5$	30.8	12:342
$BaGe_4O_9$	30.8	13:295

Higher angles were also scanned in an attempt to detect the presence of $BaGe_2O_5$ and $BaGe_4O_9$. However, their presence could not be proved, and if such compounds are formed during the decomposition they must be present in very small amounts, and less than the detectability of the diffractometer under the operating conditions chosen.

The 2:1 mole mixture forms Ba_2GeO_4, with a corresponding decrease in the amount of germania Figure 10(a). Similarly, in the decomposition of a 1:1 mole mixture, Ba_2GeO_4 is formed in increasing amounts up to a maximum correlating with the decomposition and final disappearance of barium carbonate. The 2:1 compound then decreases in amount with the formation of $BaGeO_3$ and the disappearance of germania Figure 11 (a).

The use of different mixing media does not alter the basic reaction sequences, and this is illustrated in Figures 11(a) aad 11(b); the 1:1 mixture prepared in water decomposes at a faster rate than that prepared in an acetone media. The formation of the 1:1 compound

from the 2:1 and germania, is much faster in the water mixed sample than in the acetone mix. This indicates that the mixing media alters the nature of the oxide, rather than the carbonate, since the increased reactivity is still apparent, even when all the carbonate has decomposed. Photographs obtained from the scanning electron microscope clearly illustrate the different aggregation effects obtained in water and acetone, and these are shown in Chapter 12.

6.3.3. Barium carbonate - titania system

The total interval of 2θ scanned was from 23° to 32°. This range covered the lines used for analysis:

Compound	2θ	ASTM Index No.
$BaCO_3$	24.0	-
TiO_2 (anatase)	25.4	-
Ba_2TiO_4	29.3	8:277
$BaTi_4O_9$	30.2	8:367
$BaTi_3O_7$	31.4	8:366
$BaTiO_3$	31.6	5:0626

The relative amounts of titania could not be determined, as the mixtures, after quenching from 1000°C, contained both the anatase and rutile forms of titania. The compounds $BaTi_3O_7$ amd $BaTi_4O_9$ could not be positively identified in any of the partial reaction mixtures. However, Templeton and Pask[13] reported these compounds to be present in amounts of less than 5% mole in their similar investigation, and therefore the amounts of these

compounds in this investigation may well have been less than the detectability of the diffractometer.

The 2:1 mole mixture decomposes to form the 2:1 compound, Ba_2TiO_4, and this is shown in Figure 10(b). In the 1:1 mole mixture, both the 1:1 and 2:1 compounds are apparently formed during the decomposition of the carbonate. Figure 12 shows the results for this system, and although interpretation of the diagram of difficult, this system appears to fit case B, (6.2.1.2).

6.3.4. Barium carbonate - stannic oxide system

The ranges of 2θ scanned were from 23° to 31° and 53° to 55°. This covered the angles used for analysis:

Compound	2θ	ASTM Index No.
$BaCO_3$	24.0	-
SnO_2	26.8	-
Ba_2SnO_4	29.6	12:665
$BaSnO_3$	54.6	15:780

A 2θ value of 54.6 for $BaSnO_3$ was used in preference to any of its lower angle values, due to the very close similarity of the 1:1 and 2:1 compounds' 2θ values at low angles. $BaSnO_3$ has a pervoskite structure and Ba_2SnO_4 a closely related structure, so that it is reasonable for the x-ray patterns to be so similar.

The 2:1 mole mixture only forms the 2:1 compound, Ba_2SnO_4, with a corresponding decrease in the amount of stannic oxide. Figure 13(b). Similarly, the 1:1 mole mixture forms Ba_2SnO_4 during the loss of carbon dioxide

and reaches a maximum amount corresponding to the final disappearance of barium carbonate. Figure 13(a). It is not possible to detect with certainty the first appearance of the 1:1 compound and consequently this system may be analagous to either the germania or the titania systems.

6.3.5. Barium carbonate - silica system

Completely satisfactory results could not be obtained for this system, and one of the many queries is illustrated in Table 11; namely there were discrepancies in the experimental and theoretical 2θ values for the 1:1 and 2:1 compounds.

TABLE 11: Theoretical and Experimental 2θ values of 2:1 and 1:1 compounds

Compound	ASTM		Experimental	
	2θ	I	2θ	I
Ba_2SiO_4	29.46	100	29.7	100
(6:0366)	30.28	95	30.5	84
	30.70	82	30.8	71
$BaSiO_3$	25.96	100	-	
(6:0247)	26.50	57	26.9	100
	28.50	50	28.9	100

The relative amounts of silica could not be determined, as the quenched products of partial reaction mixtures contained silica in several forms, including the α- and B- quartz modifications. A third query concerned the

inability of the 1:1 mole mixture to react completely to form $BaSiO_3$, even after two weeks of firing at 1300°C. When a precipitated form of silica was used, instead of the fragmented quartz, the reaction again did not reach completion. However, if the discrepancies and peculiarities are ignored, and a 2θ value of 29.70 is used for Ba_2SiO_4, the product formation is similar to that reported by Jander[7]; the 1:1 mole mixture decomposes to form Ba_2SiO_4 in increasing amounts, with a maximum corresponding to the final disappearance of barium carbonate, Figure 14(a). The 2:1 mole mixture also decomposes to form Ba_2SiO_4, and this is shown in Figure 14(b). Thus the silica system appears to be analagous with the germania system as expected from the chemical similarites of the two oxides, but with some peculiarities all of its own.

6.3.6. Strontrum carbonate - metal oxide systems

All the partial reaction mixtures of all the strontium carbonate-metal oxide systems were found to contain complex strontium hydroxides, and the presence of such phases caused severe difficulties in interpreting the experimental data. This situation was remedied by cooling all the samples from 1000°C to room temperature, in an atmosphere of carbon dioxide, which prevented the formation of strontium hydroxides, and resulted in the formation of strontium carbonate. The formation of the product phases could then be followed, but the true

reaction sequence could not be determined. Consequently only a few selected systems were examined in detail, but two general results were obtained; the occurrence of complex hydroxide phases indicated the formation of strontia in the reaction sequence at 1000°C, and the rates of formation of the ternary oxide products were of the same order as those observed for the barium carbonate systems.

6.4. Conclusions

Case C is the ideal reaction for kinetic studies, since only one compound is formed, and the rate of formation is directly proportional to the rate of loss of carbon dioxide. The system barium carbonate-zirconia is the sole example of this ideal situation in the five oxide systems. Case A is also suitable for kinetic studies, since the rate of loss of carbon dioxide is directly proportional to the rate of formation of the 2:1 compound. The systems barium-carbonate-germania, barium carbonate-silica and possibly barium carbonate-stannic oxide are examples of this situation. However, Case D can give results apparently identical to both Case C and Case A, under certain conditions outlined in the text (6.2.1.4.), and the techniques employed in this investigation are not sufficiently refined to give completely unquestionable results. Systems, such as the 1:1 barium carbonate-titania, are difficult to

interpret using this technique, and a study of the thermodynamics of such a system is required in order to clarify the reaction mechanism (see Chapter 2).

The barium carbonate systems show that the product formed during the decomposition of a carbonate in the presence of an oxide, is not necessarily that expected from the composition of the oxide-carbonate mixture. Barium oxide was never observed in any of the partial reaction mixtures of the barium carbonate systems, but strontium oxide was always present in partial reaction mixtures of all the strontrium carbonate systems. In view of this phenomena, the kinetic investigations in the vacuum thermobalance were restricted to the barium carbonate-metal oxide systems, the formation of strontrium oxide during a reaction makes the kinetics of such systems difficult to evaluate.

FIGURE 8: Theoretical curves for comparison with x-ray analysis data.

Figure 8a

Figure 8b

Figure 8c

Figure 8d

Figure 8e

Figure 8f

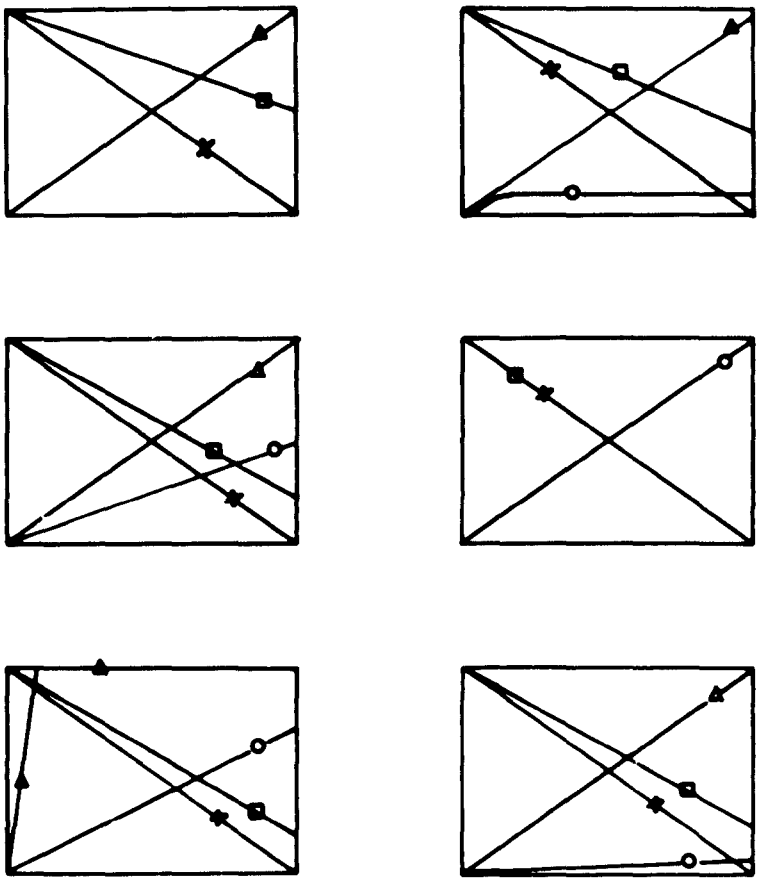

△ : Ba_2MO_4
○ : $BaMO_3$
× : $BaCO_3$
□ : MO_2

FIGURE 9a: X-ray analysis curves of $BaCO_3$-ZrO_2

FIGURE 9b: X-ray analysis curves of $2BaCO_3$:ZrO_2

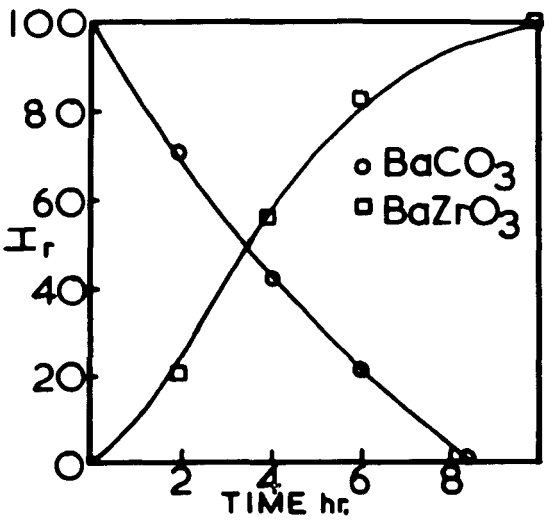
100
80
60
40
20
0
I_r
2
4
6
8
TIME hr.
$BaCO_3$
$BaZrO_3$

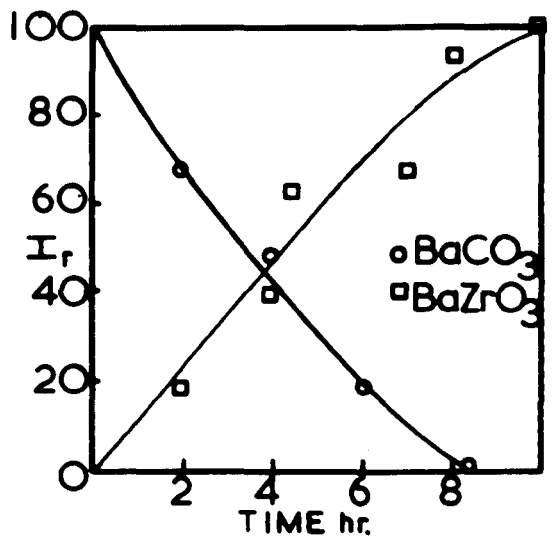
100
80
60
40
20
0
I_r
2
4
6
8
TIME hr.
$BaCO_3$
$BaZrO_3$

FIGURE 10a: X-ray analysis curves of $2BaCO_3:GeO_2$

FIGURE 10b: X-ray analysis curves of $2BaCO_3:TiO_2$

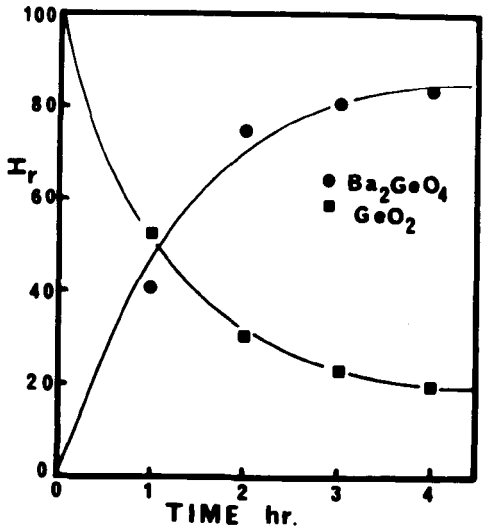
100
80
60
40
20
0
I_r
Ba_2GeO_4
GeO_2
0
1
2
3
4
TIME hr.

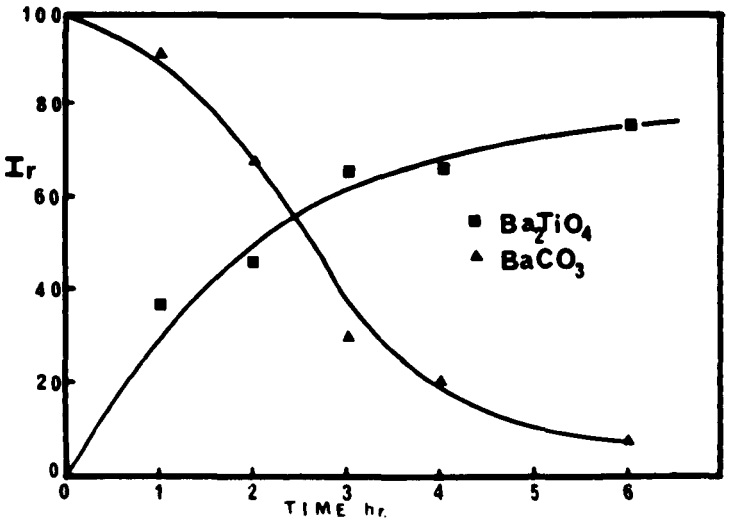
100
80
60
40
20
0
I_r
Ba_2TiO_4
$BaCO_3$
0
1
2
3
4
5
6
TIME hr.

FIGURE 11a: X-ray analysis curves of $BaCO_3$:GeO_2 (mixed in acetone)

FIGURE 11b: X-ray analysis curves of $BaCO_3$:GeO_2 (mixed in water)

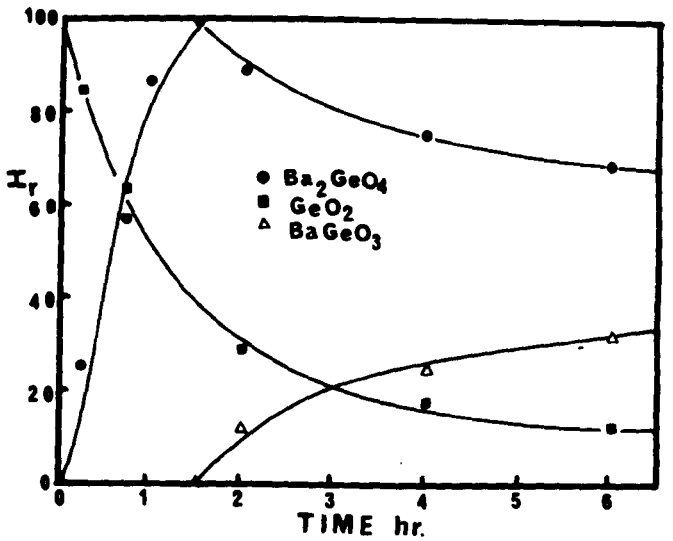
100
80
60
40
20
0
I_r
● Ba_2GeO_4
■ GeO_2
△ $BaGeO_3$
0
1
2
3
4
5
6
TIME hr.

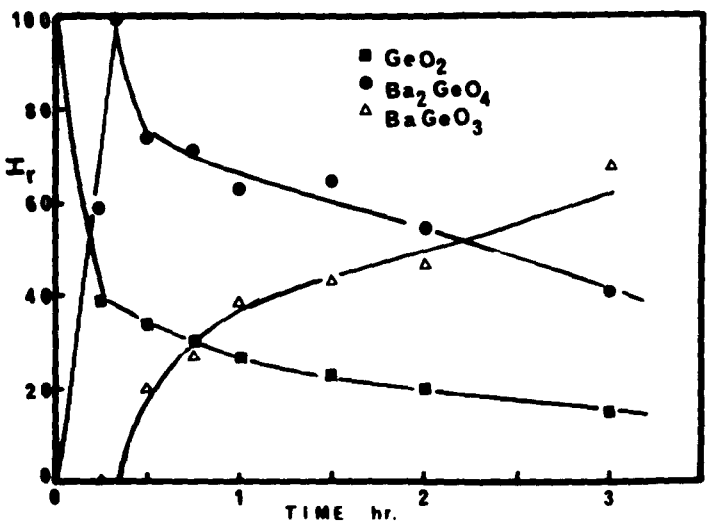
100
80
60
40
20
0
I_r
■ GeO_2
● Ba_2GeO_4
△ $BaGeO_3$
0
1
2
3
TIME hr.

FIGURE 12: X-ray analysis curves of $BaCO_3$:TiO_2

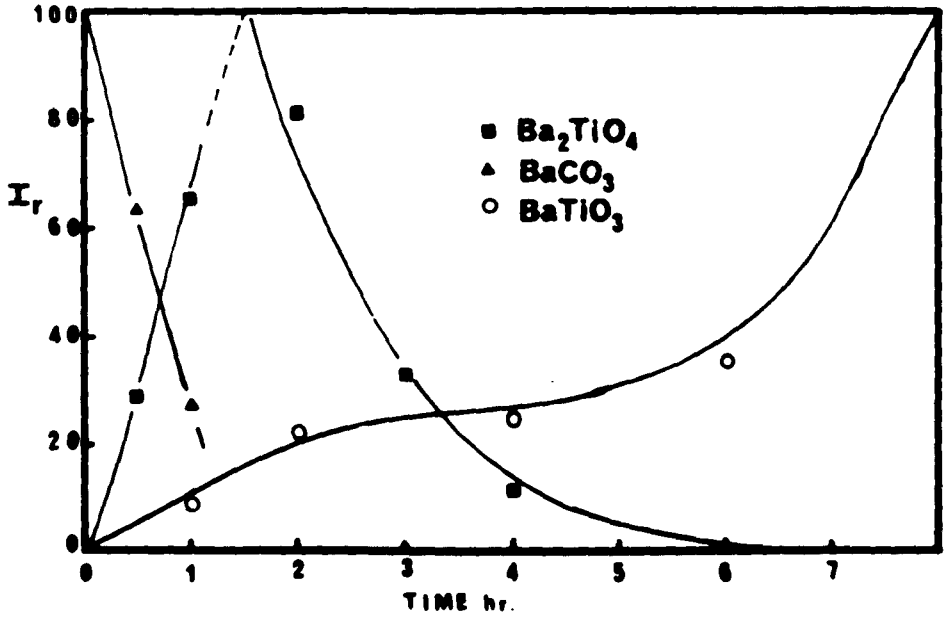
100
80
60
40
20
0
I_r
0
1
2
3
4
5
6
7
TIME hr.
Ba_2TiO_4
$BaCO_3$
$BaTiO_3$

FIGURE 13a: X-ray analysis curves of $2BaCO_3:SnO_2$

FIGURE 13b: X-ray analysis curves of $BaCO_3:SnO_2$

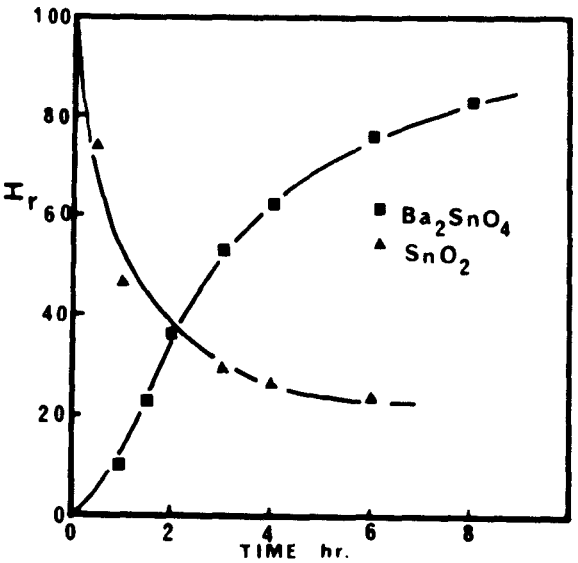
100
80
60
40
20
0
H_r
0
2
4
6
8
TIME hr.
Ba_2SnO_4
SnO_2

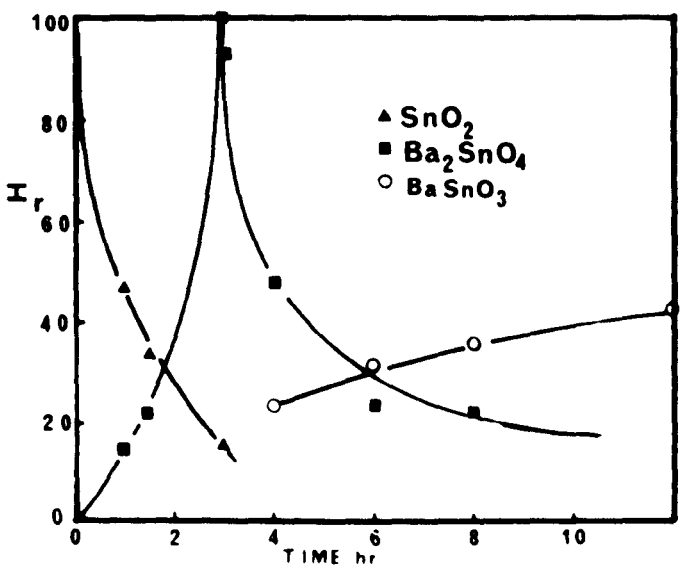
100
80
60
40
20
0
H_r
0
2
4
6
8
10
TIME hr
SnO_2
Ba_2SnO_4
$BaSnO_3$

FIGURE 14a: X-ray analysis curves of $2BaCO_3:SiO_2$

FIGURE 14b: X-ray analysis curves of $BaCO_3:SiO_2$

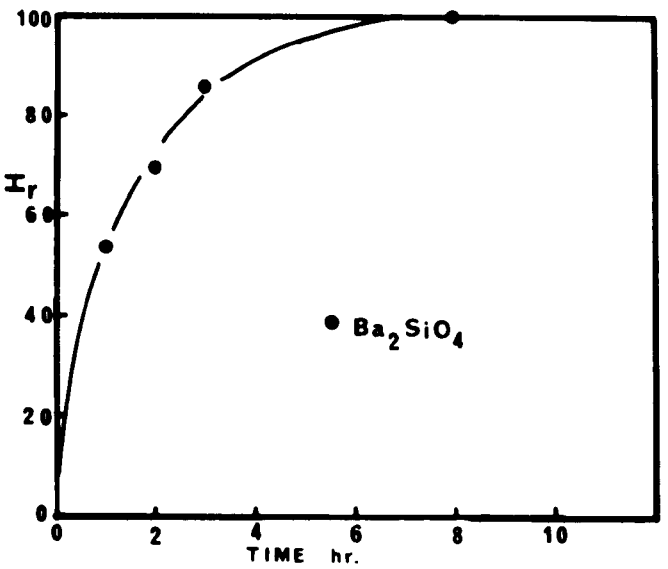
100
80
X_r
60
40
20
0
0
2
4
6
8
10
TIME hr.
Ba_2SiO_4

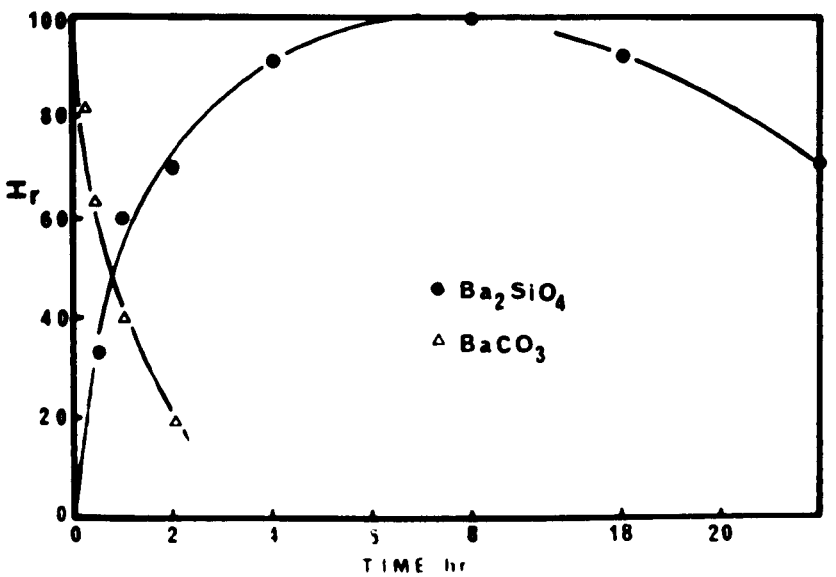
100
80
X_r
60
40
20
0
0
2
4
5
8
18
20
TIME hr
Ba_2SiO_4
$BaCO_3$

CHAPTER 7

An Investigation of Barium Carbonate-Metal Oxide Systems Using The Electron Probe

The purpose of this investigation was to study the compounds formed in barium-carbonate-metal oxide mixtures, and the sequence of compounds within each mixture, for comparison with the x-ray data discussed in Chapter 6. The instrument used for this investigation was an A.E.I. Scanning Electron Probe Micro-Analyser. Mixed phase samples were prepared from oxide powders compacted around sintered barium carbonate pellets in a platinum holder and fired, either at 1000°C in a nitrogen atmosphere, or at 800°C in vacuo in the case of barium carbonate-titania samples. The specimens were mounted in araldite, sectioned along the axis and polished with diamond paste. A thin coating of aluminium was used to prevent surface charging, and a standard technique was used to obtain the phase compositions..

7.1. Experimental Results

The amount of reaction product formed was found to be small in all the specimens examined, and in most cases the reaction product band had separated from the barium carbonate pellet. In some specimens, the reaction product was isolated from both the carbonate and the oxide, and the reaction products were frequently porous, thus reducing the accuracy of the analysis. The data

are summarised in Table 12, and although some phases appear to be non-stoichiometric, e.g. $B_{1.8}T$, there is no real evidence for non-stoichiometry as opposed to experimental error.

7.2. Discussion

In the titania system, the compound formed at the barium carbonate interface is Ba_2TiO_4 both in vacuo and in nitrogen, whilst the second phase approximates to BT_3 in vacuo and BT_4or$_5$ in nitrogen. The 1:1 compound, $BaTiO_3$ is not found in either of the specimens, but this could be formed in such small amounts that it cannot be detected using the probe, therefore its apparent abscence cannot be used as indicative of its non-occurrence in the reaction products. None of the techniques used for studying the titania-system have either supported or disproved the theory that $BaTiO_3$ is initially formed and then reacts with titania to form Ba_2TiO_4, so that the compound formation in the titania system is uncertain.

The situation in the silica system is very clear, as B_3S and B_2S are formed during the decomposition and the product sequence is $BaCO_3/B_3S/B_2S/SiO_2$. Unfortunately, the product sequence in the germania system is in some doubt, as BG was only found in an isolated grain, so that BG can occur anywhere in the sequence $BaCO_3/B_2G/BG_4/GeO_2$. Quantitative results could not be obtained for the stannic oxide system as the reaction product band was very porous, and isolated from both the barium carbonate pellet and the tin oxide.

The barium carbonate-zirconia system is somewhat puzzling, as the composition of the sole product phase is very close to Ba_2ZrO_4, but the x-ray analysis of both 1:1 and 2:1 mole mixtures of barium carbonate: zirconia indicated the formation of $BaZrO_3$ as the sole product phase. However, $B_{1.9}Z$ ($BG_{4.2}$ and $BT_{4.5}$) may be formed by solid solution of one of the reactants with a product, thus:

$$BT + T \longrightarrow BT_{4.5}$$

$$B + BZ \longrightarrow B_{1.9}Z.$$

Further work is required for complete clarification of compound formation in the zirconia system.

FIGURE 15a: Electron microprobe photograph of $BaCO_3$ pellet and TiO_2 (in vacuo)
Magnification x 1,225

FIGURE 15b: Electron microprobe photograph of $BaCO_3$ pellet and TiO_2 (in nitrogen)
Magnification x 1,225

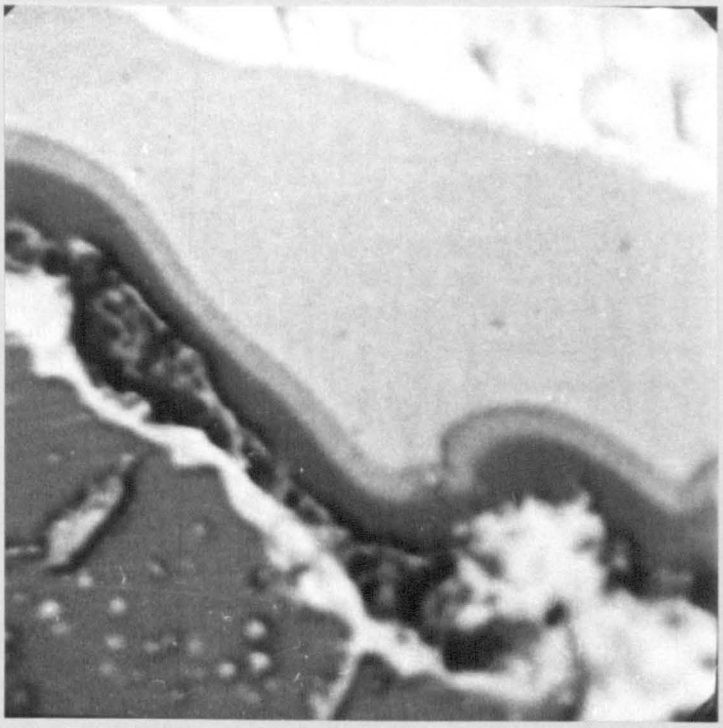
TiO_2
$BT_{3.2}$
$B_{1.8}T$
$BaCO_3$

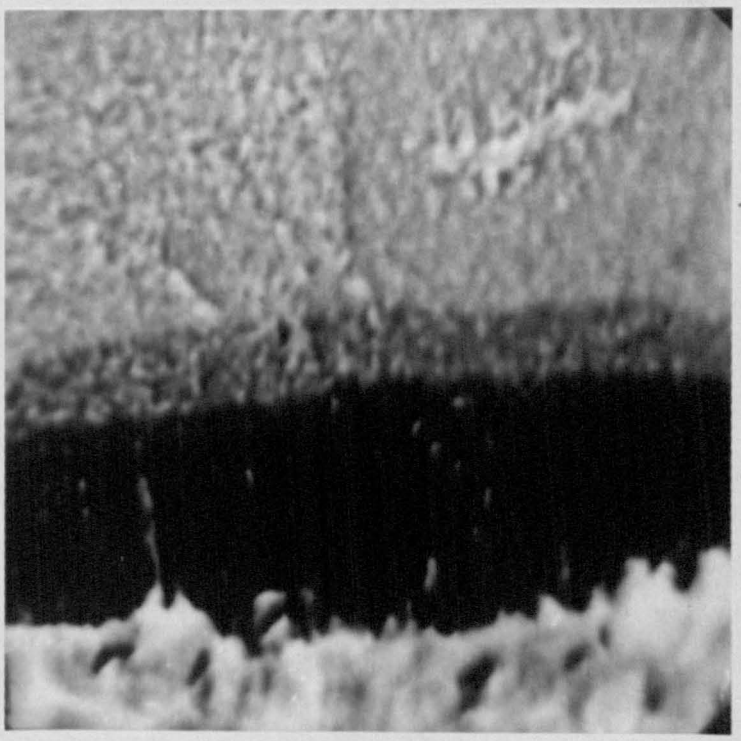
TiO_2
$BT_{4.5}$
B_2T

FIGURE 16a: Electron microprobe photograph of $BaCO_3$ pellet and SiO_2
Magnification x 700

FIGURE 16b: Electron microprobe photograph of $BaCO_3$ pellet and ZrO_2
Magnification x 470

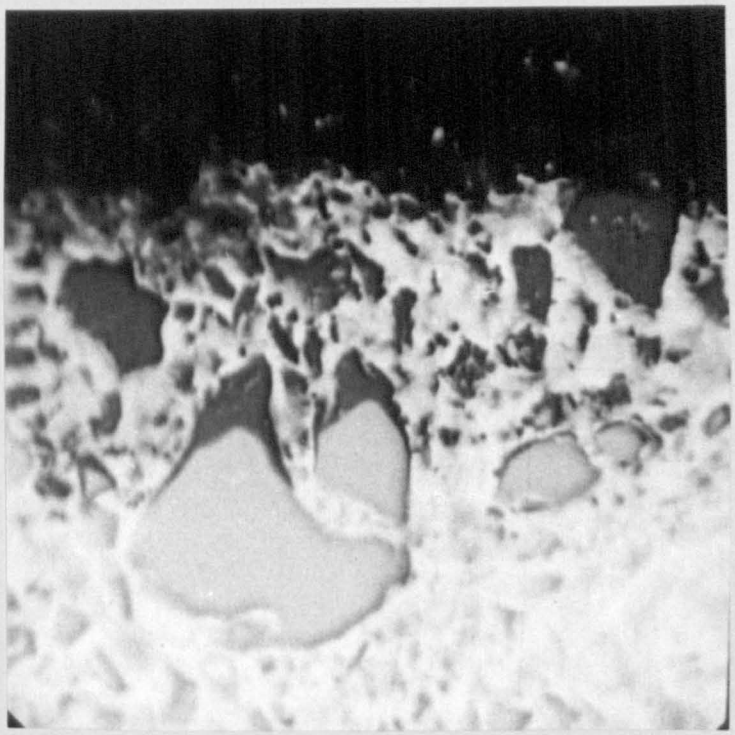
B_3S
B_2S
SiO_2

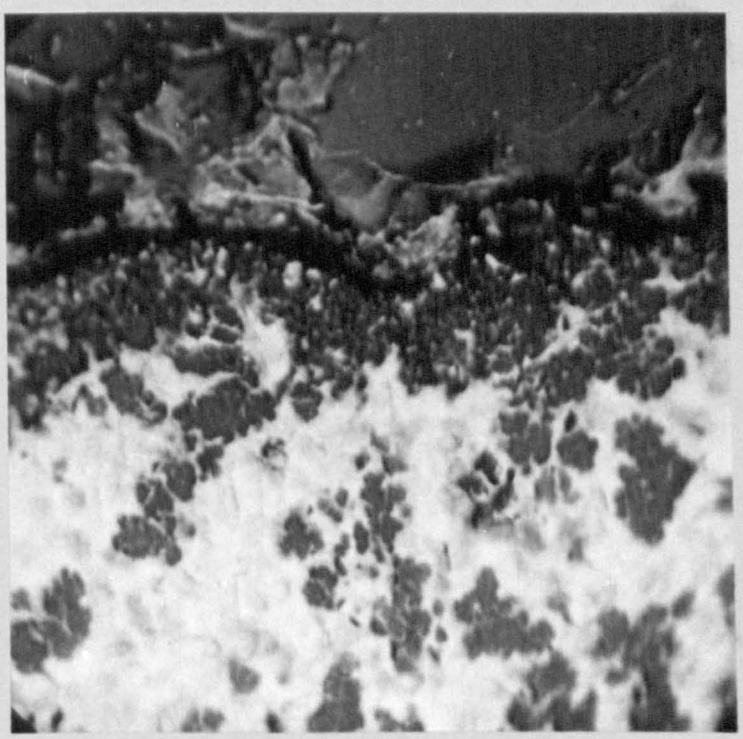
$BaCO_3$
$B_{1.9}Z$
ZrO_2

TABLE 12: Phase Compositions in $BaCO_3$:MO_2 Systems.

Sample	Weight-fraction		Mol-fraction		Phase
$BaCO_3$ + TiO_2, 800°C	B	T	B	T	
Phase 1	0.781	0.228	0.641	0.359	$B_{1.8}T$
Phase 2	0.347	0.582	0.237	0.763	$BT_{3.2}$
$BaCO_3$ + TiO_2, 1000°C					
Phase 1	0.797	0.210	0.664	0.336	$B_{2.0}T$
Phase 2	0.276	0.648	0.181	0.819	$BT_{4.5}$
$BaCO_3$ + GeO_2, 1000°C	B	G	B	G	
Phase 1	0.742	0.284	0.641	0.359	$B_{1.8}G$
Phase 2	0.596	0.449	0.476	0.524	$BG_{1.1}$
Phase 3	0.269	0.774	0.192	0.808	$BG_{4.2}$
$BaCO_3$ + SiO_2, 1000°C	B	S	B	S	
Phase 1	0.861	0.114	0.748	0.252	$B_{3.0}S$
Phase 2	0.823	0.165	0.661	0.339	$B_{2.0}S$
$BaCO_3$ + ZrO_2, 1000°C	B	Z	B	Z	
Phase 1	0.704	0.297	0.655	0.345	$B_{1.9}Z$

Stoichiometric compositions are:

B_2T B = 0.793, T = 0.207

B_2G B = 0.746, G = 0.254

B_2S B = 0.836, S = 0.164

B_2S B = 0.884, S = 0.116

B_2Z B = 0.713, Z = 0.287

CHAPTER 8

The Decomposition Kinetics of Barium Carbonate in Nitrogen

During the decomposition of barium carbonate in air at 1000°C, a liquid phase is formed, and it has been suggested that this effect is due to a eutectic in the $BaO-(BaCO_3)-CO_2$ system. Platinum crucibles are severely attacked by this liquid formation, and alumina and magnesia crucibles are stained brown. This colouration gradually disappears on standing in air over a period of weeks, and barium carbonate is reformed in the crucibles. However, when barium carbonate is decomposed in vacuum, the decomposition temperature is lowered, as predicted by thermodynamics, so that isothermal studies can be undertaken in the temperature range 700° to 800°C, without the formation of a liquid phase. Similarly, when a flowing nitrogen atmosphere is used, isothermal studies can be made up to a maximum temperature of about 1040°C without liquid formation.

Four samples of barium carbonate were characterised by SEM and the results are shown in Table 13. The spec. pure material is obviously unsuitable for use in isothermal studies of reaction mechanisms due to the wide range of particle shapes and sizes (Figure 19a).

TABLE 13: Morphology and Purity of Barium Carbonate Samples

Nomenclature	Purity	Particle Size and Shape	Figure
$BaCO_3$ (ℓ)	Analar	laths 10μ x 1μ x 1μ	17(a)+b
$BaCO_3$ (s)	Analar	spherical 0.5μ diam.	18(a)
$BaCO_3$ (s.p.)	Spec. Pure	spheres, laths and plates	19(a)

8.1. Experimental Technique

The decomposition of barium carbonate in a nitrogen atmosphere was investigated, using a Stanton thermobalance HT-SF with a 20mg. full scale deflection. All the samples were placed in the furnace at temperature in a mixed nitrogen-carbon dioxide atmosphere, which was maintained for twenty minutes to allow the samples to attain temperature. The atmosphere was then changed to pure dry nitrogen, at a flow rate of 300 ml. per min. The pre-heating in carbon dioxide caused sintering of the barium carbonate samples so that higher temperatures were required for decomposition in nitrogen than in vacuo, where extensive sintering does not occur.

8.2. Barium Carbonate Lath System ($BaCO_3$ℓ)

Sample weights of 50, 100 and 200 mg. were dispersed in acetone in cylindrical alumina crucibles and allowed to

dry slowly. The combination of the damping procedure, and the crucible geometry, resulted in the formation of cylindrical powder compacts with constant diameter and heights in the ratio 1:2:4. The preliminary heating in the nitrogen-carbon dioxide atmosphere causes shrinkage of the compacts to about 0.7 of their original volume. Quite often the reaction rates were so slow ($t_{0.50}$ > 720 min.) that it was impractical to wait for complete decomposition, and sometimes even for 50% reaction. For this reason, a LnLn analysis technique was used in interpreting the experimental results, but some data on $t/t_{0.5}$ values was obtained (Table 14).

The reaction rates for the 50 mg. samples were of the same order as the decomposition studies in vacuum (160 mins. to $\alpha = 0.50$ at 990°C), but an accurate study of this system was impossible due to the limited sensitivity of the Stanton thermobalance. However, m values of 1.18 (Figure 21a) were obtained, indicating that these data approximated to a zero order model (Figure 20a), but deviation from this model occurred at lower values of α than the results for the 100 and 200 mg. samples with zero order characteristics. At a temperature of 993°C and also when melting occurred, the zero order model was obeyed to higher values of α than at other temperatures (up to $\alpha = 0.80$ cf. $\alpha = 0.60$).

The LnLn analysis and $R_2\alpha$ data for 100 mg samples are shown in Figures 21b and 20b; the constant m value

of 1.08 indicating that the data would be best represented by an $R_2\alpha$ or $R_3\alpha$ model. An $R_2\alpha$ plot showed the highest degree of linearity (up to $\alpha = 0.60$) before deviation occurred, and some $t/t_{0.5}$ data are collected in Table 15. Two anomolous m values of 1.15 were obtained for this system at 981°C, and when melting occurred, and these results fitted a zero order model up to $\alpha = 0.80$.

Values of $m = 1.03$ for the range $\alpha = 0.00$ to 0.36 and $m \sim 0.56$ at higher values of α were obtained for the 200 mg. samples, and the results are shown in Figure 21a and Table 14. At a temperature of 981°C, and when melting occurred, this system had the same m value as that of the 100mg. system at the same temperatures.

TABLE:15: m Values Obtained From a LnLn Analysis of 200 mg. Data

Temperature°C	Initial m	Temperature°C	Initial m
1048	~1.15	991	1.03
1020	1.02	981	~1.15
1000	1.04	970	1.02

The change in m value from 1.03 to 0.56 suggests that a diffusion step becomes rate controlling at high values of α, but the reaction rates of this system were always too slow ($t_{0.50}$ = 780 mins.) for the effect to be studied in detail before melting commenced at ~1040°C.

Activation energies were calculated for the three systems, using rates detained from phase boundary and zero order models, and the results are shown in Table 16 and Figures 22(a) and (b). The Arrhenius plot for 50mg samples was not linear, and the activation energy was determined for the low temperature results. These results suggest an activation energy of about 60 kcal/mole for the decomposition of $BaCO_3(\ell)$ in nitrogen.

TABLE 16: Activation Energies of powder samples of lath barium carbonate

Sample Weight mg	Model Used	Temperature Range °C	kcal/mole Activation Energy
50	zero order ($t_{0.5}$)	950-1000	60 ± 8
100	$R_2\alpha$	923-1019	59 ± 4
200	$R_2\alpha$	970-1020	61 ± 3
200	$R_3\alpha$	970-1020	61 ± 5

8.3. Barium Carbonate Spherical System ($BaCO_3$ s)

An acetone damping technique was again used to prepare 100mg powder samples, and the preliminary heating in a carbon dioxide-nitrogen atmosphere did not cause any apparent shrinkage. The bulk density of these samples was higher than those similarly prepared from the lath barium carbonate and of the same order as the pressed pellets of the lath carbonate (see section 8.4).

The results are shown in Figures 23(a) and (b) and the LnLn analysis confirms that the system is not isokinetic. Zero order behaviour is observed when melting occurs during the decomposition, but the interpretation of the remaining data is not clear. The low temperature studies show an initial rapid loss, followed by a much slower decomposition rate, and partially reacted samples have a glassy surface character.

Pellets of the spherical carbonate were prepared for decomposition using the method outlined in section 8.4. The α v time and LnLn analysis are shown in Figures 23(a) and (b) and a $D_2\alpha$ model plot is shown in Figure 24(b). The results follow the $D_2\alpha$ model up to at least 40% reaction without deviation, suggesting that the reaction mechanism for cylindrical pellets of spherical barium carbonate is a two-dimensional diffusion controlled process.

8.4. Sintered Pellets of $BaCO_3$

100 mg pellets of barium carbonate were prepared in a 7mm. diameter die, at a pressure of $\sim$ 30,000 psi. The preliminary heating scheme was the same as that used for the powder samples, and shrinkage was not observed.

The decomposition was not isokinetic throughout the temperature range studied, as indicated by the isothermal data shown in Figure 25(a); a drastic change in the value of m is observed in the LnLn analysis for runs below 1016°C (Figure 25 b). Local melting within

the sample was observed at a minimum temperature of 1035°C, and this data followed a zero order mechanism up to at least $\alpha = 0.60$. At 1022°C and 1016°C, the m values are in the range 1.07 to 1.03, suggesting a phase boundary controlled mechanism, and initial m values of $\sim$0.55 in the range $\alpha = 0.00$ to 0.25, are observed for lower temperature runs, possibly indicating a diffusion controlled mechanism.

8.5. Discussion

The balance between maximising particle-particle contacts and minimising bed pressures is a common problem in reaction kinetic studies of two phase systems involving the evolution of a gaseous product. When single phase reactions are studied, the bulk density of the sample is important, as it effects the partial pressure of gaseous products held within the sample during the decomposition. The rate controlling step in a reaction involving the production of a gaseous phase, can be the gross diffusion of the evolved gas through the sample bed, and two factors need to be considered; for loose powder samples, it becomes more difficult for the evolved gas to escape as the sample weight is increased due to the increase in bed depth, and similarly the partial pressure of gas generated within a compacted bed during decomposition increases as the degree of compaction of the sample increases, with the related increase in bulk density. In the lath carbonate systems, the pelletized

samples (high bulk density) have lower reactivites than the loose powder samples (low bulk density). However, the reverse applies in the spherical carbonate systems, where the pelletized sample is more reactive than the powder sample at a temperature of 1020°C (Figure 23 a). This phenomenon may be related to the different reaction mechanisms; the pelletized sample follows a $D_2\alpha$ model up to 40% reaction, whereas the powder sample data deviates from this model in the range $\alpha = 0.00$ to 0.17. Further investigations of the spherical carbonate systems are required before a complete explanation of the phenomena can be made.

The powder samples of the lath barium carbonate had the lowest bulk densities of the carbonate samples investigated, and were also the easiest for determining the reaction mechanism. In each of the three systems, 50, 100 and 200 mg, anomalous m values were obtained when melting occurred during the decomposition, and at one other temperature. This other temperature can be interpreted as due to the phase change of barium carbonate: $\beta\ BaCO_3 \xrightarrow{968°C} \alpha\ BaCO_3$. The results of the DTA investigation of barium carbonate in the preliminary experiments are shown in Table 17, together with some standard values. The experimental value of 990°C obtained for the phase transition is higher than the true temperature due to the dynamic nature of the DTA technique, and consequently the phase transformation temperature recorded on

the thermobalance should be found to occur somewhere between the two values of 968° and 990°C.

TABLE 17: A Comparison of the Experimental and Literature Values[26] of the Phase Transition Temperatures of Barium Carbonate.

Experimental	Literature
820°C	806°C
990°C	968°C

Such an explanation is satisfactory for the 100 and 200mg samples, where this anomalous m value occurs at 981°C, but not for the 50mg system with a temperature of 993°C. The work of Hills[11] on the decomposition of calcium carbonate has shown that the sample temperature may fall during an isothermal decomposition when the rate of reaction is fast. In his system, samples of more than 1g. of $CaCO_3$ were totally decomposed in less than 100 minutes, and the sample temperature fell below its surroundings at the start of the decomposition, and gradually increased as the decomposition continued. This 'cooling effect' will occur in all endothermic reactions, but frequently can be avoided by controlling the conditions so that the rate of decomposition is very slow. Hence the 993°C anomaly for 50mg samples is probably due to the self-cooling effect becoming important at these

relatively fast reaction rates (160mins. to $\alpha = 0.50$) and the sample temperature falling below 993°C.

A further effect of this self-cooling would be expected in the Arrhenius plot of the 50mg. sample data as the faster the reaction rate the more the self-cooling effect will lower the sample temperature, and a linear Arrhenius plot should tend to negative curvature at fast rates of decomposition. This phenomenon can be observed in Figure 22 (b), but does not occur for the 100 and 200 mg samples where the reaction rate is much slower, and melting occurs before comparative rates can be obtained. However, the self-cooling effects should only be comparable when the reaction rates expressed as mg of CO_2/min. are similar and, since self-cooling effects are not apparent in the data for 100 and 200 mg samples when the rate in mg. of CO_2/min. is comparable with that of the 50mg. sample, one must conclude that the relative sample weights are also important; when the absolute rates of reaction (mg. CO_2/min) are comparable between two different sample weights, the self-cooling effect will be smaller in the larger sample due to its larger thermal mass.

The reaction mechanism of the 100mg compacted lath carbonate samples is isokinetic, except at the barium carbonate phase transition, and when melting occurs during the decomposition. Increased reactivity

at a phase change is predicted by the Hedvall[27] effect, and the change in reaction mechanism from phase boundary controlled to zero order results in an increased reaction rate at the temperature. The same effect is found for the 200 and 50mg systems but the reaction mechanisms at other temperatures are not perfectly clear. Considering the geometry of the 200mg powder samples, height almost equal to diameter, one might expect that neither an $R_2\alpha$ nor an $R_3\alpha$ model would completely fit the data, but the reaction mechanism for this system does appear to be phase boundary controlled up to $\alpha = 0.36$, and probably diffusion controlled at higher α values. Since the Stanton thermobalance is not suitable for an accurate study of the decomposition of 50mg samples of barium carbonate, a reaction model analysis of this system is of questionable signficance. However, the effective geometry of 50mg powder samples is equivalent to that of the 100mg powder samples, and when a phase boundary model is applicable to the latter it should also apply to the former of the rate controlling step remains constant. However, the 50mg samples do not follow a phase boundary controlled model but approximate to a zero order model up to $\alpha = 0.55$.

These results are similar to those obtained for the decomposition of calcium carbonate[28] where small samples follow a zero order model, larger samples follow

an $R_2(\alpha)$ model and even larger samples (300mg) tend to follow an $R_3(\alpha)$ model. This similarity in reaction mechanisms suggests that gross diffusion and CO_2 back pressure effects are not important in determining the reaction mechanism in powder samples of less than 200 mg.

Similarly the behaviour of powder samples and pressed pellets of the spherical barium carbonate might be expected to be comparable with the behaviour of pressed pellets of the lath carbonate, since the bulk densities of all these samples are of the same order. For these systems, it is not unlikely that the diffusion of carbon dioxide out of the sample may become an important factor in determining the slowest step of the reaction, and the results for the pressed pellets of the lath barium carbonate are worth considering in this context. This system shows an apparent phase boundary controlled mechanism at 1022° and 1016°C, and changes at lower temperatures to a mechanism that approximates to a two-dimensional diffusion controlled model, $D_2\alpha$, in the early stages of decomposition Figure 25 (b). It is unfortunate that the reaction rates are so slow in this system that a detailed mechanistic study is not feasible using a Stanton thermo-balance and again, unfortunately, the same applies to the spherical barium carbonate systems. However, the pelletised spherical barium carbonate at 1020°C does show good agreement with a $D_2\alpha$ model, and likewise the powder sample at the same temperature follows a $D_2\alpha$ model

but shows a 'false zero' i.e. the model plot does not pass through the origin Figure 24(b). At 1000°C, the powder spherical carbonate sample shows a rapid initial loss of carbon dioxide, followed by a much slower decomposition rate similar to the protective film effect recorded for the oxidation of certain metals (Cu and Al), and it appears that 'surface effects' may become important in the spherical carbonate system at low temperatures.

The activation energies of the powder samples of the lath barium carbonate are shown in Table 16, and the activation energy of about 60kcal/mole for a phase boundary controlled mechanism is comparable with the heat of formation of barium carbonate at similar temperatures ($\Delta H_{1100} \sim 55$ kcal/mole). Activation energies could not be calculated for the other samples of barium carbonate because of the complex changes in reaction mechanism and the limited data.

8.6. Summary

The investigation of the decomposition of barium carbonate in nitrogen has established the dependence of both the rate of reaction and the mechanism of decomposition on the morphology, compaction and depth (i.e. weight) of the sample. This complex kinetic behaviour is further complicated by a change in mechanism associated with the structural transformation in barium carbonate at 981°C (an example of the Hedvall effect). It has also been established that it is impossible to obtain meaningful

kinetic data when the rate of reaction is fast, because the endothermic effect within the sample leads to departures from isothermal conditions. Hills' has shown that heat-mass transfer models can be used for the decomposition of calcium carbonate when self-cooling effects are important, but similar models cannot be derived for the decomposition of barium carbonate in the particular experimental conditions used in this investigation. The temperature dependence of the reaction indicates an activation energy of about 60 kcal/mole, which is slightly greater than the heat of dissociation. The kinetics of the decomposition of barium carbonate in vacuo are reported in the next chapter.

TABLE 14: A Comparison of $t/t_{0.5}$ values for 100 mg. Samples of $BaCO_3(\ell)$ with Theoretical Data

α	$R_2\alpha$	970°C	981°C	1019°C	Zero Order
0.1	0.174	0.177	0.189	0.170	0.200
0.2	0.362	0.355	0.394	0.350	0.400
0.3	0.556	0.550	0.597	0.542	0.600
0.4	0.768	0.760	0.797	0.760	0.800
0.5	1.000	1.000	1.000	1.000	1.000
0.6	1.253	-	1.223	1.290	1.200
0.7	1.543	-	1.446	1.606	1.400
0.8	1.887	-	-	2.003	1.600
0.9	2.334	-	-	-	1.800

FIGURE 17a: Scanning electron micrograph of barium carbonate ($BaCO_3$ (ℓ))
Magnification x 5,500

FIGURE 17b: Scanning electron micrograph
Magnification x 15,500

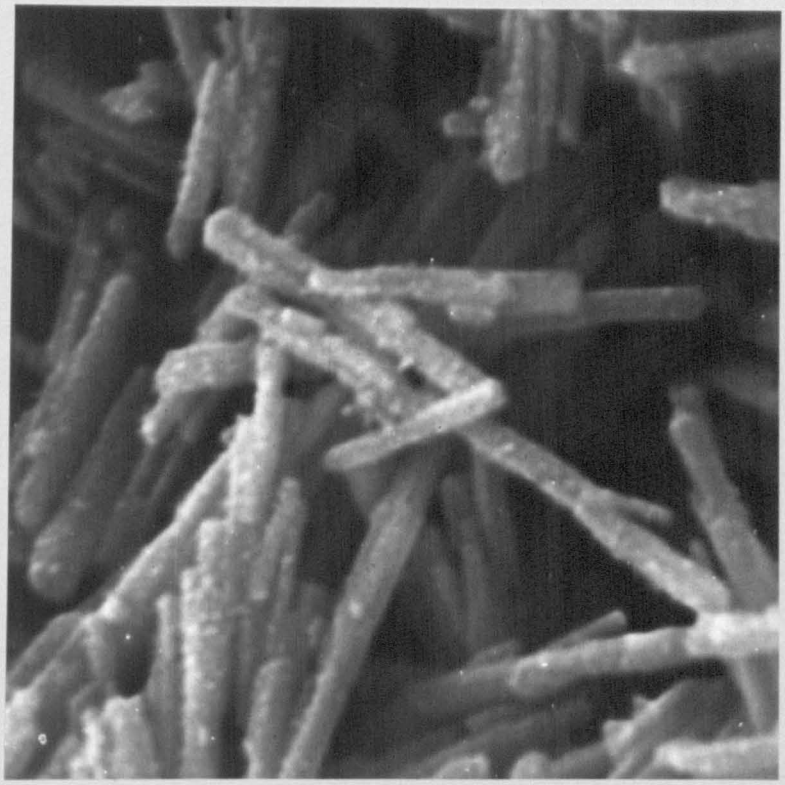

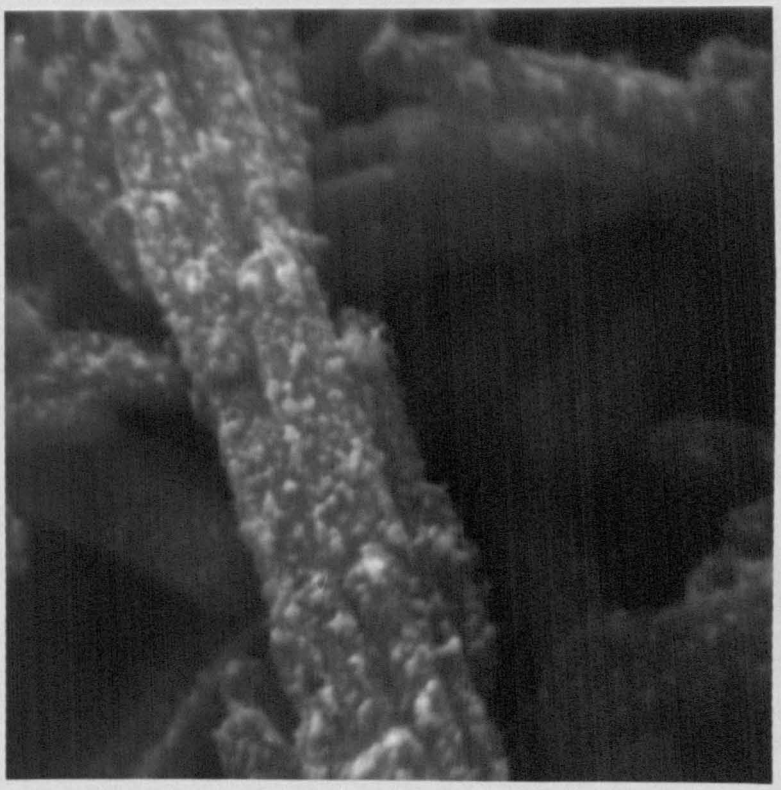

FIGURE 18a: Scanning electron micrograph of barium carbonate ($BaCO_3(s)$)
Magnification x 2,400

FIGURE 18b: Scanning electron micrograph of barium carbonate (mixed in water).
Magnification x 7,000

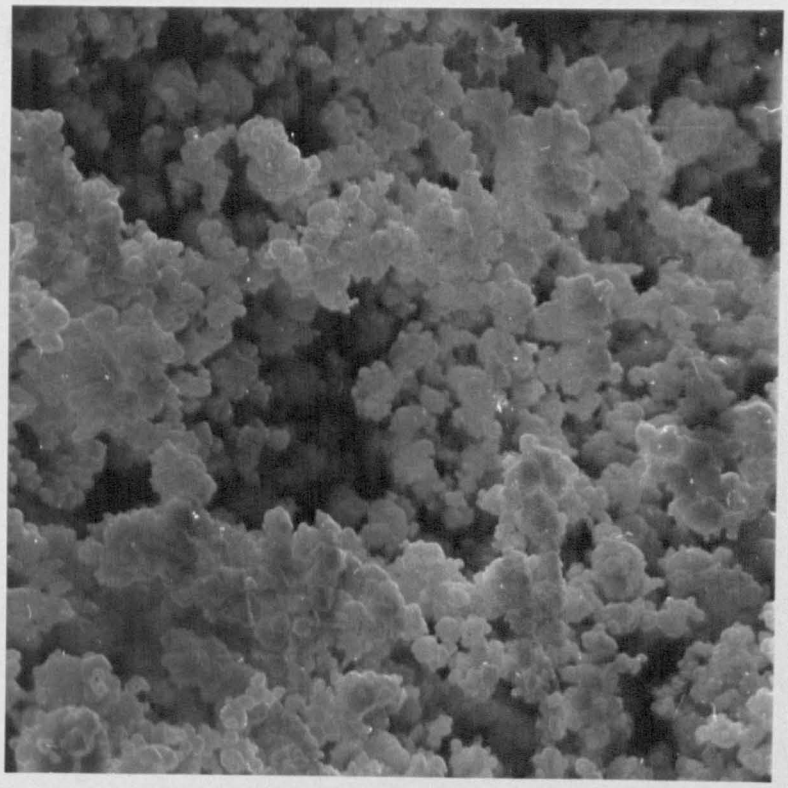

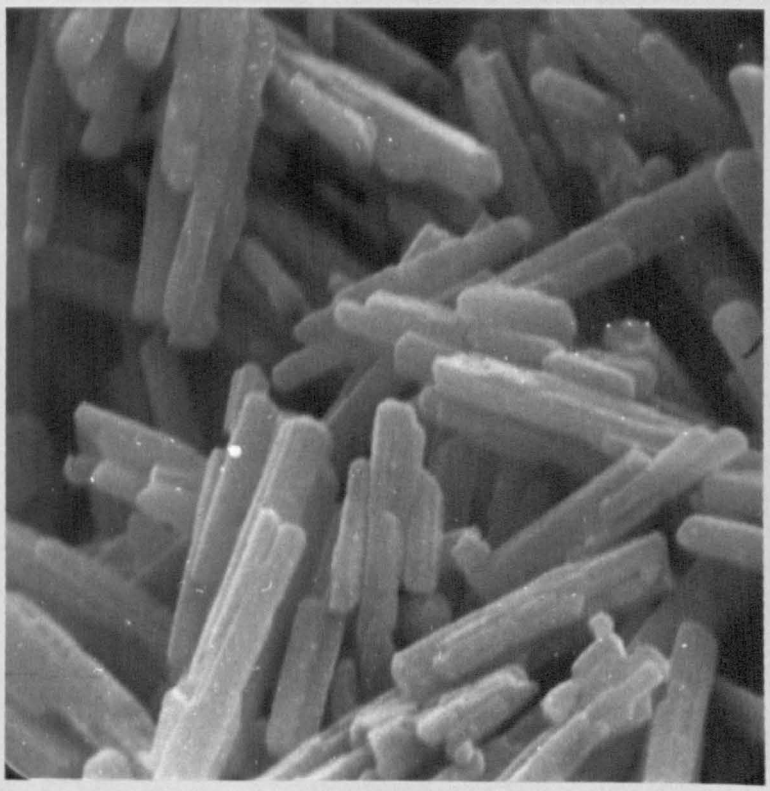

FIGURE 19a: Scanning electron micrograph of spec. pure barium carbonate Magnification x 3,000

FIGURE 19b: Scanning electron micrograph of carbonated strontium carbonate Magnification x 2,200

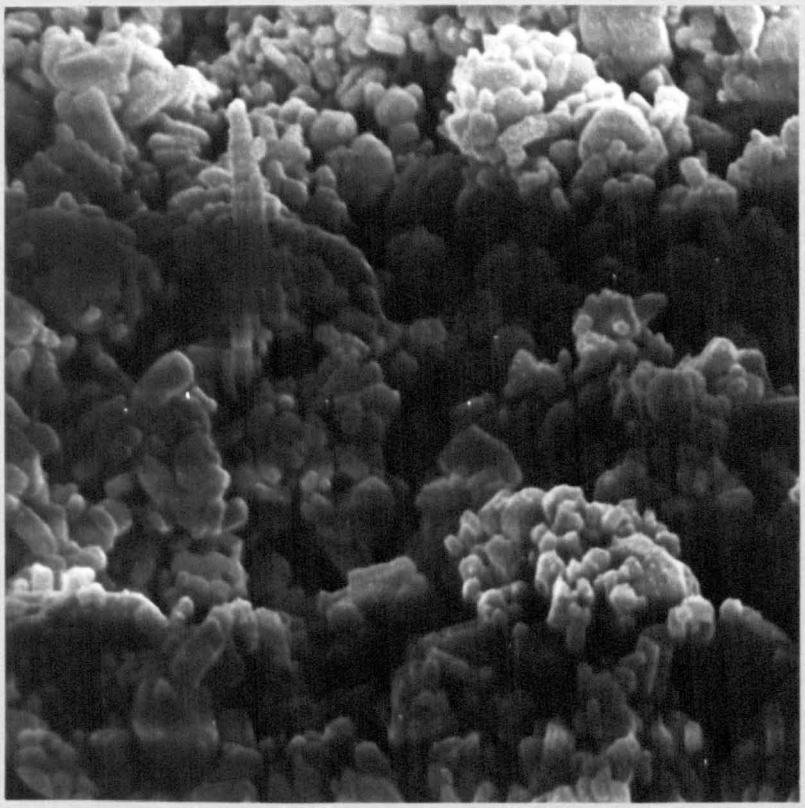

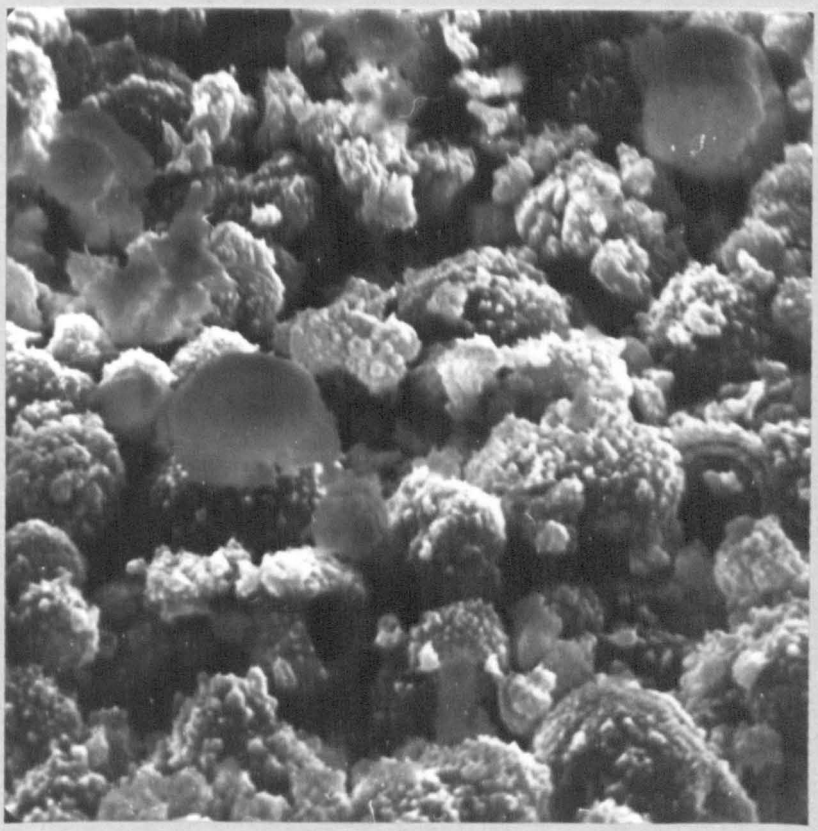

FIGURE 20a: Stanton thermobalance curves of 50mg samples of $BaCO_3(\ell)$

FIGURE 20b: $R_2\alpha$ model curves of 100mg $BaCO_3(\ell)$ Stanton thermobalance data.

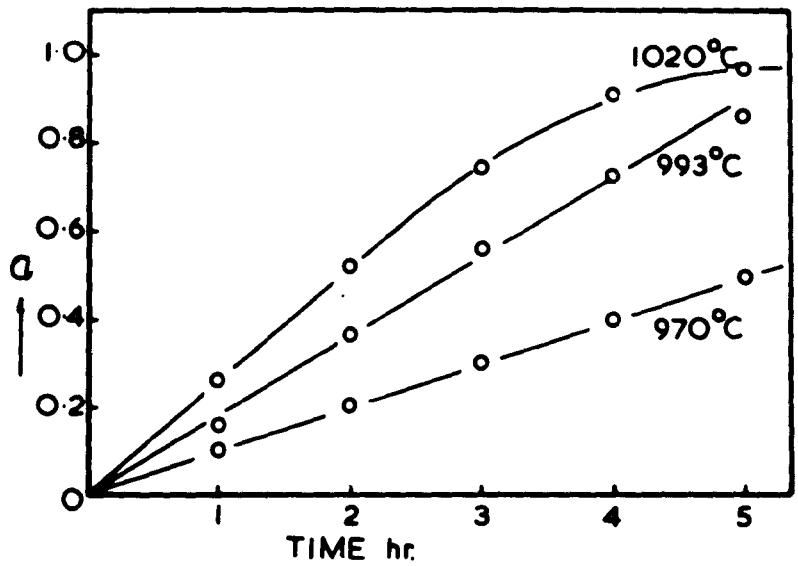
1·0
0·8
0·6
0·4
0·2
0
a
1020°C
993°C
970°C
1
2
3
4
5
TIME hr.

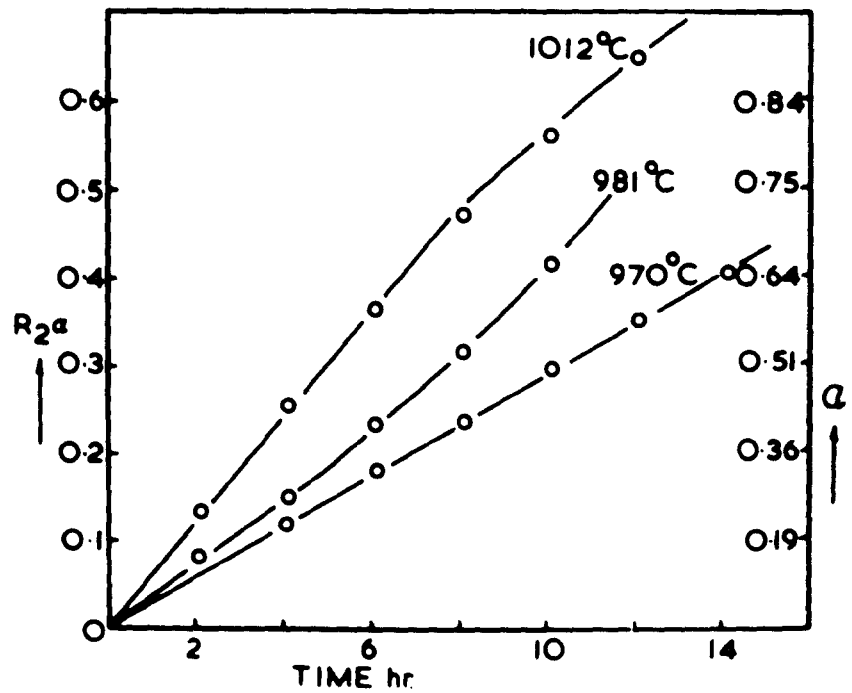
0·6
0·5
0·4
0·3
0·2
0·1
0
R2a
1012°C
981°C
970°C
0·84
0·75
0·64
0·51
0·36
0·19
a
2
6
10
14
TIME hr.

FIGURE 21a: LnLn analysis curves of Stanton thermobalance data for 200 and 50mg samples of $BaCO_3(\ell)$.

FIGURE 21b: LnLn analysis curves of Stanton thermobalance data for 100mg samples of $BaCO_3(\ell)$.

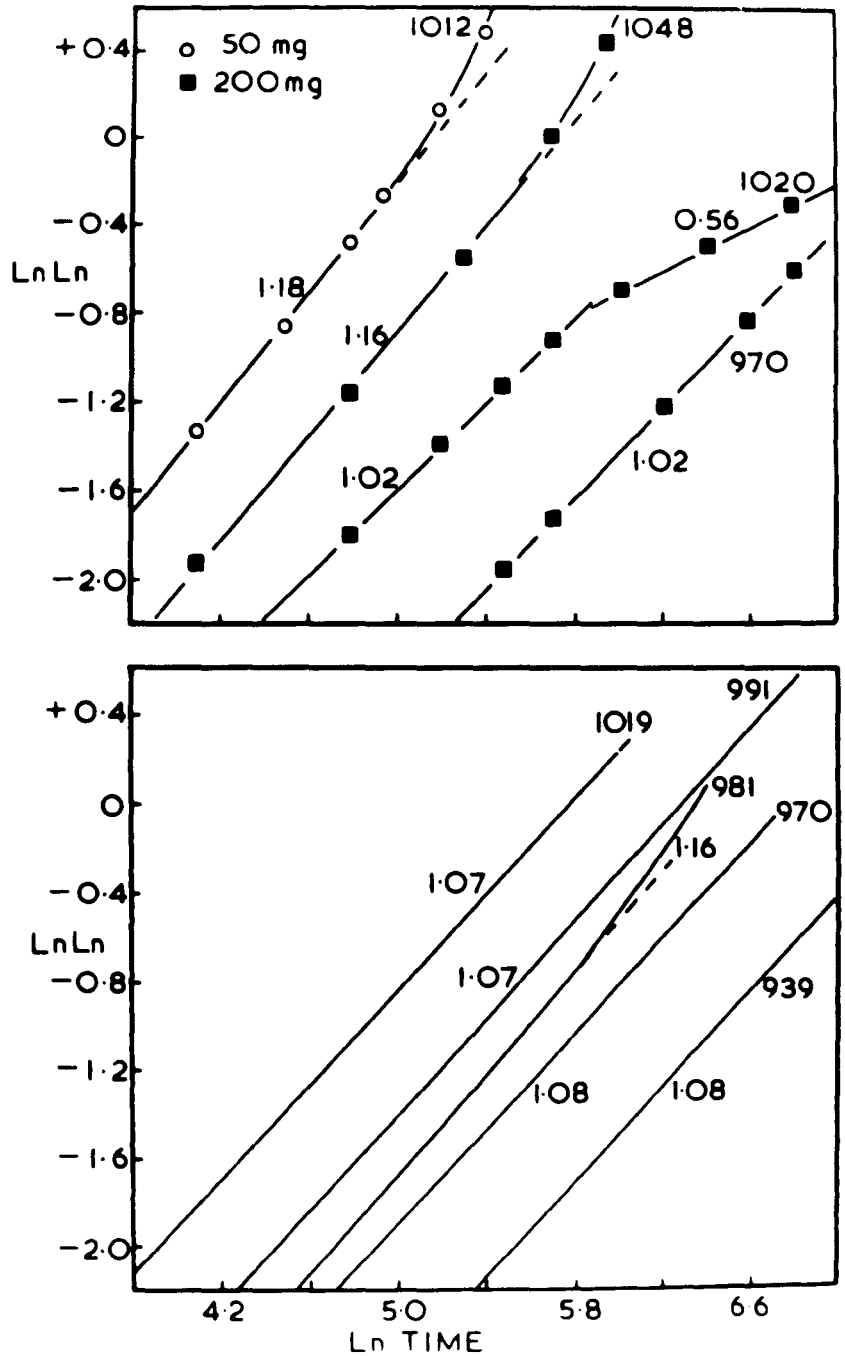
o 50 mg
■ 200mg
+0·4
0
−0·4
−0·8
−1·2
−1·6
−2·0
LnLn
1012
1048
1020
0·56
1·18
1·16
1·02
970
1·02
991
1019
981
970
1·16
1·07
1·07
939
1·08
1·08
4·2
5·0
5·8
6·6
Ln TIME

FIGURE 22a: Arrhenius plots for 200, 100 and 50mg samples of $BaCO_3(\ell)$.

FIGURE 22b: Arrhenius plot for 50mg samples of $BaCO_3(\ell)$.

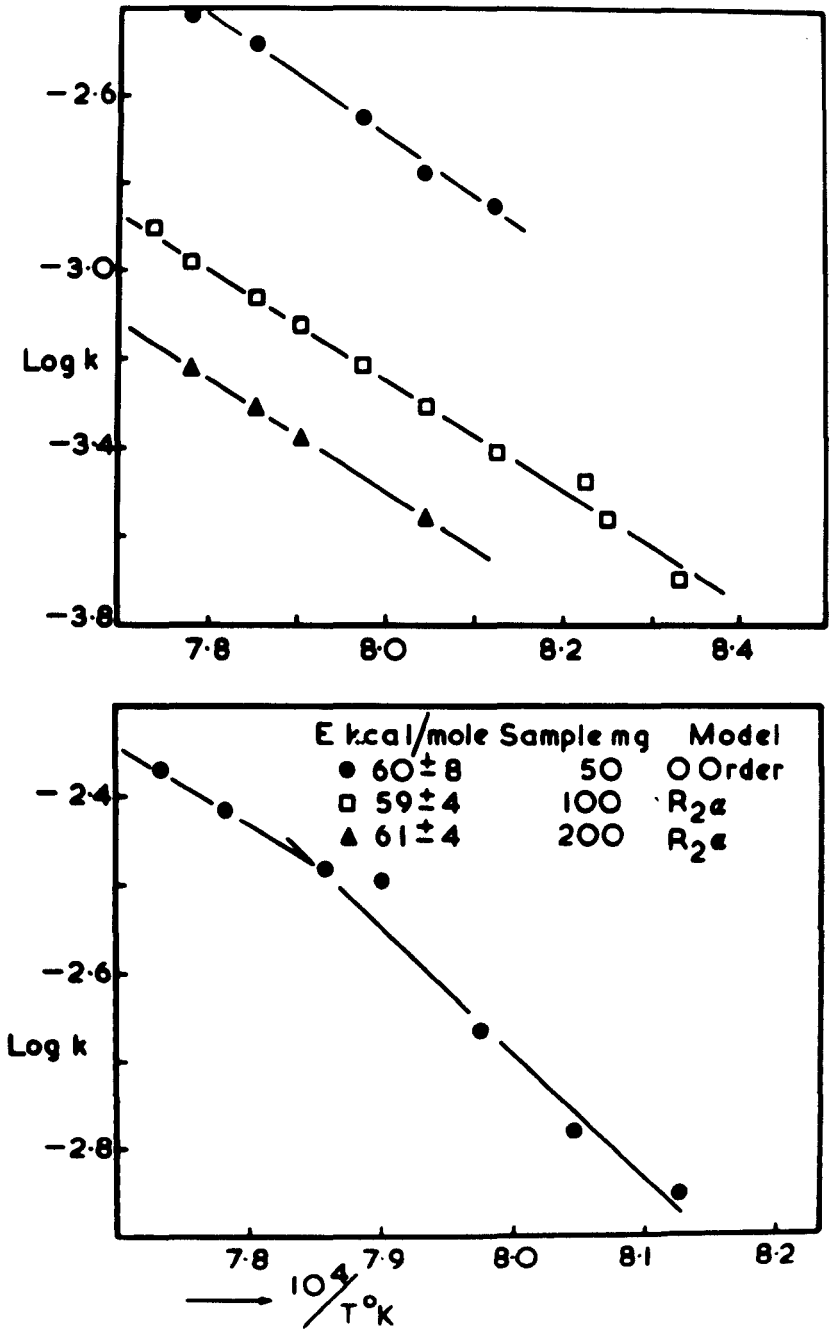
−2·6
−3·0
Log k
−3·4
−3·8
7·8
8·0
8·2
8·4
E k.cal/mole Sample mg Model
● 60±8 50 O Order
□ 59±4 100 $R_2\alpha$
▲ 61±4 200 $R_2\alpha$
−2·4
−2·6
Log k
−2·8
7·8
7·9
8·0
8·1
8·2
$10^4/T°K$

FIGURE 23a: Stanton thermobalance curves of 100mg samples of $BaCO_3(s)$

FIGURE 23b: LnLn analysis curves of 100mg $BaCO_3(s)$ Stanton thermobalance data.

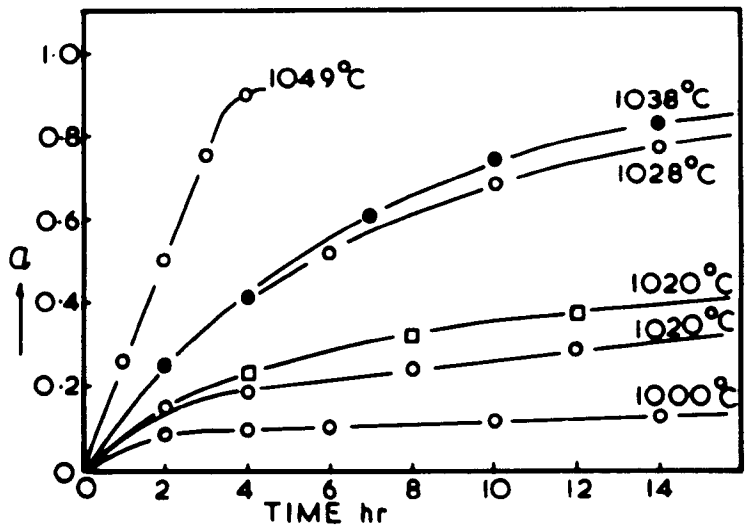
1·0
0·8
0·6
α
0·4
0·2
0
0
2
4
6
8
10
12
14
TIME hr
1049°C
1038°C
1028°C
1020°C
1020°C
1000°C

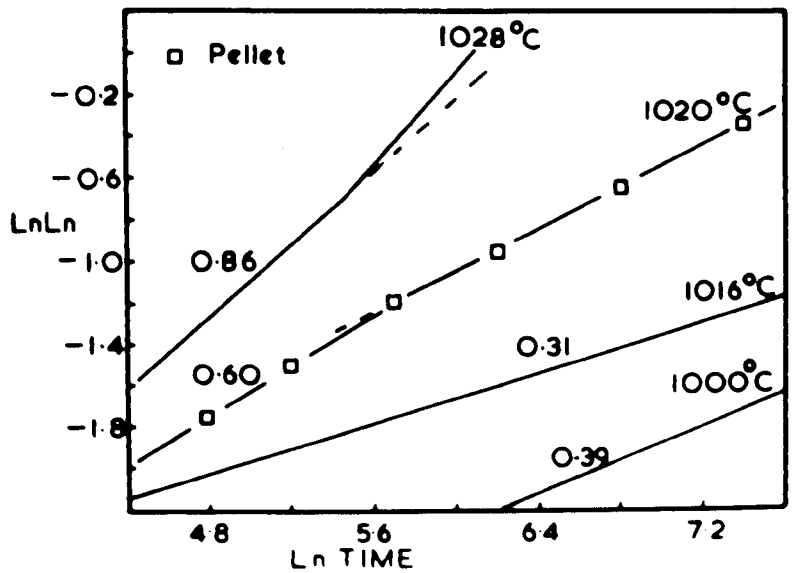
Pellet
1028°C
1020°C
1016°C
1000°C
−0·2
−0·6
LnLn
−1·0
−1·4
−1·8
0·86
0·60
0·31
0·39
4·8
5·6
6·4
7·2
Ln TIME

FIGURE 24a: LnLn analysis curves of sintered barium pellets decomposed in vacuo.

FIGURE 24b: $D_2\alpha$ model curves of 100mg $BaCO_3$ Stanton thermobalance data.

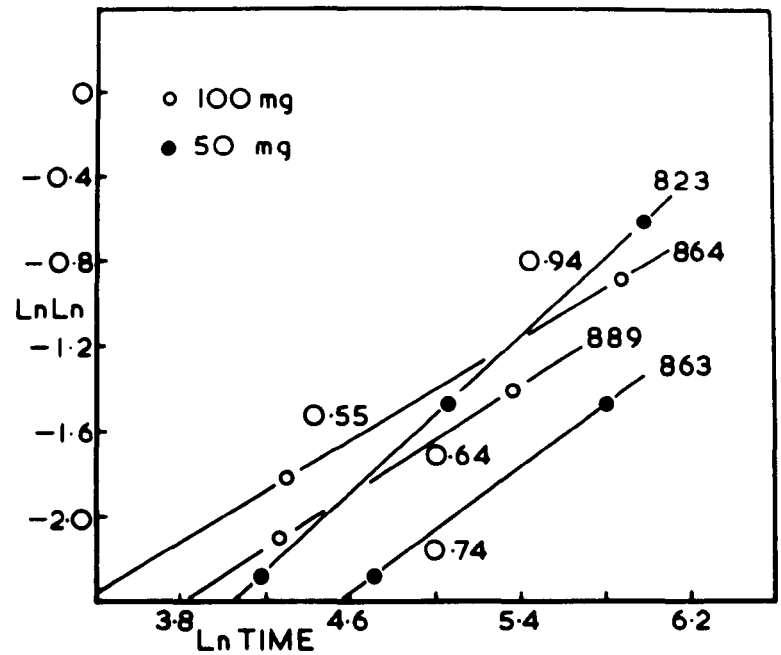
o 100 mg
● 50 mg
0
−0·4
−0·8
−1·2
−1·6
−2·0
LnLn
823
0·94
864
889
863
0·55
0·64
0·74
3·8
4·6
5·4
6·2
Ln TIME

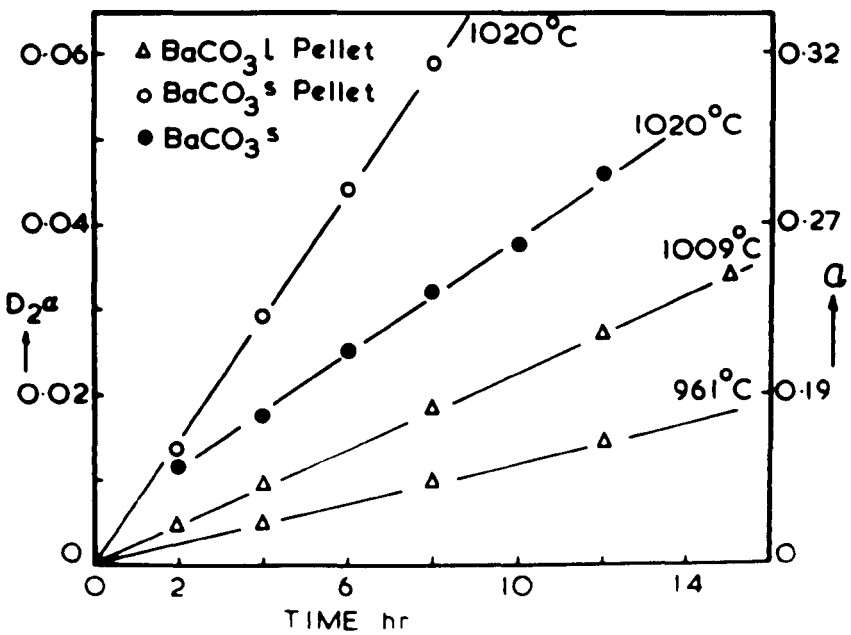
Δ BaCO3 l Pellet
o BaCO3 s Pellet
● BaCO3 s
1020°C
1020°C
1009°C
961°C
0·06
0·04
0·02
0
D2α
0·32
0·27
0·19
α
0
2
6
10
14
TIME hr

FIGURE 25a: Stanton thermobalance curves of 100mg pellets of $BaCO_3(\ell)$.

FIGURE 25b: LnLn analysis curves of Stanton thermobalance data for 100mg pellets of $BaCO_3(\ell)$.

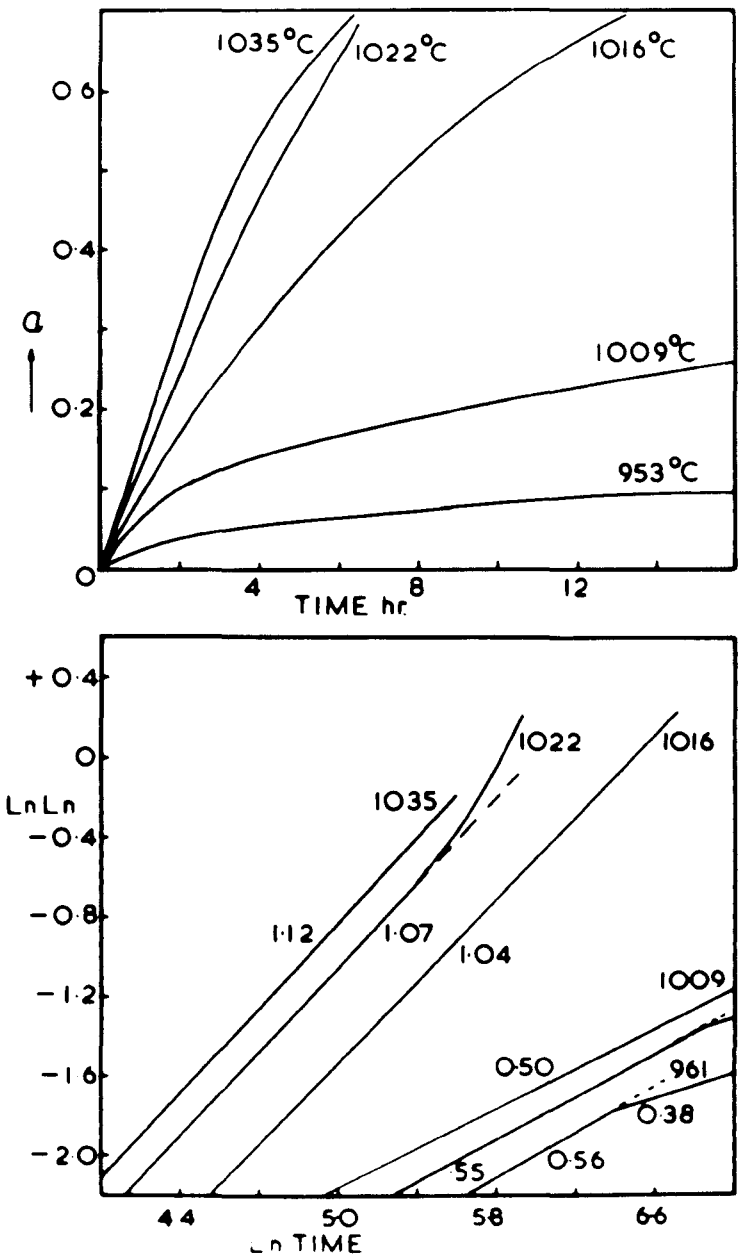
1035°C
1022°C
1016°C
1009°C
953°C
0·6
0·4
0·2
0
α
4
8
12
TIME hr
+0·4
0
−0·4
−0·8
−1·2
−1·6
−2·0
Ln Ln
1035
1022
1016
1·12
1·07
1·04
1009
0·50
961
0·38
0·56
55
44
50
58
66
Ln TIME

CHAPTER 9

The Decomposition Kinetics of $BaCO_3$ in Vacuo

It has often been suggested that the only reasonable way of studying a reaction involving the evolution of a gaseous product is to conduct the experiments in an atmosphere of the same gas. However, the occurrence of eutectics in the $(BaCO_3)$-BaO-CO_2 system prohibits detailed investigations of the solid state reactions even at low carbon dioxide pressures, and the decomposition of barium carbonate can only be studied over a wide temperature range when vacuum conditions are used to prevent liquid formation during the reaction. Whenever liquid formation occurs during the decomposition of barium carbonate in a nitrogen atmosphere, the reaction mechanism is always zero order, hence liquid formation must be avoided for meaningful analysis of the solid state reaction mechanisms. In this investigation the decomposition kinetics of two samples of barium carbonate have been examined over the temperature range from 700° to 800°C in the vacuum thermobalance discussed in Chapter 4.

9.1 Barium Carbonate Lath ($BaCO_3(\ell)$)

The samples for examination were weighed in platinum crucibles and then damped in acetone so that a consistent packing of the lath particles (Figure 17 (a) and (b)) could be obtained. In the preliminary investigations, three platinum crucibles of almost the same dimensions were used, and the LnLn analysis of the data for 100 mg samples

indicated that the initial m value of the analysis at constant temperature was related to the crucible geometry. The Arrhenius plot for these samples was constructed from rates obtained from the function $0.8\sqrt{-\ln(1-\alpha)}$, and the apparent activation energy was found to be related to the initial m value and the crucible geometry (Table 18 and Figure 32(a)).

TABLE 18: The Effect of Crucible Geometry on the Initial m Value and Apparent Activation Energy of 100mg Samples $BaCO_3$ (ℓ)

Crucible	bed depth of sample mm	m values		Activation Energy kcal/mole
		initial	final	
1	3	0.74	1.00	36
2	3-2	0.78	1.00	39
3	2	0.80	1.00	53

The LnLn analysis of the data obtained for crucible 3 is shown in Figure 26(a), and the process is not isokinetic, as the change in slope from 0.80 to 1.00 occurs at lower values of α as the temperature is lowered.

The rate of decomposition increased progressively with decreasing sample weight, but the reaction was only isokinetic in the decomposition of 25mg samples. Since the total weight loss was only 5mg, the thermobalance was

not suitable for accurate kinetic studies of the decomposition of 25mg samples, but the reaction mechanism can be regarded as isokinetic in the temperature range 770° to 731°C, but changes at 719°C and below Figure 27(b). The limited sensitivity of the thermobalance introduces small errors in the value of α calculated for 25mg samples, but the errors involved cannot possibly account for the total induction times recorded for the 696° and 718°C samples, Figure 28(a), and the longer induction period as the temperature is reduced is a genuine effect. A first order model (Figure 28(b)) was used to calculate the reaction rate, and the activation energy was 62 kcal/mole.

The micrographs of the lath barium carbonate, Figures 17(a) and (b) show that the surface of the laths is covered with specks, and this coating can be removed by shaking the carbonate in acetone or water. Since all the oxide-carbonate mixtures investigated in later Chapers were prepared in acetone or water, the decomposition kinetics of a water mixed barium carbonate sample were studied to see if this surface phenomena altered the reaction mechanism. 100mg and 25mg samples were used and the LnLn analysis is shown in Figure 30(b). The surface phenomena has no drastic effect on the reaction mechanism, but the reaction rates for 25mg samples mixed in water are slightly slower than those of the raw carbonate samples, and the inhibition period is smaller (cf. 5 mins. and 25 mins.).

The activation energy was ~68kcal/mole, (Figure 35) and the reaction mechanism was isokinetic over a temperature range in which the raw carbonate samples showed a change in mechanism.

9.2. Barium Carbonate Spherical $BaCO_3(s)$

The electron micrograph of this material is shown in Figure 18(a), and the experimental technique was the same as that used for the lath system. The bed depth of a 100mg sample of the spherical carbonate was at least a factor of $\frac{1}{2}$ that of the lath sample and could not be measured. Three almost identical crucibles were again used, but a bed depth effect was not observed, and the LnLn analysis is shown in Figure 31(a). The negative curvature, shown as a change in m value from 0.84 to 0.66, indicates that the data should be analysed using the Austin-Rickett approach, and this analysis is shown in Figure 32(b). An Arrhenius plot was constructed using the $t\alpha$ method, Figure 31(b), and the data for 25mg samples are shown in Figures 33(a) and (b). A photographic method was used to determine the volume shrinkage occurring during the decomposition of 100mg samples, (Figure 34), and this gave a Z factor of 0.72 to 0.80 comparing favourably with the value of 0.78 calculated for the decomposition of barium carbonate to barium oxide at constant density.

9.3. Barium Carbonate Sintered Pellets

Samples of the lath carbonate were pressed at ~30,000 psi., and sintered for thirty minutes at 1000°C, in an atmosphere of carbon dioxide, so that a comparison could be made between the behaviour of these samples and those decomposed in nitrogen (section 8.4). 100 and 50mg samples were used, and the LnLn analysis is shown in Figure 24(a). The decomposition data for pelletized samples in nitrogen indicate that the decomposition in vacuo is likely to be diffusion or nucleation controlled as the reaction temperature in vacuo is 200°C lower than in nitrogen, and reaction mechanism are likely to change with decreasing temperature in the order phase boundary to diffusion to nucleation controlled. However, anomalous m values are obtained in the LnLn analysis of vacuum samples and the temperature dependence of the reaction rates indicates that the samples are inconsistent, and a carefully controlled sintering procedure would be needed to produce suitable pellets.

9.4. Discussion

The variation of apparent activation energy with the bed depth of 100mg samples of the lath samples, and the related changes in the initial m values and reaction rates, are very confusing, until these reults are related to those obtained for the decomposition of compacted powder samples in a nitrogen atmosphere. The maximum reaction rate before self-cooling effects become

important in the decomposition of 50mg samples in nitrogen is $t_{0.5}$ = 150 minutes, and this rate is similar to the rates used in the vacuum studies. Heat transfer to the sample to maintain isothermal conditions when self-cooling occurs should be more rapid in the vacuum conditions where a platinum crucible is used rather than an alumina one, therefore this maximum value is probably too low for the decomposition of 50mg samples in vacuo.

The results for 100mg lath samples show that the process is not isokinetic in the temperature range investigated, and indicate that self-cooling effects are present, even when the reaction rate is $t_{0.5}$ = 200 minutes. Unfortunately, the vacuum thermobalance is not suitable for slower reaction rates and, in addition, its limited sensitivity prevents accurate analysis of the decomposition kinetics of 25mg samples. However, the results for the decomposition of 25mg samples show that the process is isokinetic, and self-cooling is not evident at a reaction rate of $t_{0.5}$ = 55 minutes.

The Arrhenius plot for 100mg samples of the spherical barium barbonate shows a negative curvature at fast reaction rates, similar to the lath system, and the LnLn analysis, Figure 31(a), indicates that the process is not isokinetic. If the anomalous results were due solely to self-cooling phenomena, the spherical carbonate system should be more similar to the lath system than is found experimentally, and the smaller bed depth of the

spherical samples must have some effect on the self-cooling; the maximum reaction rate before self-cooling is evident in 100mg spherical samples is $t_{0.5}$ =130 minutes (cf. $t_{0.5} \geq$ 200 minutes in 100mg lath samples). The Austin-Rickett analysis of the spherical carbonate data shows that a linear function can be obtained when $n \sim 1.10$ (at least up to $\alpha = 0.85$), but this is meaningless in terms of any reaction model and, in any case, the process is not isokinetic. The Arrhenius plot, Figure 31(b), was constructed using rates obtained by the $t\alpha$ method at $\alpha = 0.25$, 0.50 and 0.75, and the negative curvature at fast reaction rates can be seen for the $t_{\alpha=0.50}$ and $t_{\alpha=0.75}$ methods. The apparent linearity of the $t_{\alpha=0.25}$ values is attributable to either the inherent errors at fast reaction rates or the progressive change in activation energy with the different t_α methods.

Both the 25mg samples of the lath and the spherical barium carbonate show an induction period which cannot be attributed to experimental errors. The spherical carbonate samples have a constant induction period, whilst the lath system only shows this behaviour for samples pre-mixed in water; the raw lath carbonate samples showing a progressive increase in the induction period as the temperature is lowered. These effects would not be expected if the sole cause was the time period

required for the sample to attain temperature as in this situation the lower the temperature the shorter the time period. The lath samples follow a first order model after the induction period, and good agreement is obtained up to 85% decomposition (Figure 28(b)) and similarly, the spherical samples follow an $R_3\alpha$ model (Figure 33(B)) up to at least 50% reaction before deviation occurs. An explanation of the induction periods may be found in considering nucleation phenomena. The induction periods for the raw lath carbonate samples can be used to yield a linear function when plotted on a log time v $\frac{1}{T°K}$, and the equation of the line is,

$$\frac{10^4}{T} = 2.15 \log t + 9.6$$

9.5 Summary

The investigation of the decomposition of barium carbonate in vacuo has shown that it is difficult to obtain meaningful kinetic data when the rate of reaction exceeds some maximum tolerable value which depends on the sample weight and morphology. The self-cooling effect, always associated with endothermic reactions and leading to departures from isothermal conditions within a sample, depends on the heat of formation, but the extent of the effect is related to the reaction rate expressed as mg of CO_2/minute. Hence meaningful kinetic data can be obtained for the decomposition of 25mg samples, even though this may be impossible for the decomposition of

100mg samples at comparable reaction rates expressed as α. Unfortunately, the limited sensitivity of the thermobalance prevents absolute measurements for 25mg samples, but the results indicate that the lath system follows a first order model and the spherical an $R_3\alpha$ model with an activation energy of about 62 kcal/mole.

The implications of this investigation to carbonate-metal oxide systems are as follows:

(a) carbonate-metal oxide mixtures containing $\sim$25mg of barium carbonate must be used for self-cooling effects to be minimized, but this sample size is not suitable for absolute reaction mechanism studies due to the limited sensitivity of the vacuum thermobalance,

(b) meaningful kinetic data may be obtained for carbonate-metal oxide mixtures containing 100mg of carbonate when very slow reaction rates are used.

FIGURE 26a: LnLn analysis curves of 100mg samples of $BaCO_3(\ell)$ in vacuo.

FIGURE 26b: Arrhenius plots of 100mg samples of $BaCO_3(\ell)$ in vacuo using the t_α method.

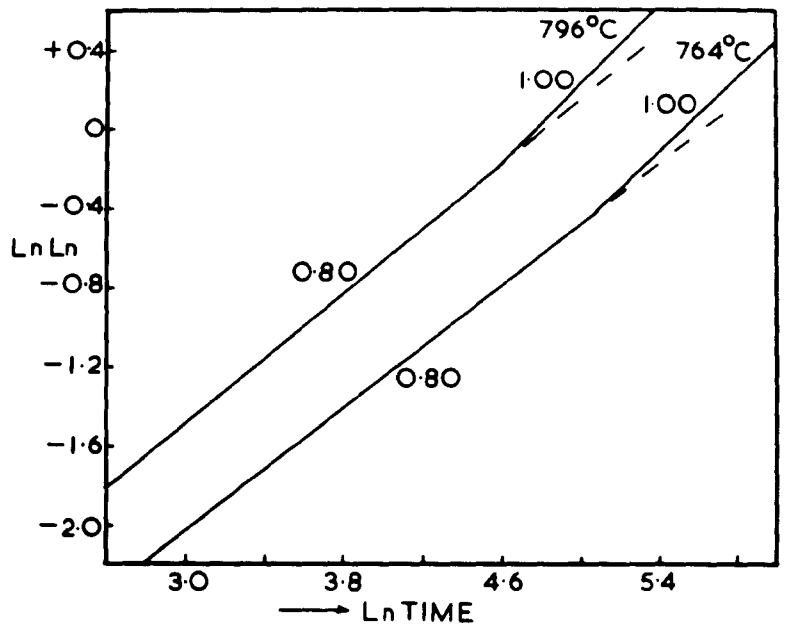
796°C
764°C
1·00
1·00
0·80
0·80
+0·4
0
−0·4
−0·8
−1·2
−1·6
−2·0
Ln Ln
3·0
3·8
4·6
5·4
Ln TIME

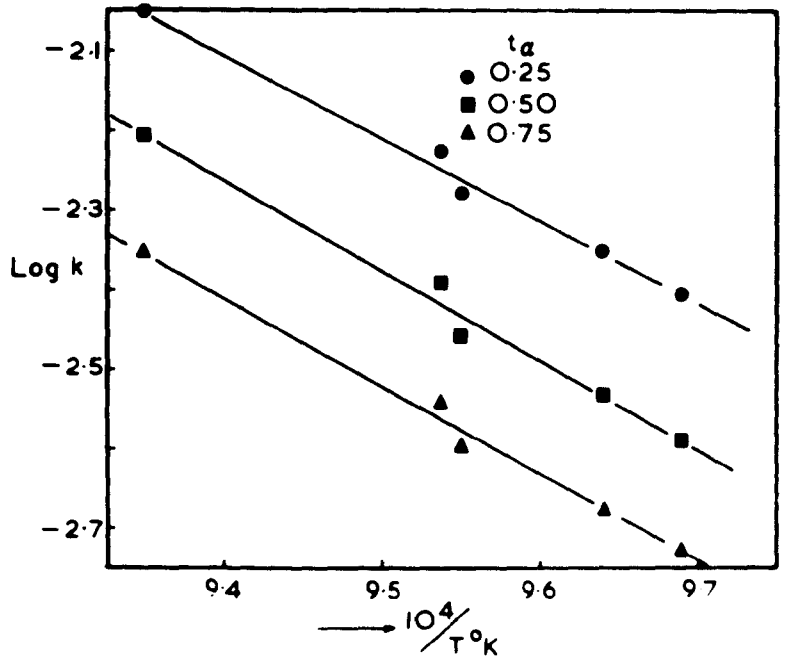
tα
0·25
0·50
0·75
−2·1
−2·3
−2·5
−2·7
Log k
9·4
9·5
9·6
9·7
10⁴/T °K

FIGURE 27a: LnLn analysis curves of 25mg samples of $BaCO_3(s)$ in vacuo.

FIGURE 27b: LnLn analysis curves of 25mg samples of $BaCO_3(\ell)$ in vacuo.

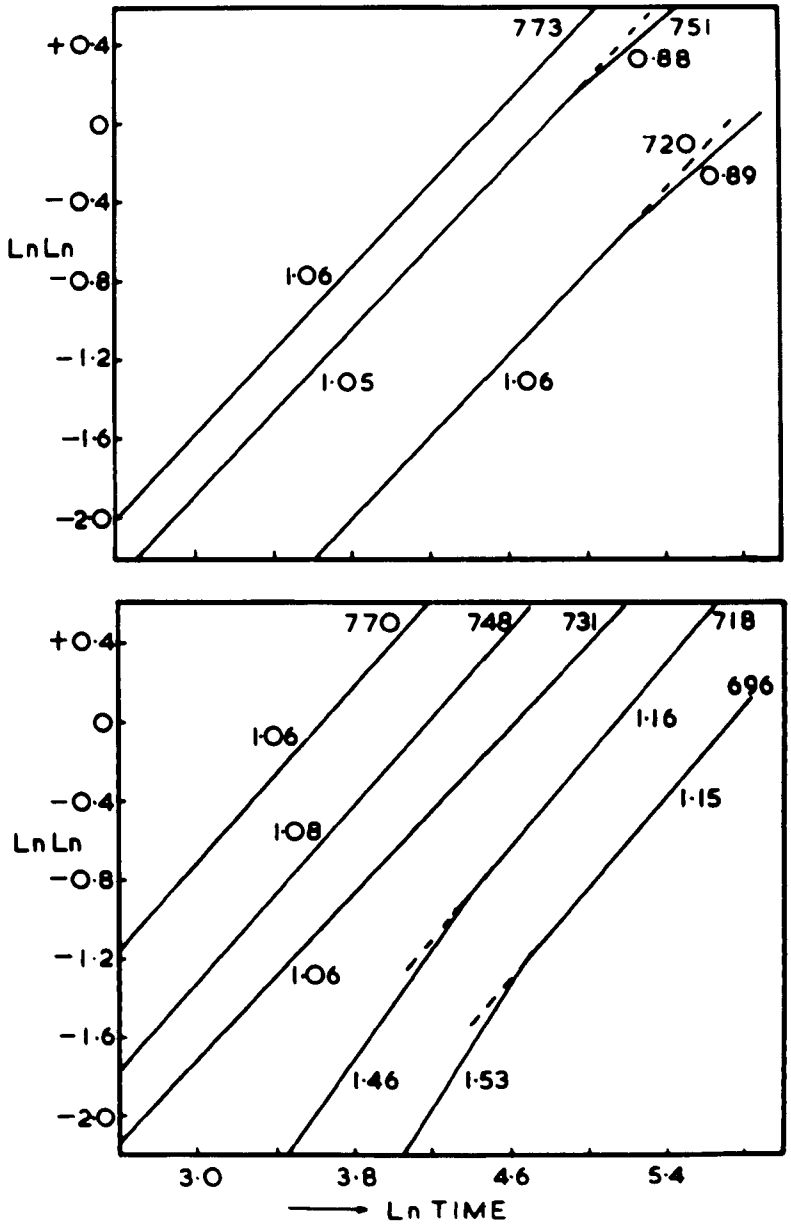
773
751
0·88
720
0·89
1·06
1·05
1·06
+0·4
0
−0·4
−0·8
−1·2
−1·6
−2·0
Ln Ln
770
748
731
718
696
1·06
1·08
1·06
1·16
1·15
1·46
1·53
3·0
3·8
4·6
5·4
Ln TIME

FIGURE 28a: Isothermal weight change curves for 25mg $BaCO_3$(ℓ) in vacuo.

FIGURE 28b: First order model curves for 25mg $BaCO_3$(ℓ) in vacuo.

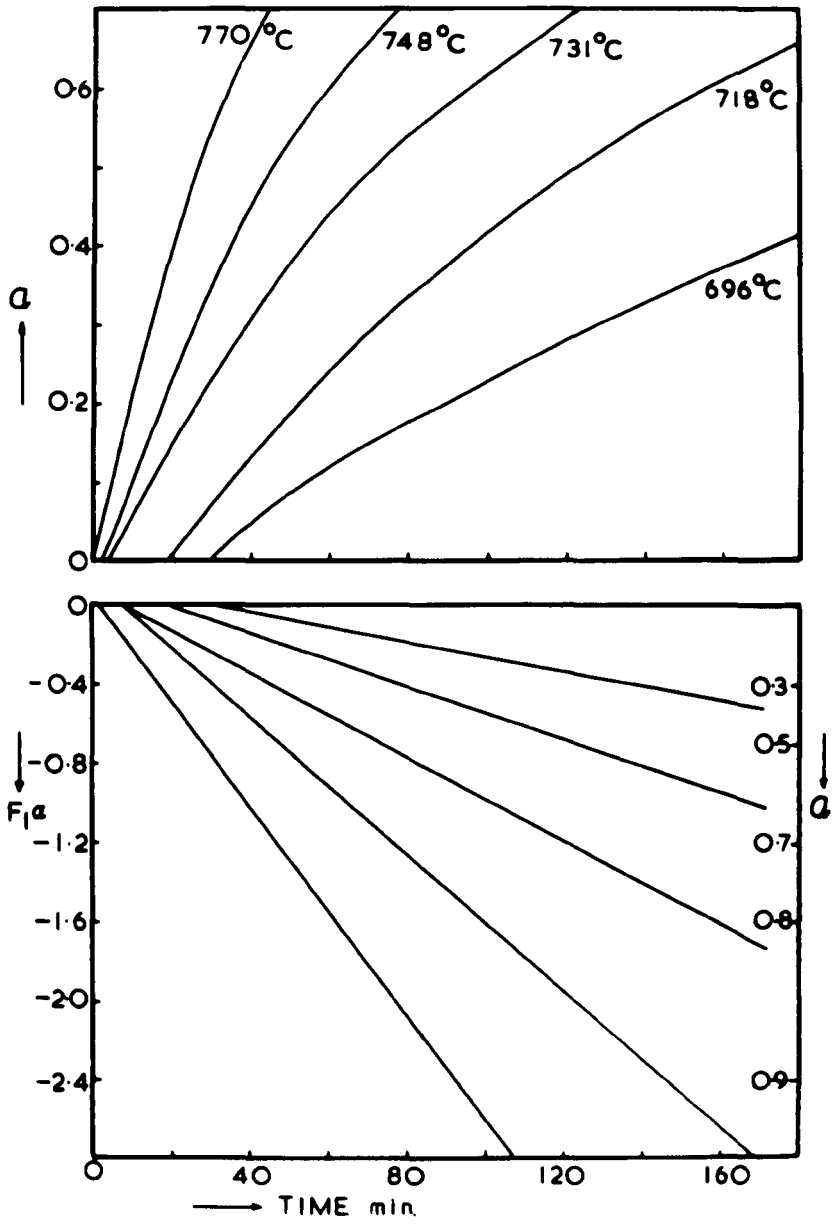
770°C
748°C
731°C
718°C
696°C
0·6
0·4
0·2
0
a
0
-0·4
-0·8
-1·2
-1·6
-2·0
-2·4
F1a
0·3
0·5
0·7
0·8
0·9
a
0
40
80
120
160
TIME min.

FIGURE 30a: First order model plots for 25 and 100mg samples of $BaCO_3(\ell)$, (mixed in water).

FIGURE 30b: LnLn analysis curves for 25 and 100mg samples of $BaCO_3(\ell)$, (mixed in water).

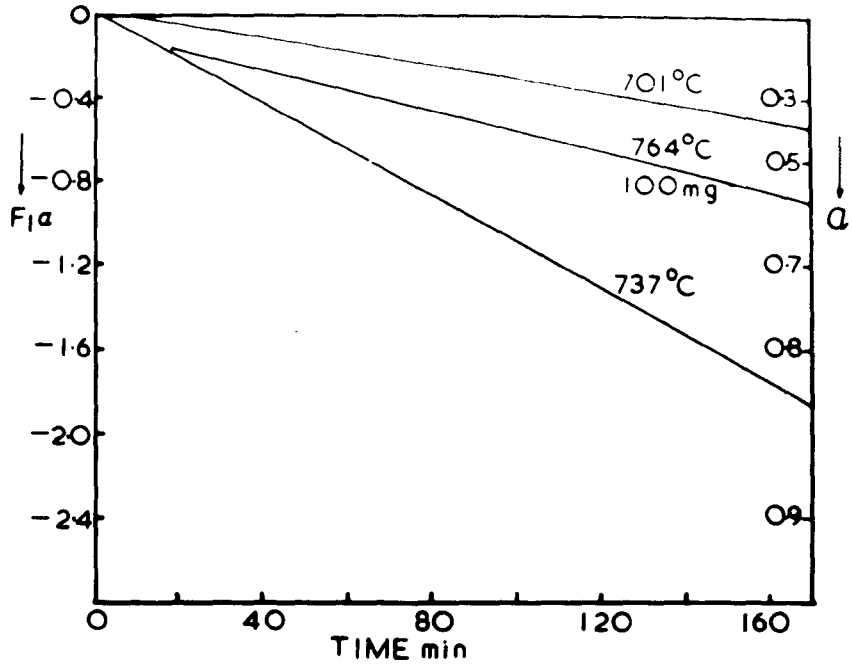
0
-0·4
-0·8
-1·2
-1·6
-2·0
-2·4
F/a
701°C
764°C
100mg
737°C
0·3
0·5
0·7
0·8
0·9
a
0
40
80
120
160
TIME min

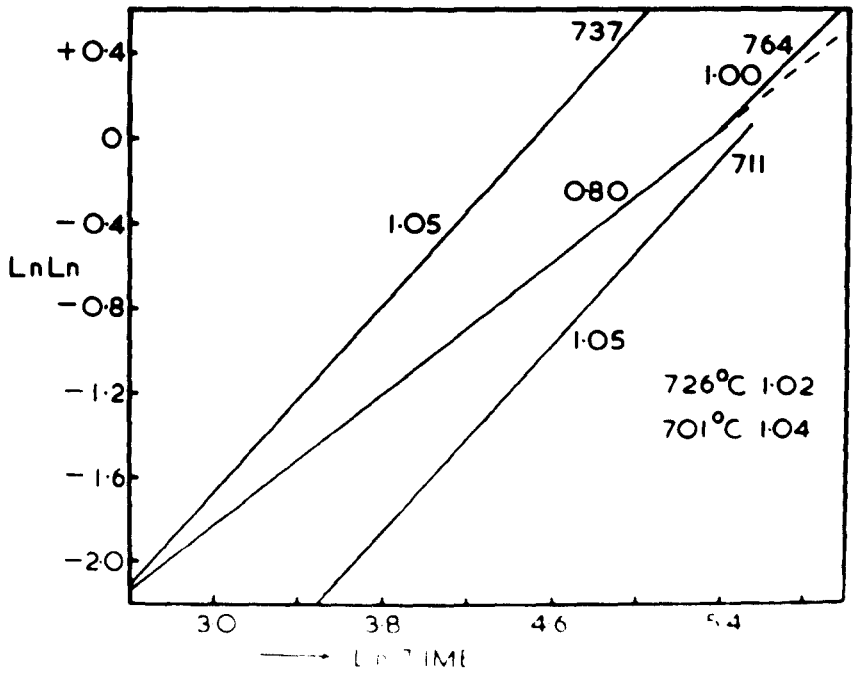
+0·4
0
-0·4
-0·8
-1·2
-1·6
-2·0
LnLn
737
764
1·00
711
0·80
1·05
1·05
726°C 1·02
701°C 1·04
3·0
3·8
4·6
5·4

FIGURE 31a: LnLn analysis curves for 100mg samples of $BaCO_3(s)$ in vacuo.

FIGURE 31b: Arrhenius plots for 100mg samples of $BaCO_3(s)$ in vacuo using the t_α method.

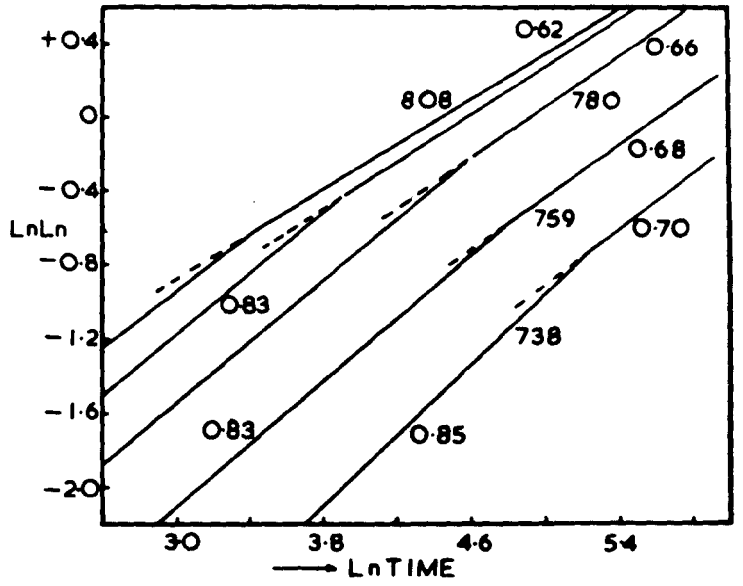
+0·4
0
−0·4
−0·8
−1·2
−1·6
−2·0
LnLn
0·62
0·66
808
780
0·68
759
0·70
0·83
738
0·83
0·85
3·0
3·8
4·6
5·4
LnTIME

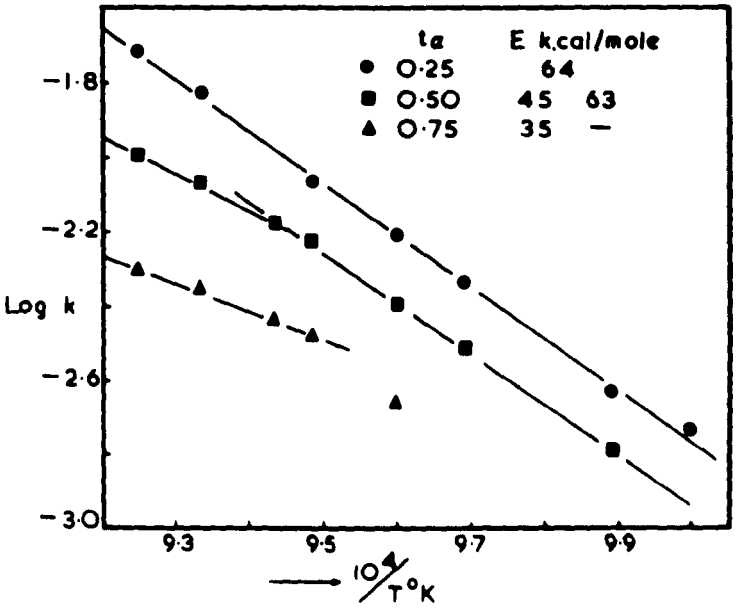
tα
E k.cal/mole
0·25
64
0·50
45
63
0·75
35
—
−1·8
−2·2
−2·6
−3·0
Log k
9·3
9·5
9·7
9·9
10⁴/T°K

FIGURE 32a: Arrhenius plots for 100mg samples of $BaCO_3(\ell)$ in crucibles 1, 2 and 3.

FIGURE 32b: Austin-Rickett analysis of 100mg samples of $BaCO_3(s)$ in vacuo.

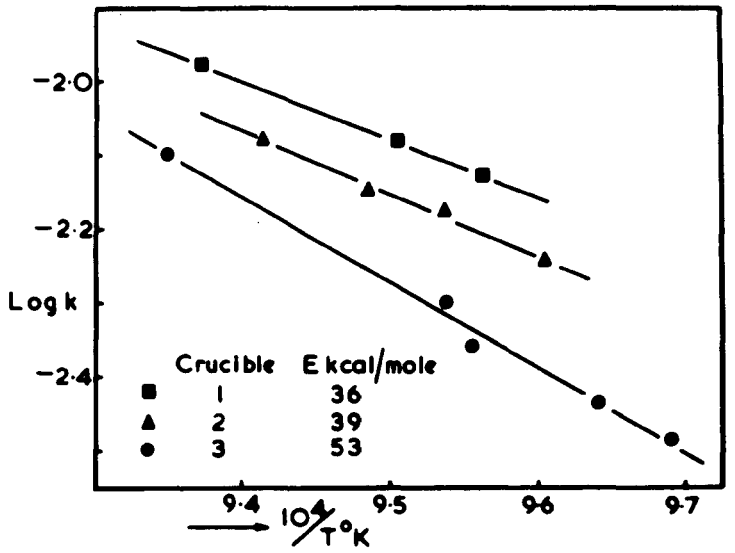
-2·0
-2·2
Log k
-2·4
Crucible E kcal/mole
1 36
2 39
3 53
9·4
9·5
9·6
9·7
10⁴/T°K

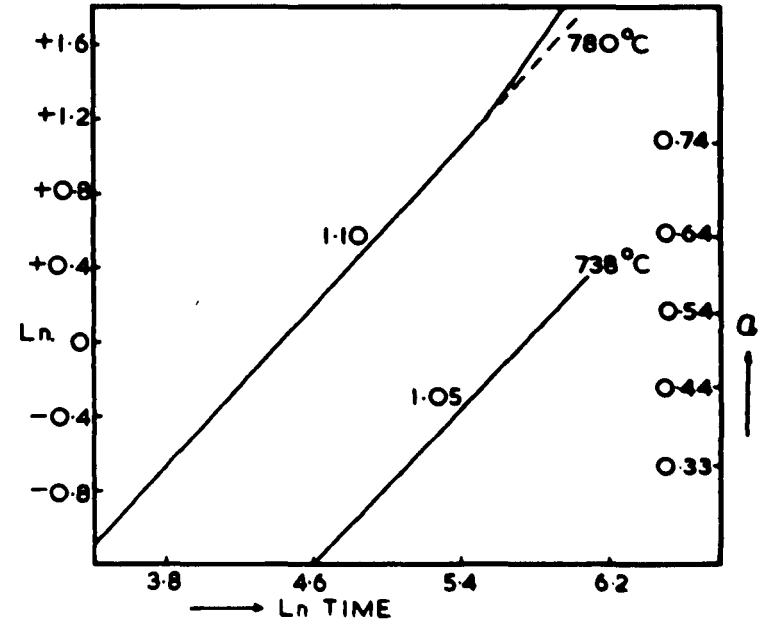
+1·6
+1·2
+0·8
+0·4
Ln. O
-0·4
-0·8
780°C
738°C
1·10
1·05
0·74
0·64
0·54
0·44
0·33
a
3·8
4·6
5·4
6·2
Ln TIME

FIGURE 33a: Isothermal weight change curves for 25mg samples of $BaCO_3(s)$ in vacuo.

FIGURE 33b: $R_3\alpha$ model plots for 25mg samples of $BaCO_3(s)$ in vacuo.

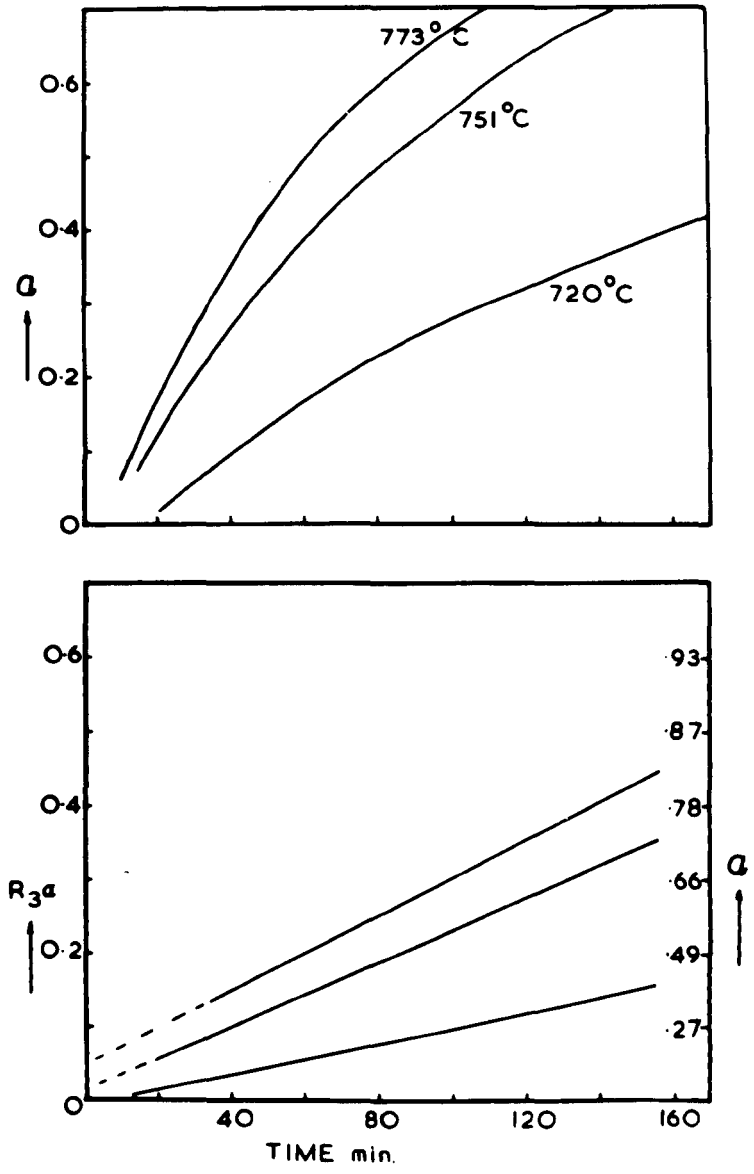
773°C
751°C
720°C
0·6
0·4
0·2
0
a
0·6
0·4
0·2
0
R_3^a
·93
·87
·78
·66
·49
·27
a
40
80
120
160
TIME min.

FIGURE 34a: 100mg sample of $BaCO_3(s)$ prior to decomposition.

FIGURE 34b: Decomposition product of 100mg samples of $BaCO_3(s)$ in vacuo.

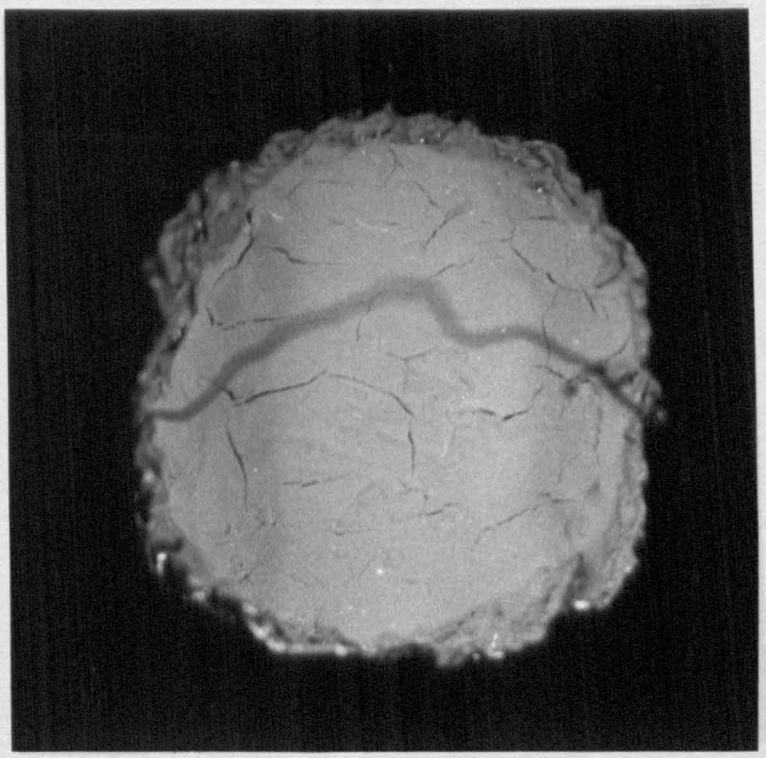

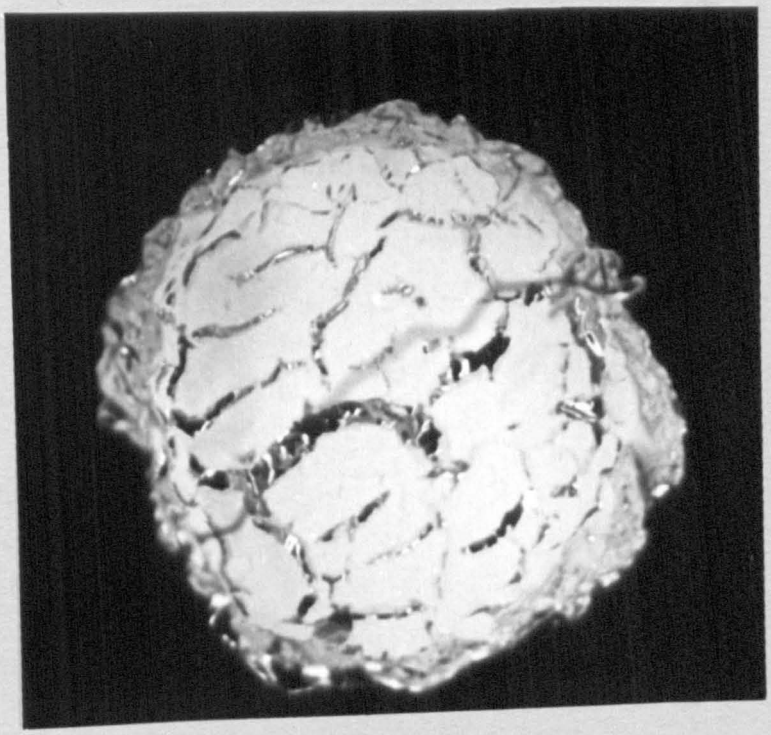

FIGURE 34c: Scanning electron micrograph of barium oxide ($BaCO_3(\ell)$ decomposed in vacuo)
Magnification x 2,600

FIGURE 34d: Scanning electron micrograph
Magnification x 6,800

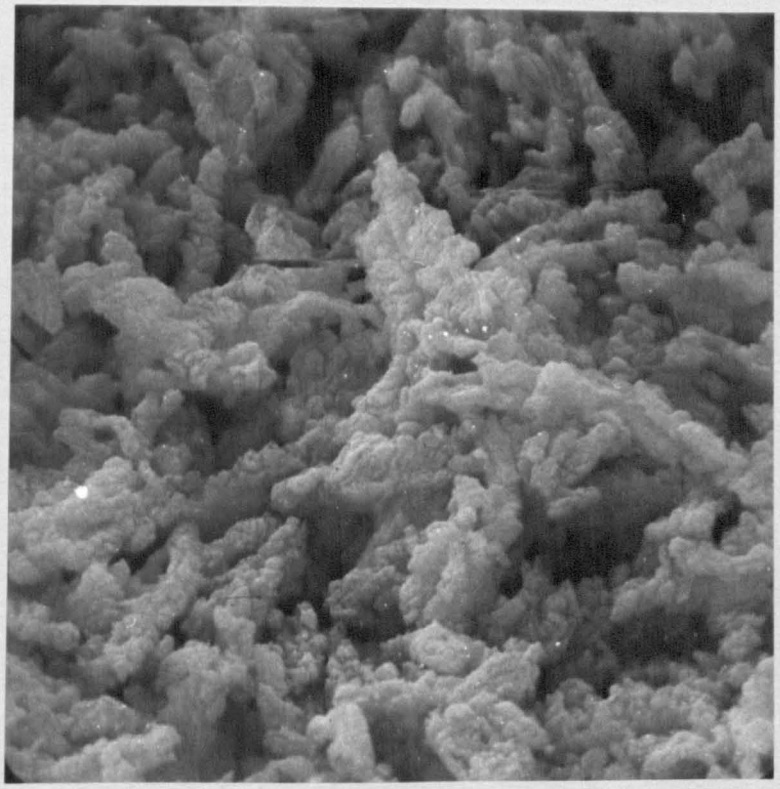

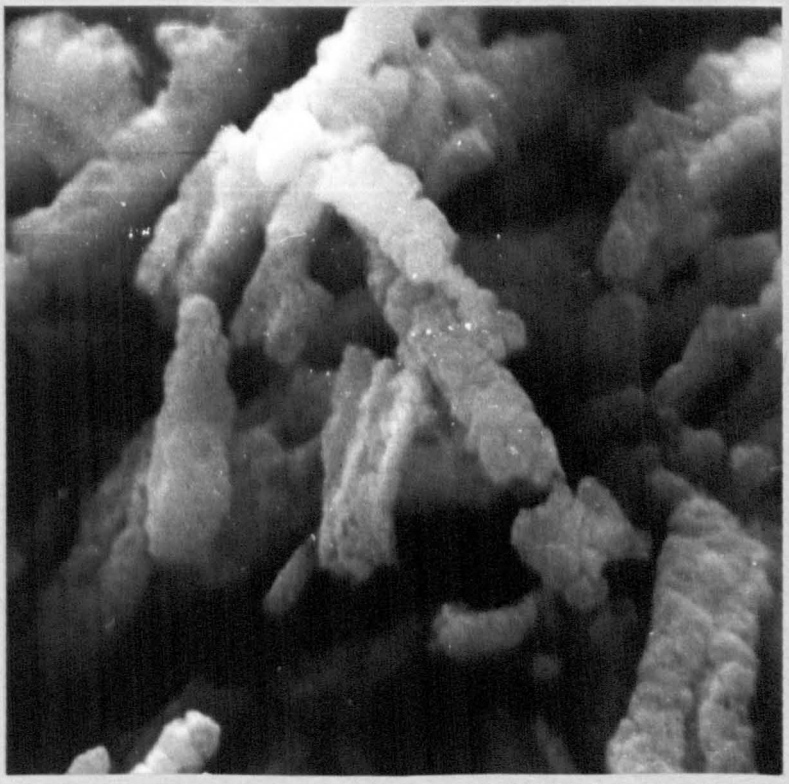

FIGURE 35: Arrhenius plots for 25mg samples of $BaCO_3(\ell)$ and $BaCO_3(s)$ in vacuo.

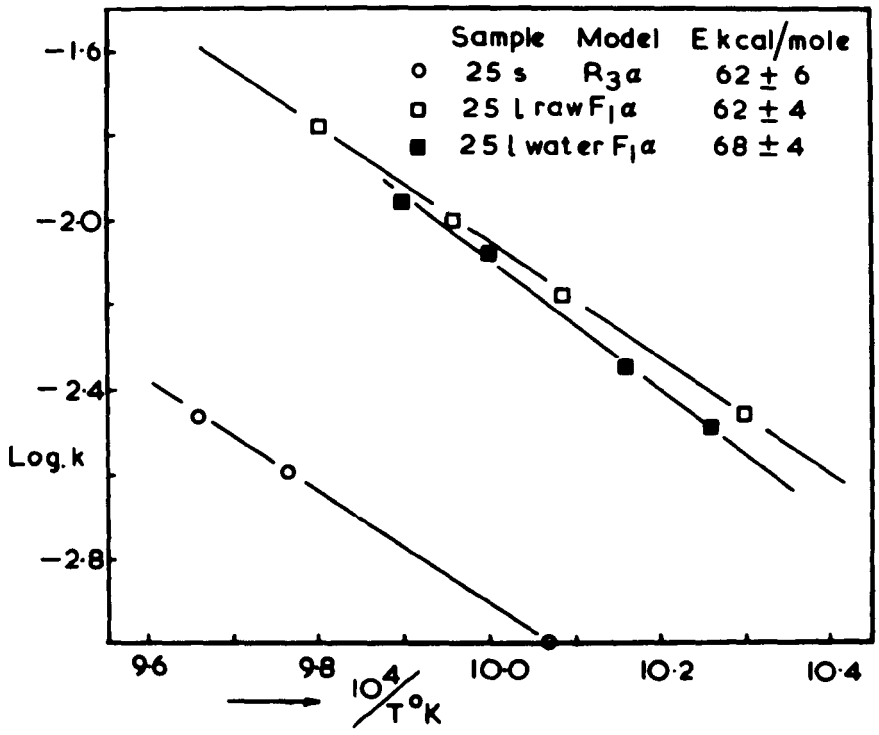
Sample Model E kcal/mole
25 s $R_3\alpha$ 62 ± 6
25 l raw $F_1\alpha$ 62 ± 4
25 l water $F_1\alpha$ 68 ± 4
−1·6
−2·0
−2·4
−2·8
Log. k
9·6
9·8
10·0
10·2
10·4
$10^4/T°K$

CHAPTER 10

The Decomposition Kinetics of $BaCO_3$-ZrO_2 in Vacuo

The preliminary studies of the barium carbonate-zirconia system using TG, x-ray analysis and infrared spectroscopy indicated that only one compound was formed during the decomposition of both the 1:1 and 2:1 mole mixtures of barium carbonate:zirconia. X-ray analysis of partial reaction products of the 1:1 mixture indicated that the rate of formation of barium zirconate was directly proportional to the rate of decomposition of barium carbonate (see Figure 9(a)). Therefore this system was thought to be an ideal one for kinetic studies relating the formation of barium zirconate with the rate of evolution of carbon dioxide. However, SEM of barium carbonate-zirconia mixtures showed that not all the mixtures were suitable for kinetic model studies, and that all mixtures containing the lath barium carbonate were totally unsuitable, due to the aggregation of the zirconia particles and the small number of zirconia-carbonate point contacts. Figure 36(b). The mixtures containing the spherical barium carbonate can be considered as approximating to a system of small carbonate particles coating larger zirconia particles, but the aggregation of the zirconia particles prevents complete surface contact between carbonate and oxide, regardless of the molecular composition of the mixture. Figure 35(a). Scanning electron micrographs indicated that the mixing

media, water or acetone, had little effect on the aggregation of the zirconia particles, but suggested that the overall size of the aggregates was slightly smaller in water than in acetone prepared samples. For this reason water prepared mixtures were used for all the isothermal experiments.

100mg samples were weighed in platinum crucibles and then damped in acetone so that a consistent packing could be obtained.

10.1. $BaCO_3(\ell):ZrO_2$

Although this system had been found to be unsuitable for kinetic model studies on the basis of the SEM results, it was thought desirable to undertake a limited investigation of the system so that an activation energy could be calculated, and compared with one obtained for the spherical barium carbonate-zirconia mixtures.

The LnLn analysis shown in Figure 36(a) gives an average m value of 0.85, and indicates that the reaction mechanism is isokinetic throughout the temperature range studied. An activation energy of 63 kcal/mole was obtained, using both the $t_{\alpha=0.50}$ method, and from the function $- \ln(1 - \alpha) = (kt)^{0.8}$ in the range $\alpha = 0.00$ to 0.40. X-ray analysis of final reaction products and partial products of reaction did not indicate the presence of barium zirconate and only barium carbonate, zirconia and a complex barium hydroxide phase were found to be present. In the SEM micrographs, Figures 37(a) and (b),

the zirconia particles are unreacted, and the barium carbonate has retained its lath form. The lath form is also shown by a totally decomposed sample, which has been exposed to the atmosphere for about one hour, (Figure 37(b)), and the whiskers are most likely the barium hydroxide phase detected in the x-ray analysis.

10.2. $\underline{BaCO_3(s):ZrO_2}$

This system was investigated over a temperature range of 150°C and showed some interesting effects. The use of a reduced time scale technique (Table 19) proved ineffective in accounting for the anomalous experimental results, and an Arrhenius plot, using the $t_{\alpha=0.50}$ method, contained discontinuities, Figure 38(b). However, a LnLn analysis of the data indicated that the results should be considered over three temperature ranges corresponding to m values of 1.16, 1.06 and 0.88, Figure 36(b). Using this approach, the Arrhenius plot can be subdivided into three temperature ranges having linear functions corresponding to the temperature ranges with constant m values.

At temperatures below 740°C, the LnLn analysis yields an m value of $\sim$0.88 comparable to that obtained for the decomposition of barium carbonate alone. X-ray analysis of partial reaction products indicated the presence of barium carbonate, zirconia and a complex barium hydroxide, (possibly a barium hydroxide hydrate),

but did not detect any barium zirconate. Infrared analysis was used to detect the hydroxide phase, since none of the barium hydroxides listed in the ASTM index corresponded with the x-ray pattern of this hydroxide. SEM micrographs of partial reaction products also indicated that the carbonate had not reacted with the zirconia, and a typical micrograph is shown in Figure 39(b).

In the temperature range from 740° to 766°C, the LnLn analysis yields an m value of $\sim$1.06, indicating a phase boundary controlled mechanism, and a linear function is obtained, using an $R_3\alpha$ model up to $\alpha = 0.75$, and an $R_2\alpha$ model up to $\alpha = 0.40$. The activation energy calculated from rates obtained from an $R_3\alpha$ model is 110 kcal/mole, and 120 kcal/mole using $t_{\alpha=0.50}$. The accuracy cannot be better than 15% because of the small temperature range considered. All the techniques used for phase identification indicated that barium zirconate was not formed during the decomposition of barium carbonate, and the reaction occurring in this temperature range is

$$BaCO_3 \longrightarrow BaO + CO_2\uparrow$$

The LnLn analysis for the temperature range 801° to 854°C yields m values in the range 1.08 to 1.16, and unfortunately the experimental data is not suitable for an accurate model analysis, as the reaction rates are rather fast. A zero order model gave the best agreement, and linear functions were obtained up to $\alpha = 0.60$.

An activation energy of 36 kcal/mole was calculated, using the zero order model. Barium zirconate was not detected in any partial reaction products, and a typical SEM micrograph is shown in Figure 39(a).

10.3. Discussion

Since the formation of barium zirconate was never observed in any of the partial reaction products, the reaction that is being studied is the decomposition of barium carbonate to barium oxide in the presence of zirconia. The mechanism and activation energy of the two carbonate systems should therefore be related to the decomposition of the two carbonates alone, and this is clearly illustrated by the data for the lath carbonate-zirconia mixtures where an m value of $\sim$0.85 and an activation energy of 63 kcal/mole are obtained. However, the data for the spherical carbonate system is not so easily explained, and the relative reaction rates must first be considered. Self cooling effects and bed pressure phenomena are likely to occur in the temperature range from 801° to 854°C where the reaction rates are relatively fast, and the activation energy of 36 kcal/mole is similar to that obtained for the spherical carbonate alone (35-45 kcal/mole) at equivalent reaction rates. The LnLn data for temperatures below 766°C indicates a change in reaction mechanism from phase boundary controlled, with an activation energy of $\sim$115 kcal/mole, to a mechanism and activation energy comparable to those

obtained for the decomposition of barium carbonate alone. However, the Arrhenius plot, using $t_{\alpha=0.50}$, suggests that the data could be considered as one mechanism in the temperature range from 766° to 854°C, and a second mechanism in the range from 702° to 749°C and, at this time, sufficient data are not available for a fair evolution to be made.

FIGURE 35a: Scanning electron micrograph of 1:1 mole $BaCO_3(s):ZrO_2$ Magnification x 5,200

FIGURE 35b: Scanning electron micrograph of 1:1 mole $BaCO_3(\ell):ZrO_2$ Magnification x 2,100

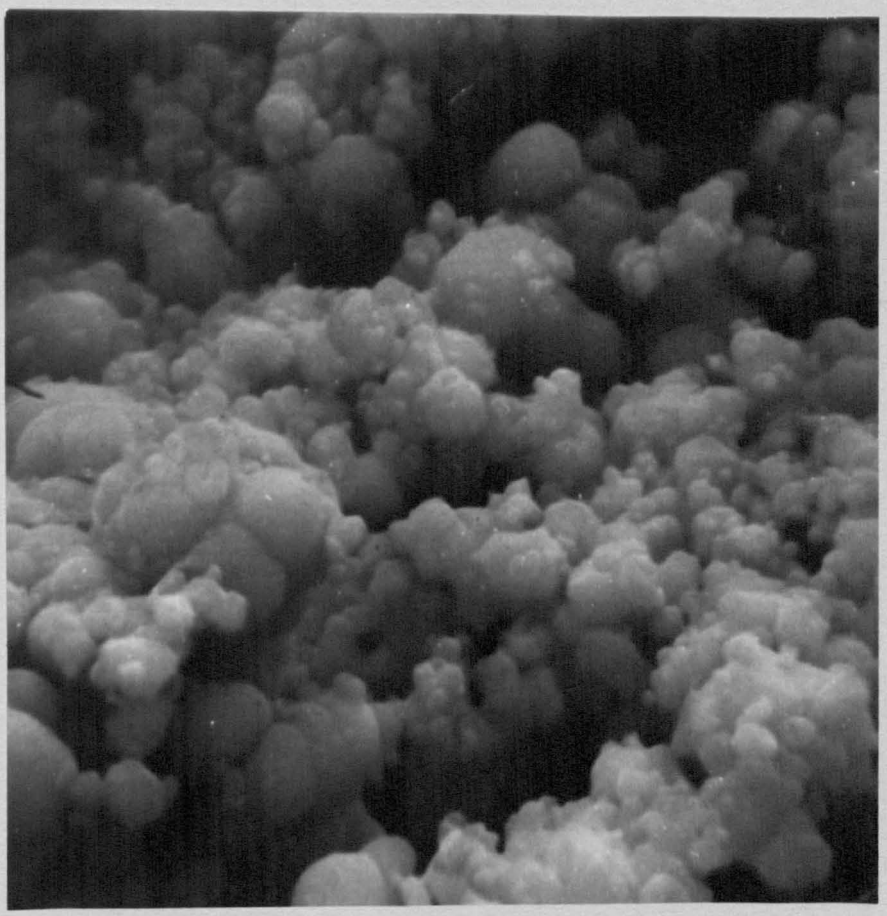

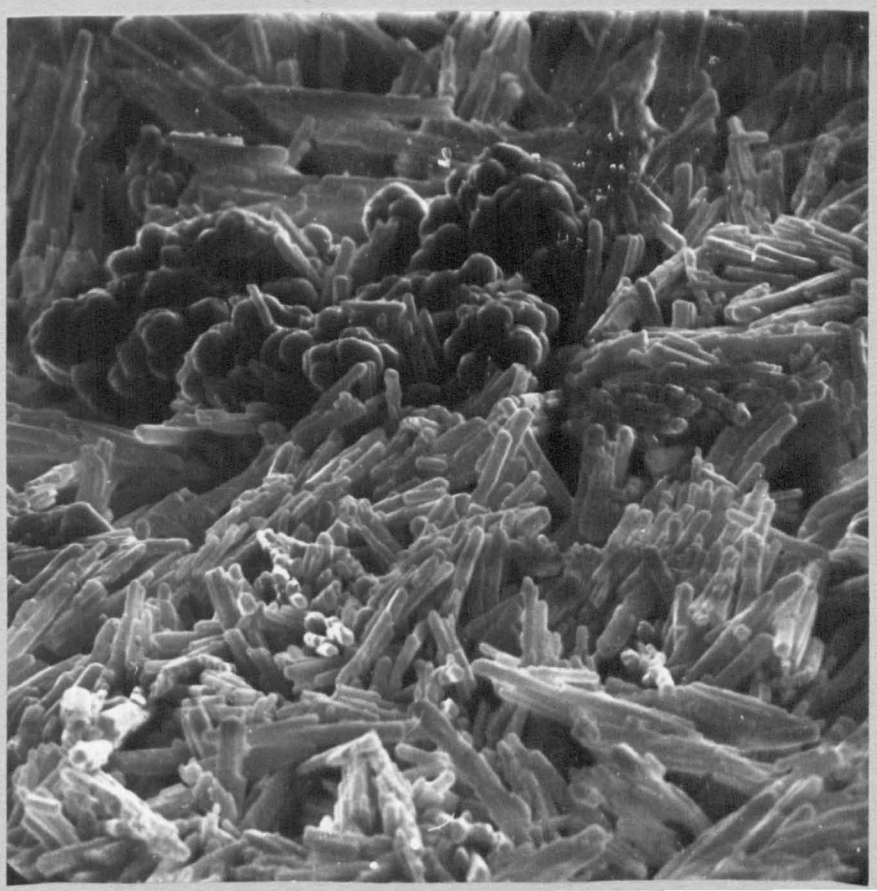

FIGURE 36a: LnLn analysis curves for $BaCO_3(s)$: ZrO_2 samples in vacuo.

FIGURE 36b: LnLn analysis curves for $BaCO_3(\ell)$: ZrO_2 samples in vacuo.

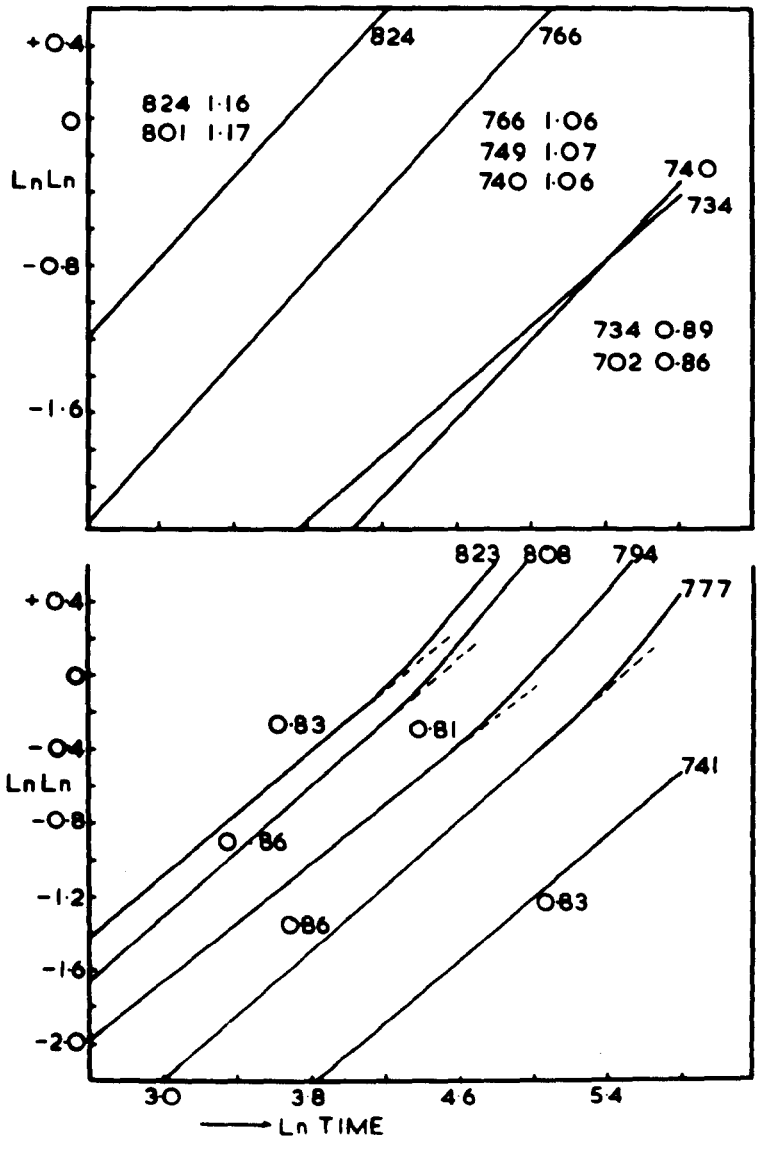
+0·4
0
LnLn
-0·8
-1·6
824
766
824 1·16
801 1·17
766 1·06
749 1·07
740 1·06
740
734
734 0·89
702 0·86
823
808
794
777
+0·4
0
-0·4
LnLn
-0·8
-1·2
-1·6
-2·0
0·83
0·81
0·86
0·86
741
0·83
3·0
3·8
4·6
5·4
Ln TIME

FIGURE 37a: Scanning electron micrograph of $BaCO_3(\ell):ZrO_2$ after decomposition in vacuo
Magnification x 1,400

FIGURE 37b: Scanning electron micrograph
Magnification x 2,400

FIGURE 38a: Isothermal weight change curves for $BaCO_3(\ell):ZrO_2$, $BaCO_3(s):ZrO_2$, $BaCO_3(s)$ and $BaCO_3(\ell)$ samples in vacuo.

FIGURE 38b: Arrhenius plots for $BaCO_3(s):ZrO_2$ and $BaCO_3(\ell):ZrO_2$ samples in vacuo.

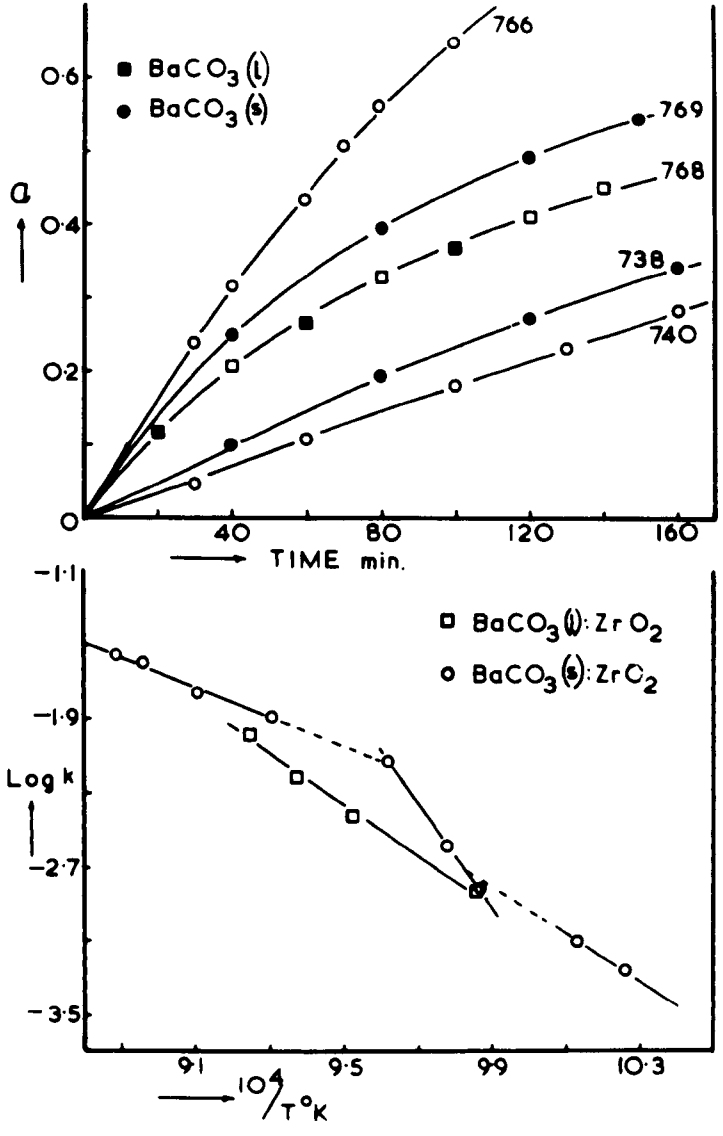
■ BaCO3 (l)
● BaCO3 (s)
766
769
768
738
740
α
0·6
0·4
0·2
0
40
80
120
160
TIME min.
□ BaCO3 (l): ZrO2
○ BaCO3 (s): ZrO2
−1·1
−1·9
−2·7
−3·5
Log k
9·1
9·5
9·9
10·3
10⁴/T°K

FIGURE 39a: Scanning electron micrograph of $BaCO_3$(s):ZrO_2 after decomposition in vacuo at 848°C
Magnification x 2,500

FICURE 39b: Scanning electron micrograph
702°C
Magnification x 2,300

TABLE 19: Reduced time scale values for $BaCO_3(s):ZrO_2$ Systems.

α	$t/t_{0.5}$ at various temperatures °C		
	824	766	702
0.1	0.186	0.174	0.100
0.2	0.368	0.348	0.255
0.3	0.580	0.543	0.452
0.4	0.765	0.761	0.702
0.5	1.000	1.000	1.000
0.6	1.315	1.304	-
0.7	1.631	1.630	-
0.8	2.105	2.109	-
0.9	2.842	2.976	-

CHAPTER 11

The Decomposition Kinetics of $BaCO_3$-TiO_2 Systems in Vacuo

The thermodynamics of the barium carbonate-titania system have been discussed in Chapter 2, and two major conclusions were drawn; firstly, $BaTiO_3$ is always the first product of reaction, regardless of the molecular composition of the mixture, but may immediately react with barium carbonate to form Ba_2TiO_4 as apparently the initial reaction product. Secondly, $BaTiO_3$ can be formed on cooling from the reaction temperature by the reaction

$$Ba_2TiO_4 + CO_2 \longrightarrow BaTiO_3 + BaCO_3$$

The preliminary x-ray investigations of partial reaction products of 1:1 molecular mixtures of barium carbonate: titania (Chapter 6), showed that both Ba_2TiO_4 and $BaTiO_3$ were present in quenched samples, and the Ba_2TiO_4 was present in larger amounts than the $BaTiO_3$. However, the sample weights used in this investigation were such that a bed pressure of carbon dioxide may have been generated within the sample so $BaTiO_3$ was probably formed on quenching from 1000°C. The kinetic investigations in vacuo were therefore extended to include pelletized samples, so that the effects of bed pressures could be studied, and the results compared with data for the powder samples.

SEM was used as a preliminary screening test for the suitability of mixtures for kinetic model studies, and some typical micrographs are shown in Figures 40(a) and (b). The mixtures of spherical barium carbonate and titania were thought to be unsuitable for model studies, due to the similar particle sizes and resultant mixing geometry, but the 1:1 mixture was investigated so that an activation energy could be determined. Lath carbonate mixtures were thought to be ideal for kinetic investigations so they approximated more to small oxide particles coating the carbonate laths as the composition was changed from 2:1 to 1:1, and finally 1:2 carbonate:titania. The effects of different mixing media were similar to those in the tin oxide system, where the use of a water media results in a fluffy oxide appearance and acetone gives a granular form. (Chapter 13). However, the fluffy oxide appearance disappears on heating, so all the mixtures were prepared in water and then damped in acetone to give consistent packing.

The sample weights were chosen so that each sample contained 100mg of barium carbonate so that the reaction rates could be directly compared with those of barium carbonate alone. All the partially reacted samples were blue, due to the reduction of titania in vacuo to a non-stoichiometric form, which is an n-type semiconductor. The platinum crucibles were found to be stained after use,

and consistent results could only be obtained after the crucible had been used once. This effect was noted, but not investigated further.

11.1. $BaCO_3(s):TiO_2$

Although this system was partially rejected for kinetic model studies on the basis of the SEM investigation, it was thought that it would be interesting to examine a system rejected on such gounds. The LnLn analysis, Figure 41(b), indicates that the reaction can be considered as first order at the higher temperatures, and deviating from first order at the lower temperatures. An isothermal at 710°C shows the effect of the platinum crucible when first used as indicated by the anomalous m value (Figure 41(b)). An activation energy of 70 kcal/mole was calculated, using a first order model up to $\alpha = 0.65$, and the Arrhenius plot is shown in Figure 42(b). X-ray analysis of partial reaction products did not detect the presence of $BaTiO_3$. Ba_2TiO_4 was apparently the sole reaction product during the decomposition of the barium carbonate.

11.2. $BaCO_3(\ell):TiO_2$

The LnLn analysis of the data for 1:1 mole mixtures of barium carbonate-titania yields m values in the range 0.98 to 1.02, indicating a first order mechanism (Figure 43(a)). In fact, first order kinetics were followed up to at least 90% reaction, and the observed activation energy was 69 kcal/mole. $BaTiO_3$ was never

detected in any of the partial reaction products, and only appeared after the total decomposition of the carbonate. Ba_2TiO_4 appeared to be the sole product of reaction during the decomposition, and this system is analogous to the 1:1 spherical carbonate-titania system. SEM micrographs of partially reacted samples are shown in Figures 44(a), (b) and (c).

A LnLn analysis of the 2:1 mole mixture of barium carbonate:titania is shown in Figure 45(b). The reaction mechanism is not clear, but an activation energy of 71 kcal/mole, calculated from a first order model up to $\alpha = 0.50$, is in good agreement with that obtained for the 1:1 carbonate:titania system. X-ray analysis of the partial reaction products indicated that Ba_2TiO_4 was the sole product of reaction during the decomposition of the carbonate.

The 1:2 barium carbonate:titania system proved to be more similar to the 2:1 system than the 1:1 in reaction mechanism, and the LnLn analysis is shown in Figure 45(a). The observed activation energy was 69 kcal/mole, using a first order model up to $\alpha = 0.50$. Very small amounts of $BaTiO_3$ were detected in partially reacted samples, but Ba_2TiO_4 was again the major reaction product during the decomposition of the carbonate.

Pelletized samples of 1:1 mole mixtures of the lath barium carbonate-titania were prepared in a 7mm

die at a pressure of ~30,000 psi. The LnLn analysis of data for these samples is shown in Figure 43(b), and an m value of ~0.89 is observed. An activation energy of 69 kcal/mole was calculated, using a first order model on data in the temperature range from 685° to 760°C. Above 760°C, the Arrhenius plot is displaced to lower rates, and an activation energy of ~87 kcal/mole is obtained. Ba_2TiO_4 was the major product phase detected by x-ray analysis, but a small amount of $BaTiO_3$ was also detected.

11.3. Discussion

Ba_2TiO_4 is always found as the major reaction product during the decomposition of barium carbonate in all mixture compositions, and $BaTiO_3$ is only observed in very small amounts for partial reaction products of 1:1 pellets and 1:2 powders of barium carbonate:titania. The $BaTiO_3$ detected in partially reacted samples of 1:2 barium carbonate:titania increases in amount as the decomposition proceeds, and is probably formed by the reaction of Ba_2TiO_4 with titania. In contrast, the $BaTiO_3$ observed in partial reaction products of 1:1 barium carbonate:titania pellets may be formed on cooling from the reaction temperature when, due to the carbon dioxide pressure within the pellet, the following reaction occurs: $Ba_2TiO_4 + CO_2 \longrightarrow BaTiO_3 + BaCO_3$. $BaTiO_3$ is not observed in partial reaction products of 1:1 powder

mixtures indicating that the above process does not occur, therefore in powder samples of 1:1 barium carbonate titania, there is a negligible carbon dioxide pressure within the sample during the decomposition.

The activation energy for all the carbonate-titania systems investigatid is 70 kcal/mole in the temperature range from 660° to 760°C, and this is very similar to the heat of formation of Ba_2TiO_4 calculated as 66 kcal/mole at 800°C (see Chapter 14). Thermodynamics directs that $BaTiO_3$ must always be the first product of reaction, but the activation energy of the barium carbonate-titania systems indicates that this is not the rate controlling step, and the subsequent reaction between barium carbonate and $BaTiO_3$ to form Ba_2TiO_4 is the slowest step in the overall reaction. This step is controlled by a first order process when 1:1 mole powder mixtures are used, and the SEM micrographs, Figures 44(a), (b) and (c), illustrate that the process does appear to be a classical first order mechanism, and not merely a process following a first order algebraic equation. The reaction mechanisms for 2:1 and 1:2 barium carbonate:titania mixtures are not clear, and cannot be explained directly in terms of a classical model. The interpretation of the process mechanism for 1:1 barium carbonate:titania pellets would be expected to be difficult, due to bed pressure effects in pelletized samples. The Arrhenius plot for this system (Figure 42(b)) shows the bed pressure effect counteracting the increased reactivity

due to increased particle-particle contacts, and displacing the Arrhenius plot at high temperatures. The latter effect is not unexpected, as a bed pressure can be considered as equivalent to an externally applied pressure on a sample, and Tinsley[29] has shown similar displacements in the Arrhenius plots for the decomposition of calcium carbonate when a range of carbon dioxide atmospheres is used.

The problem of maximising particle-particle contacts, and yet minimising bed pressures, is common in reaction kinetic studies of two phase mixtures. This investigation has indicated an effective bed pressure during the decomposition of pelletized samples when the reaction rate exceeds $t_{\alpha=0.25} \sim 100$ minutes. When the effective bed pressure is high, the Ba_2TiO_4 formed at the reaction temperature may completely react with carbon dioxide in the bed to form $BaTiO_3$ on cooling, consequently, without knowledge of the thermodynamics of this system, it would be concluded that $BaTiO_3$ was the sole reaction product during the decomposition of the carbonate.

All the results of this investigation indicate that the kinetic mechanism data and phase formation results for any carbonate-titania mixtures studied as pelletized samples should be examined very carefully for bed pressure effects on the reaction process, and phase formation during cooling from the reaction temperature. However,

this investigation has shown that meaningful kinetic data can be obtained for powder samples of barium carbonate-titania mixtures when the experimental conditions are carefully controlled.

FIGURE 40a: Scanning electron micrograph of 1:1 mole $BaCO_3(s):TiO_2$ (mixed in water)
Magnification x 10,000

FIGURE 40b: Scanning electron micrograph of 1:1 mole $BaCO_3(\ell):TiO_2$
Magnification x 5,200

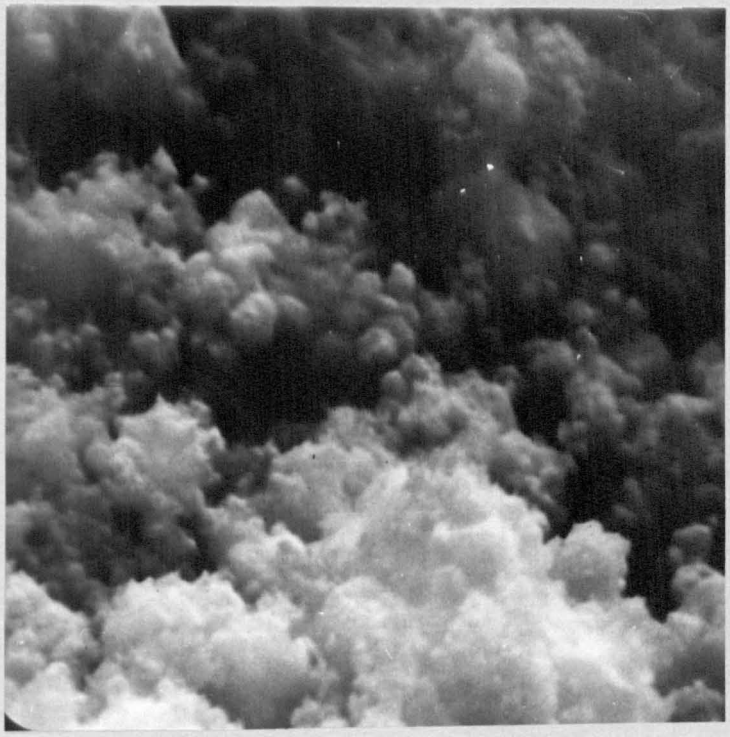

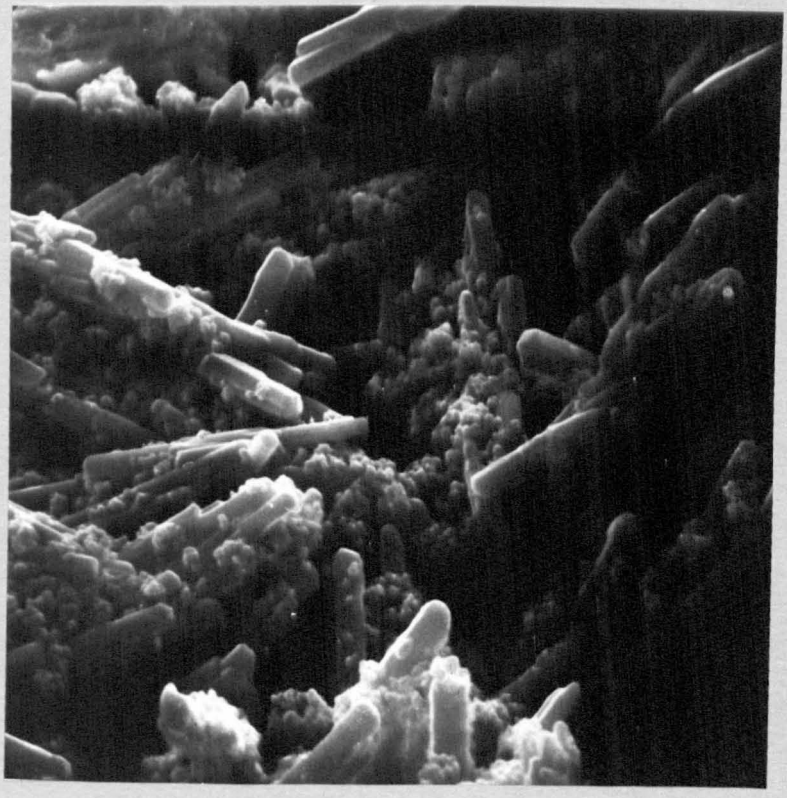

FIGURE 41a: Isothermal weight change curves for $BaCO_3:TiO_2$, $2BaCO_3:TiO_2$, $BaCO_3:2TiO_2$ and $BaCO_3$ in vacuo.

FIGURE 41b: LnLn analysis curves for $BaCO_3$(s): TiO_2 samples in vacuo.

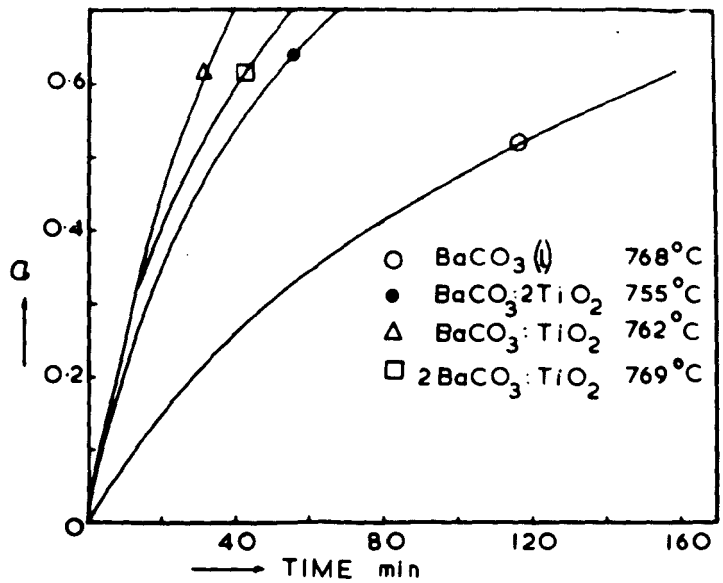
0·6
0·4
0·2
0
α
○ BaCO3 (l) 768°C
● BaCO3:2TiO2 755°C
△ BaCO3:TiO2 762°C
□ 2BaCO3:TiO2 769°C
40
80
120
160
TIME min

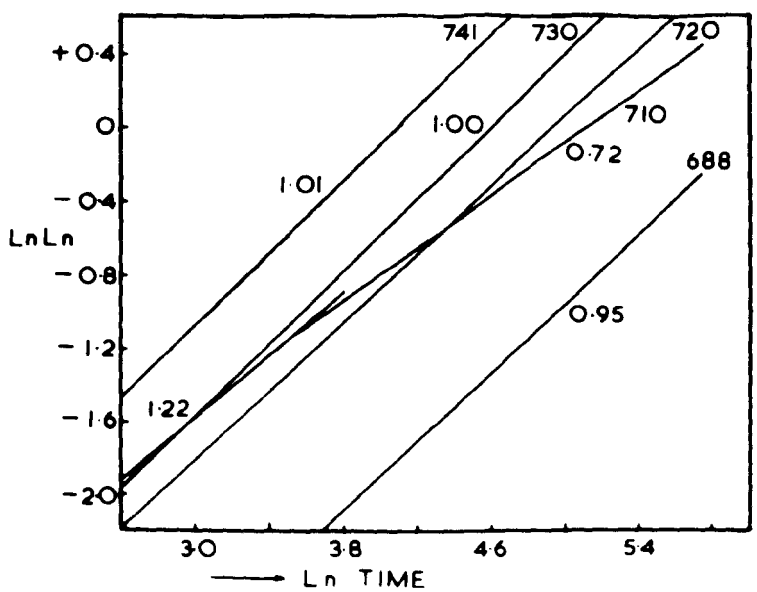
+0·4
0
−0·4
−0·8
−1·2
−1·6
−2·0
LnLn
741
730
720
1·00
710
0·72
688
1·01
0·95
1·22
3·0
3·8
4·6
5·4
Ln TIME

FIGURE 42a: First order model curves for barium carbonate-titania mixtures in vacuo.

FIGURE 42b: Arrhenius plots for barium carbonate-titania mixtures in vacuo.

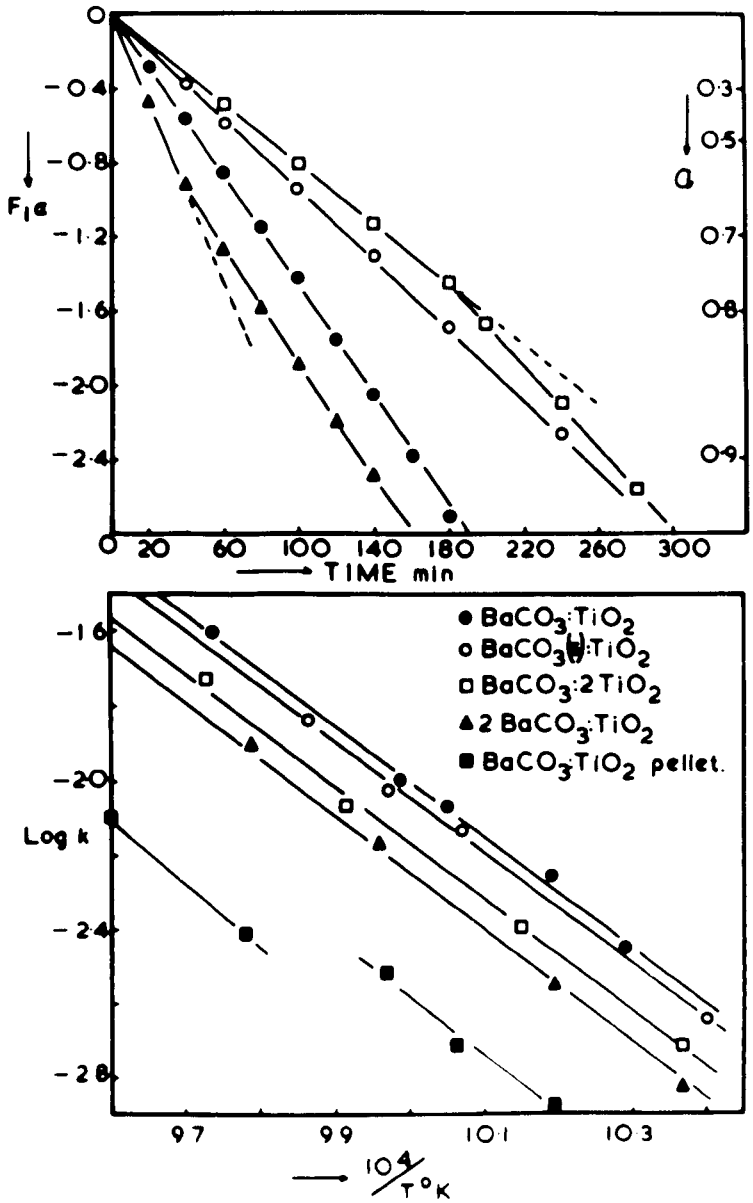
0
-0·4
-0·8
-1·2
-1·6
-2·0
-2·4
F(α)
0·3
0·5
0·7
0·8
0·9
α
0 20 60 100 140 180 220 260 300
TIME min
-1·6
-2·0
-2·4
-2·8
Log k
● BaCO3:TiO2
○ BaCO3:TiO2
□ BaCO3:2TiO2
▲ 2 BaCO3:TiO2
■ BaCO3:TiO2 pellet.
9·7 9·9 10·1 10·3
10⁴/T°K

FIGURE 43a: LnLn analysis curves $BaCO_3$ (ℓ): TiO_2 powder samples in vacuo.

FIGURE 43b: LnLn analysis curves for $BaCO_3$ (ℓ): TiO_2 pellets in vacuo.

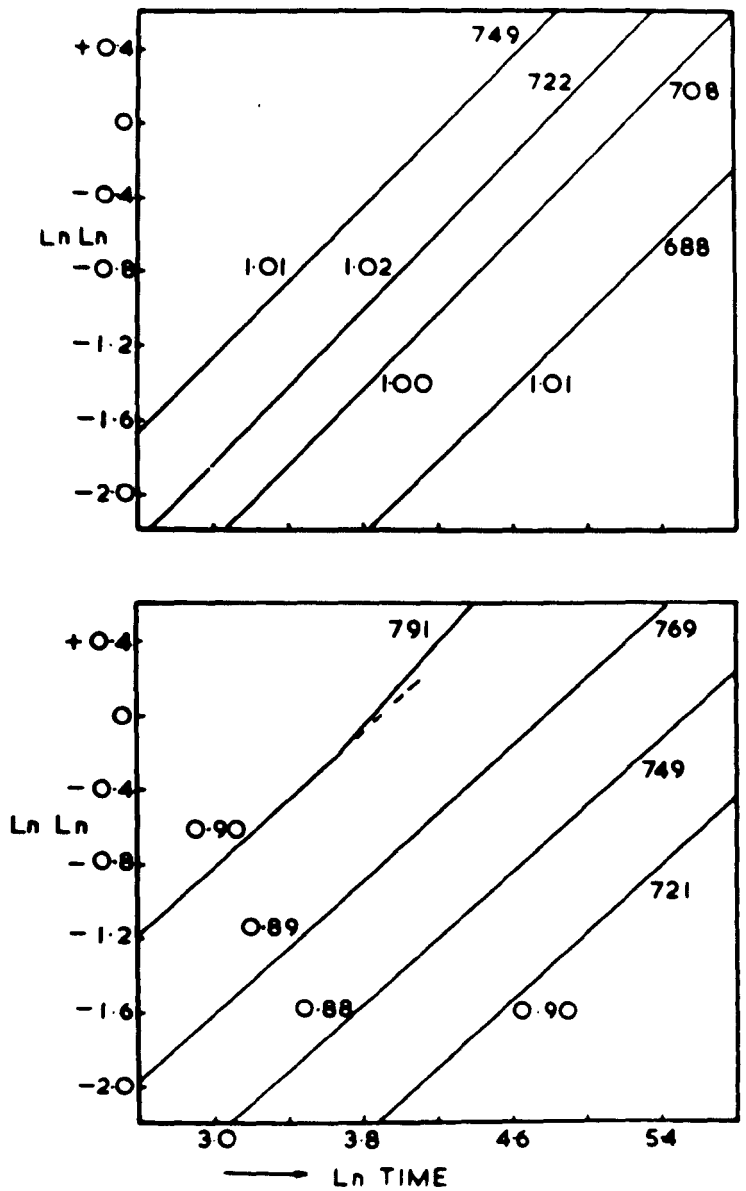
+0·4
0
−0·4
Ln Ln
−0·8
−1·2
−1·6
−2·0
749
722
708
688
1·01
1·02
1·00
1·01
+0·4
0
−0·4
Ln Ln
−0·8
−1·2
−1·6
−2·0
791
769
749
721
0·90
0·89
0·88
0·90
3·0
3·8
4·6
5·4
Ln TIME

FIGURE 44a: Scanning electron micrograph of 1:1 mole $BaCO_3(\ell):TiO_2$ decomposed in vacuo

$\alpha = 0.35$ Magnification x 5,800

FIGURE 44b: Scanning electron micrograph

$\alpha = 0.70$ Magnification x 6,000

FIGURE 44c: Scanning electron micrograph

$\alpha = 1.00$ Magnification x 5,500

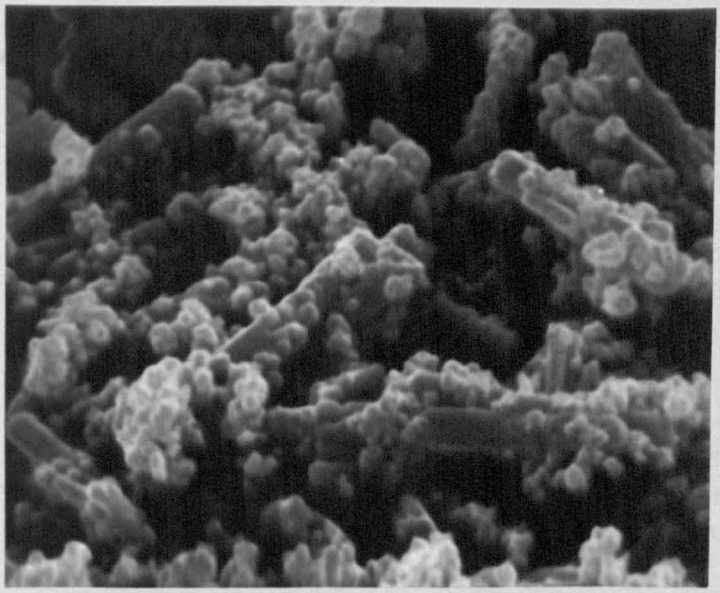

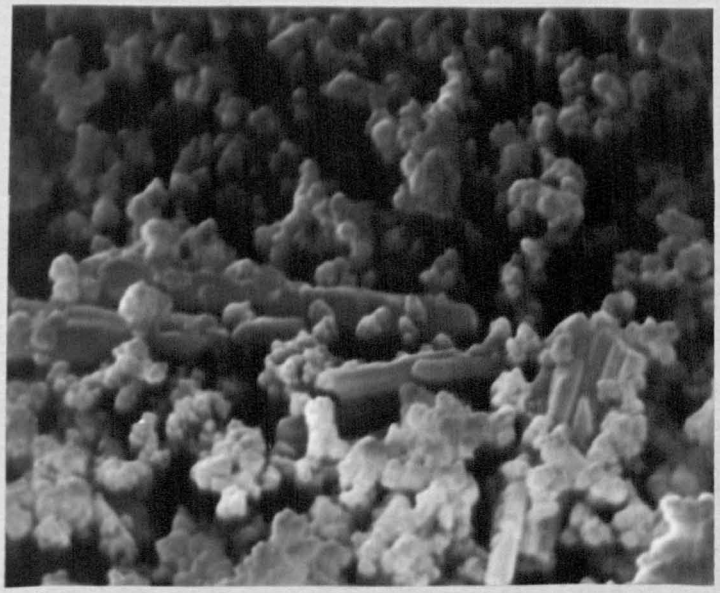

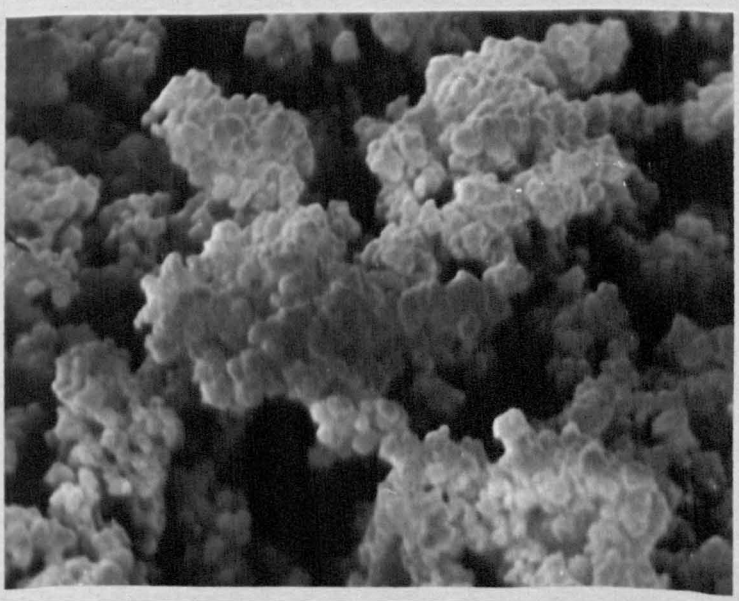

FIGURE 45a: LnLn analysis curves for $BaCO_3$(ℓ): $2TiO_2$ samples in vacuo.

FIGURE 45b: LnLn analysis curves for $2BaCO_3$(ℓ): TiO_2 samples in vacuo.

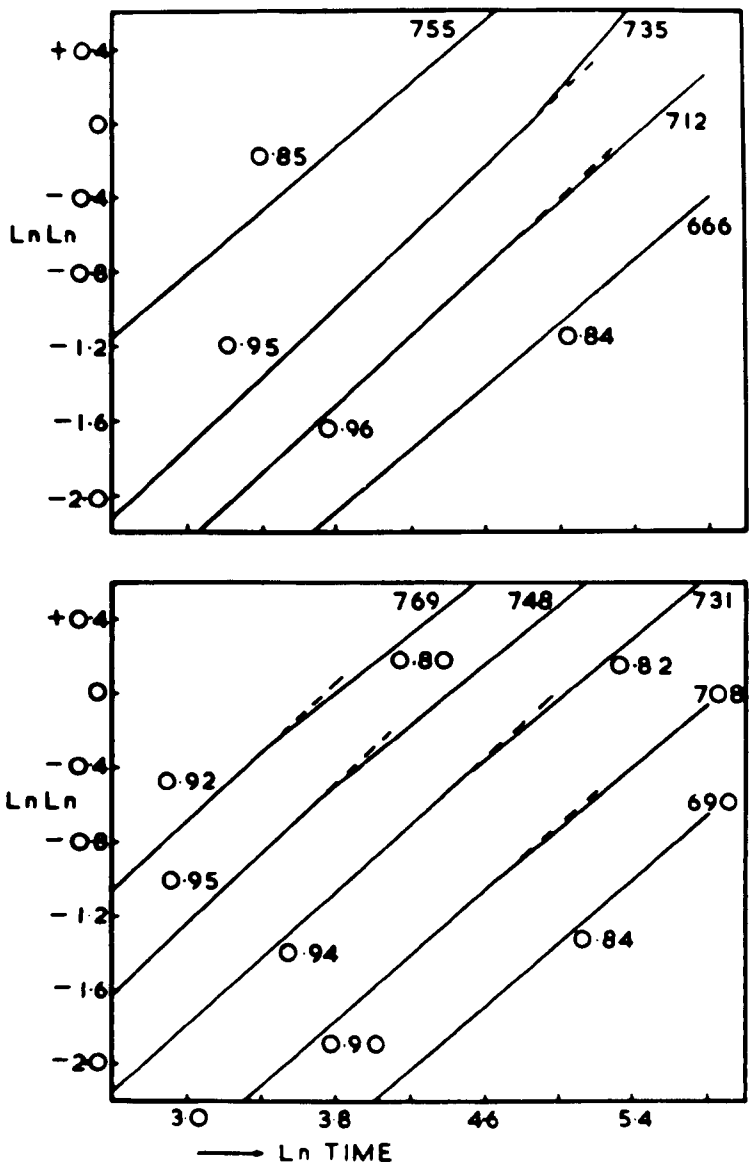
755
735
712
666
0·85
0·95
0·96
0·84
+0·4
0
−0·4
−0·8
−1·2
−1·6
−2·0
Ln Ln
769
748
731
708
690
0·80
0·82
0·92
0·95
0·94
0·90
0·84
3·0
3·8
4·6
5·4
Ln TIME

CHAPTER 12

The Decomposition Kinetics of $BaCO_3$-GeO_2 Systems in Vacuo

The x-ray analysis of partial reaction products of the 1:1 barium carbonate:germania system showed that this system was an example of the situation in which only the 2:1 compound, Ba_2GeO_4, is formed during the evolution of carbon dioxide, and the reaction between germania and Ba_2GeO_4 to form $BaGeO_3$ begins when the carbonate decomposition is complete (cf. $BaCO_3$-TiO_2 systems). The SEM investigation of this system showed that the degree of contact between oxide and carbonate was never as good as that in the titania system, and therefore, instead of investigating changes of mechanism with different compositions, the germania system was studied in terms of the number of particle-particle contacts related to the effects of different mixing media. The x-ray analysis of partial reaction products in air indicated that the different mixing media did not alter the compound formation sequence, but only the speed of formation, and the SEM investigation showed that this was related to the different aggregation states of germania in the two mixing media (Figures 46(a) and (b)).

12.1. Experimental

151mg samples of $BaCO_3$(s):GeO_2, mixed in acetone, were examined in detail, using the vacuum thermobalance,

and this sample weight corresponded to an effective weight of barium carbonate of 100mg, so that the data could be compared directly with that for the decomposition of barium carbonate alone. The LnLn analysis, Figure 47(b), indicates that the process is not isokinetic, and the mechanism appears to change from zero order to first order, and finally a 0.8 law as the temperature falls from 786° to 688°C. In the temperature range from 700° to 750°C the observed activation energy was 66 kcal/mole, and x-ray analysis indicated that Ba_2GeO_4 was the sole reaction product during the decomposition of the carbonate. However, in the temperature range from 750 to 790°C, the observed activation energy was ~90 kcal/mole, and again Ba_2GeO_4 was the sole reaction product.

151mg samples of $BaCO_3(\ell):GeO_2$ were used to investigate the effects of different mixing media on the rate of reaction, since the mixing geometry of this system is more susceptible to the mixing media than that of the spherical carbonate-germania mixtures. The data for both lath- and spherical-carbonate mixtures are shown in Figure 48(a), and the increase in reactivity, due to mixing in water, is much greater for the lath carbonate mixtures than the spherical carbonate samples. Since the increase in reactivity was so large that the initial 40% reaction of water prepared samples could not be followed on the thermobalance and a weight loss

was observed, even before the sample could possibly have reached temperature, the water mixtures were studied, using thermogravimetry in a nitrogen atmosphere. The Stanton thermobalance used in the investigation of the decomposition of barium carbonate (Chapter 8) was utilised for this purpose, and a heating rate of 7°C/min. was maintained from room temperature to 1200°C. 200mg samples of the lath carbonate-germania mixtures were used, and the data are shown in Figure 48(b). A sample that had been mixed in water and dried, was damped in acetone before heating, and the decomposition curve for this sample was identiaal to that of the water prepared sample.

A 30mg sample of the water mixed carbonate-germania was dried overnight at ~150°C. The decomposition of this sample in vacuo was investigated using an A.E.I. MS10 mass spectrometer, and the first detectable product was water vapour at ~400°C. At higher temperatures, (above 450°C), carbon dioxide, carbon monoxide and oxygen were observed. The temperature difference between the detection of water vapour and the reaction occurring at 200° to 400°C in the thermogravimetry, was related to the operating conditions of the mass spectrometer, and there is no doubt that the weight loss at 200°-400°C in the thermobalance is due to the loss of water. The 'germania complex' causing this loss of water was calculated to have a formula approximately to $GeO_2:\frac{1}{2}H_2O$, and infrared

analysis of a water prepared mixture did not indicate the presence of hydroxide groups. A sample of germania that had been mixed in water and dried, was heated in the thermobalance, and no weight loss was observed. This indicates that the formation of the complex, $GeO_2:\frac{1}{2}H_2O$, depends on the presence of barium carbonate in the water mixing stage, therefore, is probably related to the pH of the mixing media. X-ray analysis of acetone and water prepared samples that had not been reacted showed that the germania was in different forms in the two samples, and this is illustrated in Table 20.

TABLE 20: Experimental and Literature 2θ Values for GeO_2

	2θ	Values
GeO_2 ($BaCO_3(\ell):GeO_2$ Acetone)	26.0	38.0
'GeO_2' ($BaCO_3(\ell):GeO_2$ Water)	28.5	37.3
Literature GeO_2	25.96	37.93
Literature GeO_2 (tetragonal)	28.68	37.44

12.2. Discussion

As predicted by the SEM investigation, the reaction mechanisms of all the barium carbonate-germania mixtures could not be determined, but the observed activation energy of 66 kcal/mole is very similar to the heat of formation of Ba_2GeO_4 (61 kcal/mole), indicating that the formation of this compound is the rate controlling step in the decomposition of 1:1 barium carbonate:germania mixtures. The activation energy of $\sim$90 kcal/mole in

the temperature range 750° to 790°C is of questionable significance as the reaction rates in this temperature range are of the same order as those in the barium carbonate-zirconia and barium carbonate alone systems, where anomalous results are obtained. Since the sample weights (151mg) used in the barium carbonate-germania studies were larger than those used in the barium carbonate-zirconia and barium carbonate systems (100mg), bed pressure effects may be expected to be more important at fast reaction rates than self-cooling effects resulting in an increase in the observed activation energy at fast reaction rates.

The effect of a water mixing media on the aggregation of germania particles is illustrated in Figure 46(b). The micrograph does not indicate the formation of a 'water complex' of germania as might be expected in the titania and tin systems, where the oxide changes from a granular form in an acetone mix to a fluffy appearance after mixing in water (see Figures 49(a) and (b). However, the mass spectrometer data, together with the thermal analysis results, proves that the initial weight loss in barium carbonate-germania samples prepared in water, is solely due to the loss of water. One interesting aspect of this phenomenon concerns the similarity of the experimental weight losses of acetone and water prepared samples; the total weight loss in both these systems agrees with the theoretical

weight loss within the limits of experimental error, and it appears that the increase in weight loss due to the loss of water from the germania complex just happens to compensate almost exactly for the reduced weight loss from the smaller amount of barium carbonate in the mixture. Therefore, in isothermal experiments, the initial weight loss due to water may go unnoticed if the temperature is high enough for the decomposition of the carbonate to proceed sufficiently rapidly, and the increased reactivity of water prepared samples would be wrongly thought to be related only to the increased particle-particle contacts in such mixtures. The exact nature of the germania complex could not be determined, as the infrared analysis indicated the presence of water in the range 3500 to 3100 cm^{-1}, thus masking any hydroxide peaks. The x-ray analysis data also did not clarify the situation but only served to illustrate a change in the form of the germania (Table 20).

FIGURE 46a: Scanning electron micrograph of 1:1 mole $BaCO_3$(ℓ):GeO_2 (mixed in acetone)
Magnification x 2,200

FIGURE 46b: Scanning electron micrograph of 1:1 mole $BaCO_3$(ℓ):GeO_2 (mixed in water)
Magnification x 2,200

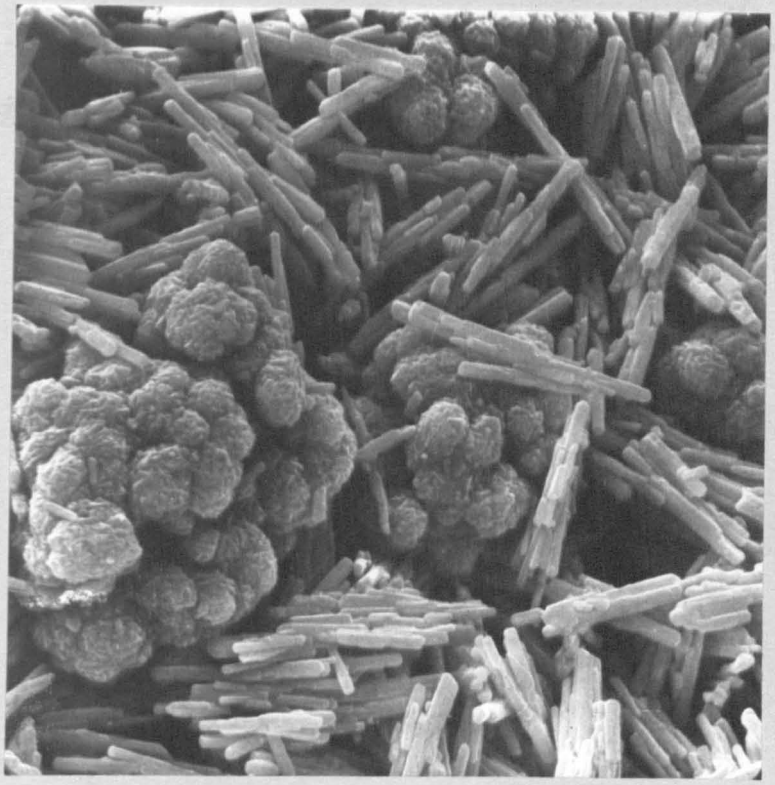

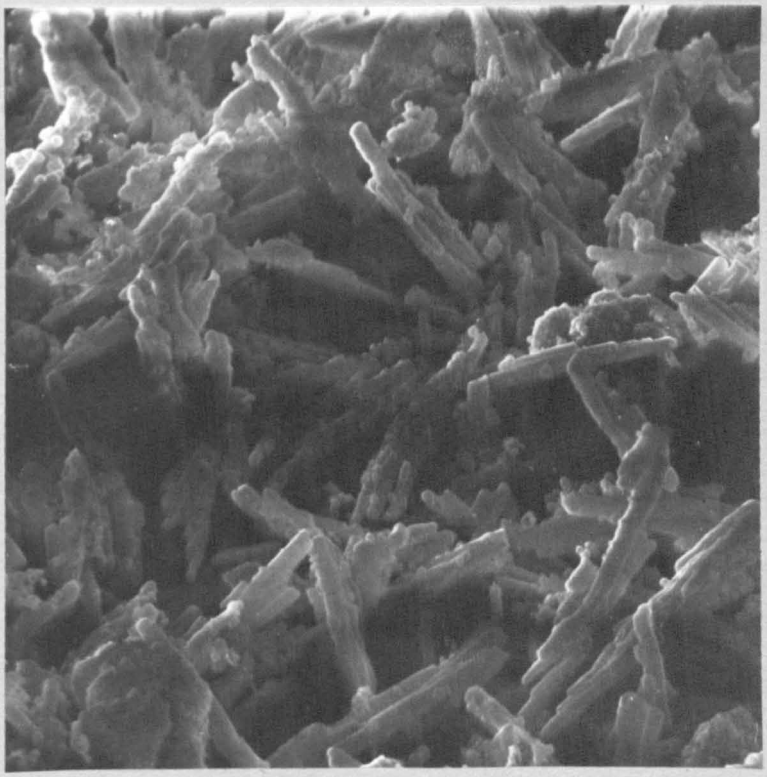

FIGURE 47a: Arrhenius plot for $BaCO_3$(s):GeO_2 samples in vacuo.

FIGURE 47b: LnLn analysis curves for $BaCO_3$(s): GeO_2 samples in vacuo.

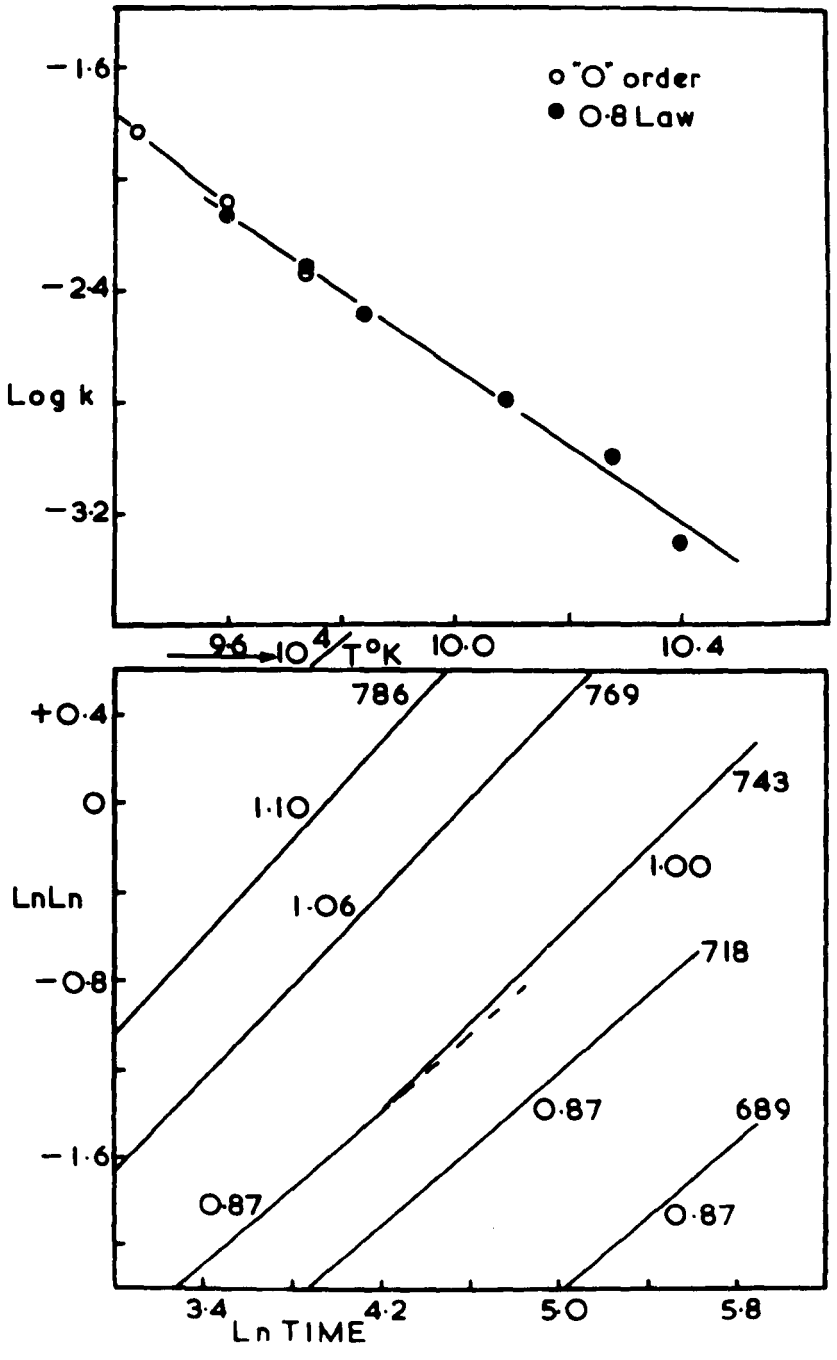
o "O" order
● 0·8 Law
−1·6
−2·4
−3·2
Log k
9·6
10⁴/T°K
10·0
10·4
+0·4
0
−0·8
−1·6
LnLn
786
769
743
718
689
1·10
1·06
1·00
0·87
0·87
0·87
3·4
4·2
5·0
5·8
Ln TIME

FIGURE 48a: Isothermal weight change curves for barium carbonate-germania samples in vacuo.

FIGURE 48b: Thermogravimetric curves for $BaCO_3$(ℓ):GeO_2 samples prepared in water and acetone.

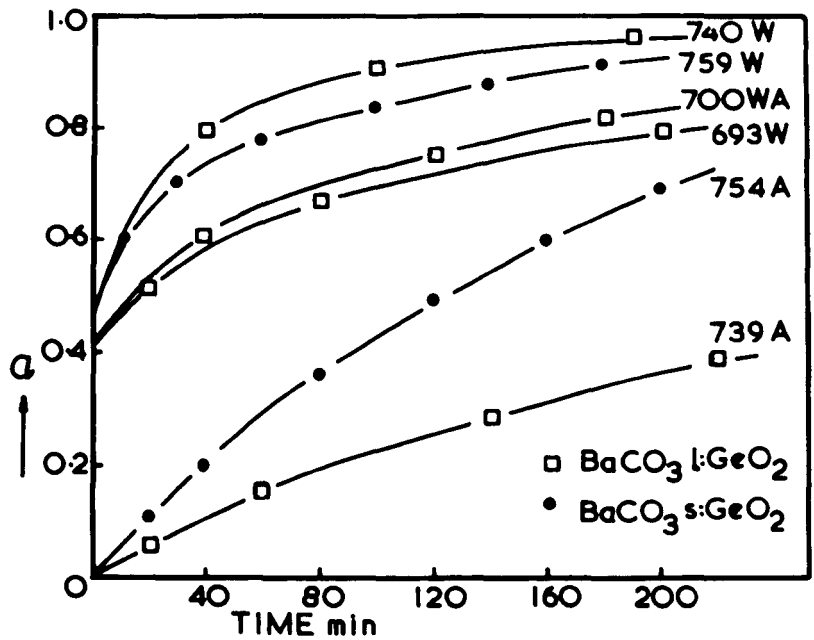
1·0
0·8
0·6
0·4
0·2
0
a
740 W
759 W
700WA
693W
754 A
739 A
□ BaCO3 l:GeO2
• BaCO3 s:GeO2
40
80
120
160
200
TIME min

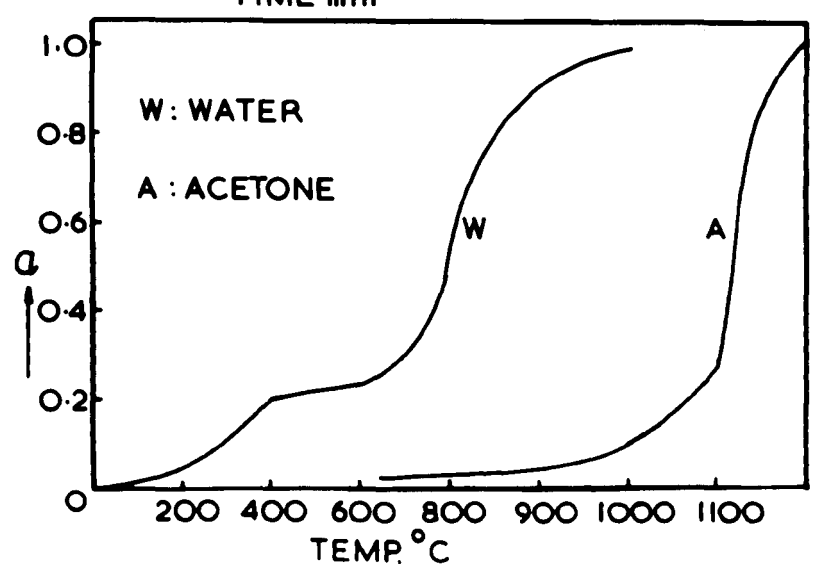
1·0
0·8
0·6
0·4
0·2
0
a
W: WATER
A : ACETONE
W
A
200
400
600
800
900
1000
1100
TEMP. °C

CHAPTER 13

The Decomposition Kinetics of $BaCO_3$-SnO_2 and $BaCO_3$-SiO_2 Systems in Vacuo

13.1. Barium Carbonate-Stannic Oxide

The preliminary experiments on this system indicated that the 2:1 compound, Ba_2SnO_4, was formed during the evolution of carbon dioxide and only reacted with the excess tin oxide to form $BaSnO_3$ when the decomposition of the carbonate was complete (Figure 13). However, there was always some uncertainty concerning the nature of the product formed in this system, since the two compounds, $BaSnO_3$ and Ba_2SnO_4, are very similar in structure and cannot be easily differentiated using x-ray and infrared techniques. SEM showed that the mixing geometry of the barium carbonate tin oxide system was very similar to that of the barium carbonate-tiania system, and that reaction mixtures containing the lath barium carbonate were more suitable for kinetic model studies than those containing the spherical carbonate, Figures 49(a) and (b).

13.1.1. Experimental

150mg samples were used for the vacuum studies, and an acetone damping technique was used to give consistent packing of the acetone prepared mixtures. Absolute α values could not be obtained, since metallic tin was always formed on heating the sample to attain complete

decomposition, and consequently the time zero catheto-meter reading could only be obtained by extrapolation of the readings obtained in the initial stages of reaction (see Chapter 4).

A mixture containing the spherical barium carbonate followed a first order model up to at least 94% reaction, and this is shown in Figure 50(a), together with some data for 1:1 lath carbonate:stannic oxide samples. The α v t and LnLn analysis of the lath system are shown in Figures 51(a) and (b), and a change in reaction mechanism is indicated by the change in m value from 0.86 to $\sim$0.36. The change in mechanism was accompanied by differences in the nature of the deposits found on the crucible for partially reacted samples, and this effect is illustrated in Table 21.

TABLE 21: Nature of the Deposits on Platinum Crucibles In the $BaCO_3$-SnO_2 System

Temperature °C	Kinetic Model	Nature of crucible deposits
$\sim$900	unknown	black metallic coating on the crucible
790	first order	no deposits
766	$\sim$first order	slight black spotting on the crucible
745	m $\sim$0.36	severe spotting
703	unknown	golden coating

The anomalous reaction rate of the 783°C sample (Figure 51(a)) could not be explained in terms of the errors involved in the approximated α values, and the Arrhenius plot for the 1:1 barium carbonate:stannic oxide system, using a first order model, is shown in Figure 50(a).

13.1.2. Discussion

The free energy data for silica, titania zirconia and stannic oxide indicates that stannic oxide is the least stable of these four oxides, Figure 53. The minimum P_{CO}/P_{CO_2} to prevent reduction of stannic oxide at 800°C is 1:4, and any P_{CO}/P_{CO_2} greater than this value will result in $SnO_2 \longrightarrow Sn + [O_2]$. The minimum P_{CO}/P_{CO_2} at 800°C for silica, titania and zirconia are 10^8:1, 10^9:1 and 10^{12}:1 respectively, and therefore the reduction of stannic oxide to a lower oxide or the metal is much more likely than a reduction of any of the other oxides. However, the effective atmosphere generated within the vacuum thermobalance under working conditions, is unknown, so that a reduction of stannic oxide can be shown to be possible, but not predictable.

When there is little or no attack on the platinum crucible, both the spherical and lath carbonate mixtures are very similar to the 1:1 barium carbonate:titania system in that they follow a first order model up to very high values of fraction reacted, and this may be related to the similar mixing geometry of these systems.

However, the reduction of stannic oxide during the decomposition of 1:1 barium carbonate:stannic oxide samples, makes a meaningful kinetic model examination of this system difficult, and so this system was not studied as extensively as the titania systems.

13.2. Barium Carbonate-Silica

The preliminary experiments on the barium carbonate-silica system indicated that this system would be the most difficult to evaluate. The reaction products of isothermal decomposition in air did not conform to any established data (see Table 11), and the SEM investigation indicated that none of the barium carbonete:silica mixtures were suitable for kinetic model studies. The optimum mixing geometry was found in the 1:1 spherical carbonate:silica system where quartz fragments are coated by spherical particles of barium carbonate Figure 54(a). The coating is not continuous, but the degree of contact is much higher than in mixtures containing a precipitated form of silica Figure 54(b).

13.2.1. Experimental

125mg samples were used in this investigation so that the data could be directly compared with the data for all the other carbonate-metal oxide mixtures. Acetone damping was used to give consistent packing of the powder mixture in the platinum crucible. The

LnLn analysis, Figure 52(b), illustrates that although the mechanism is unknown, the process appears to be isokinetic at low temperatures, but changing at the highest temperatures. The observed activation energy is ~50 kcal/mole in the temperature range from 700° to 760°C, and 39 kcal/mole in the range from 780° to 815°C.

13.2.2. Discussion

The reaction mechanism of barium carbonate: silica mixtures cannot be interpreted in terms of classical reaction models, and this was predicted by the results of the SEM investigation of the mixing geometry of these mixtures. However, the observed activation energy of ~50 kcal/mole is similar to the value for the heat of formation of Ba_2SiO_4, indicating that the formation of this compound is the rate controlling step in the decomposition of 1:1 mole mixtures of barium carbonate:silica. In the temperature range 780° to 815°C, the observed activation energy is ~39 kcal/mole, which is very similar to the values obtained for the barium carbonate-zirconia system, and the decomposition of barium carbonate at temperatures where self-cooling effects are thought to be important due to the fast reaction rates. It was unfortunate that a silica sample could not be obtained so that the mixing geometry of barium carbonate-titania samples was simulated in the barium carbonate-

silica system and hence confirm that a first order reaction model is obtained in reaction mixtures having a 1:1 barium carbonate:titania type mixing geometry, as indicated by the data for the tin and titania systems.

FIGURE 49a: Scanning electron micrograph of 1:1 mole $BaCO_3(\ell):SnO_2$ (mixed in acetone)
Magnification x 2,300

FIGURE 49b: Scanning electron micrograph of 1:1 mole $BaCO_3(\ell):SnO_2$ (mixed in water)
Magnification x 2,300

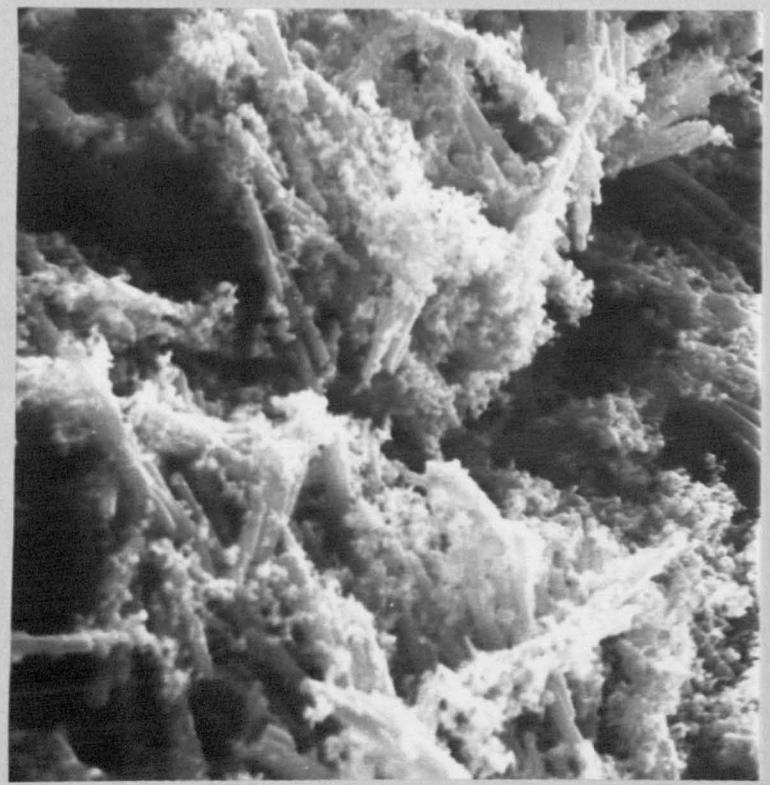

FIGURE 50a: Arrhenius plot for $BaCO_3(\ell):SnO_2$ samples in vacuo.

FIGURE 50b: First order model curves for $BaCO_3(\ell):SnO_2$ and $BaCO_3(s):SnO_2$ samples in vacuo.

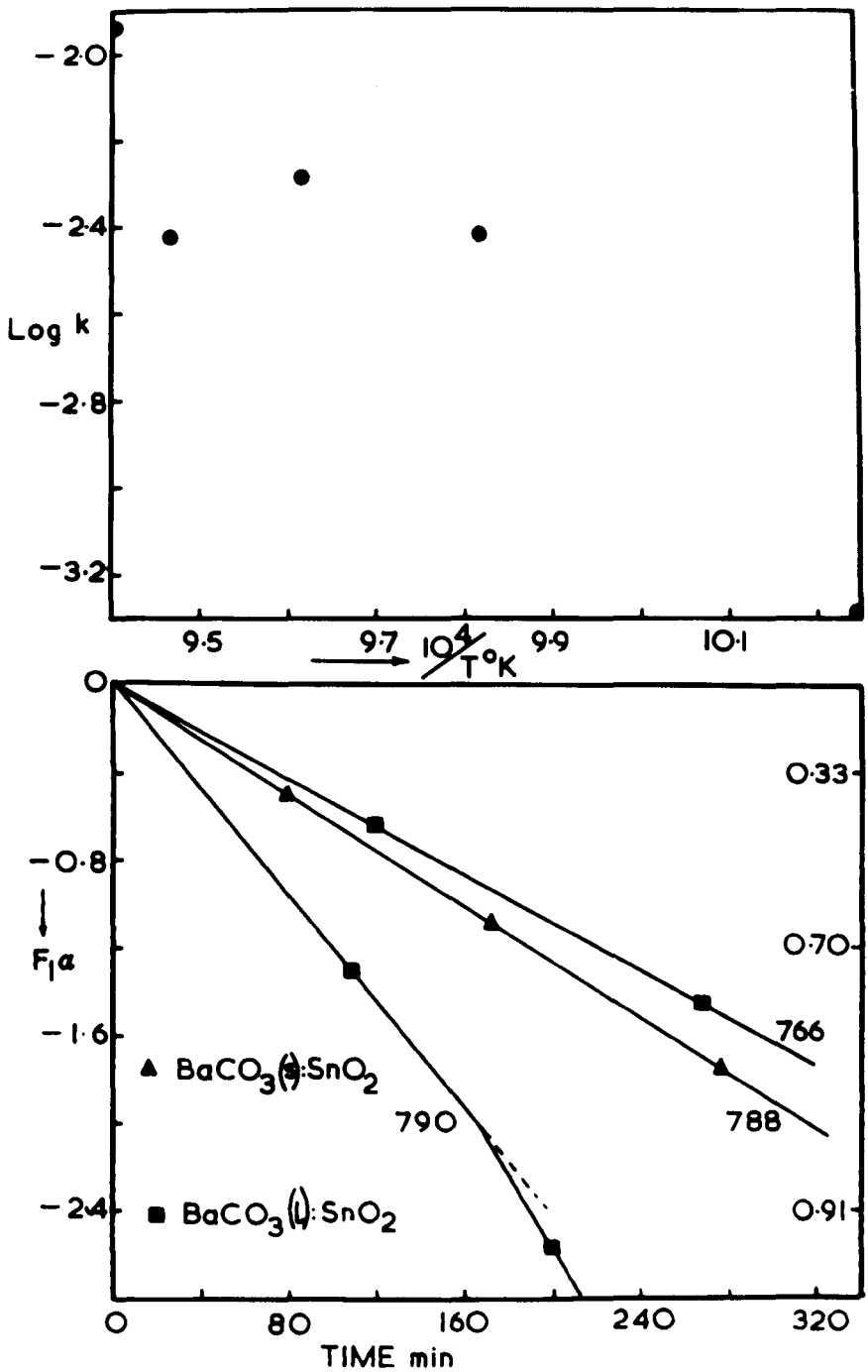
-2·0
-2·4
Log k
-2·8
-3·2
9·5
9·7
10⁴/T°K
9·9
10·1
0
0·33
-0·8
0·70
F1a
a
-1·6
766
▲ BaCO3(i):SnO2
790
788
-2·4
■ BaCO3(i):SnO2
0·91
0
80
160
240
320
TIME min

FIGURE 51a: Isothermal weight change curves for $BaCO_3(\ell)$:SnO_2 samples in vacuo.

FIGURE 51b: LnLn analysis curves for $BaCO_3(\ell)$: SnO_2 samples in vacuo.

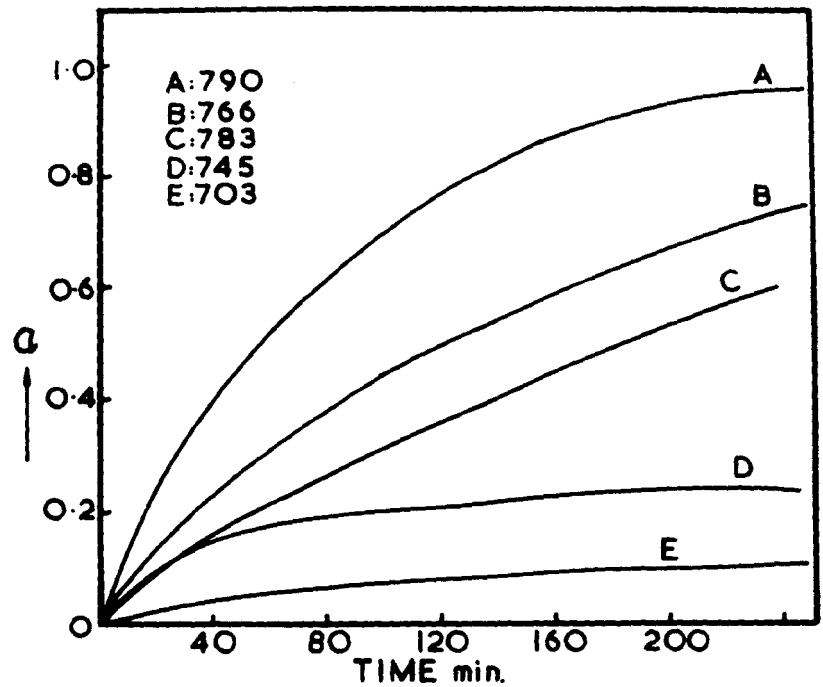
A:790
B:766
C:783
D:745
E:703
1·0
0·8
0·6
0·4
0·2
0
a
A
B
C
D
E
40
80
120
160
200
TIME min.

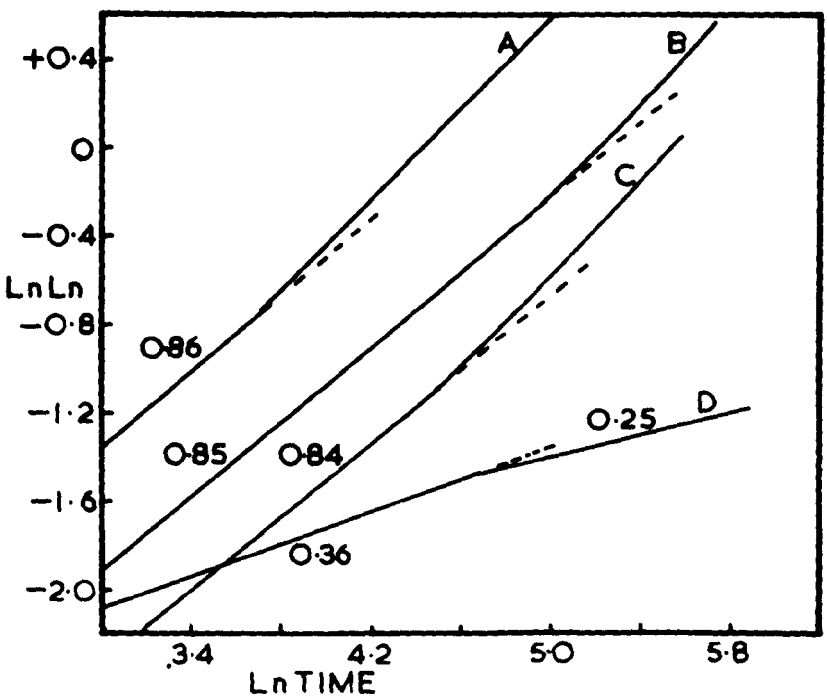
+0·4
0
−0·4
−0·8
−1·2
−1·6
−2·0
LnLn
A
B
C
D
0·86
0·85
0·84
0·36
0·25
3·4
4·2
5·0
5·8
Ln TIME

FIGURE 52a: Isothermal weight change curves for $BaCO_3(s):SiO_2II$ samples in vacuo.

FIGURE 52b: LnLn analysis curves for $BaCO_3(s):SiO_2II$ samples in vacuo.

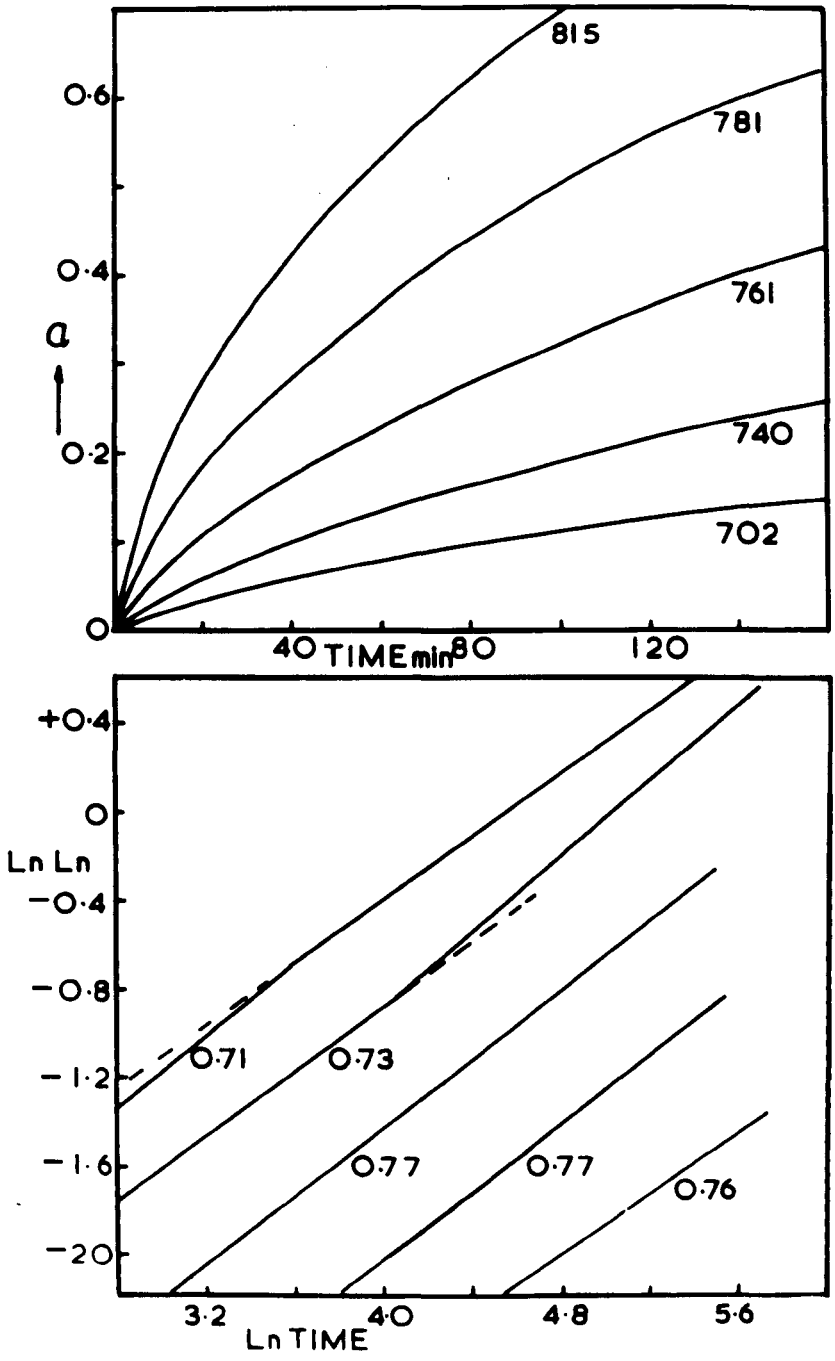
815
781
761
740
702
0·6
0·4
a
0·2
0
40
TIME min
80
120
+0·4
0
Ln Ln
−0·4
−0·8
−1·2
−1·6
−2·0
0·71
0·73
0·77
0·77
0·76
3·2
4·0
4·8
5·6
Ln TIME

FIGURE 53: Free energy data for SnO_2, SiO_2, TiO_2 and ZrO_2.

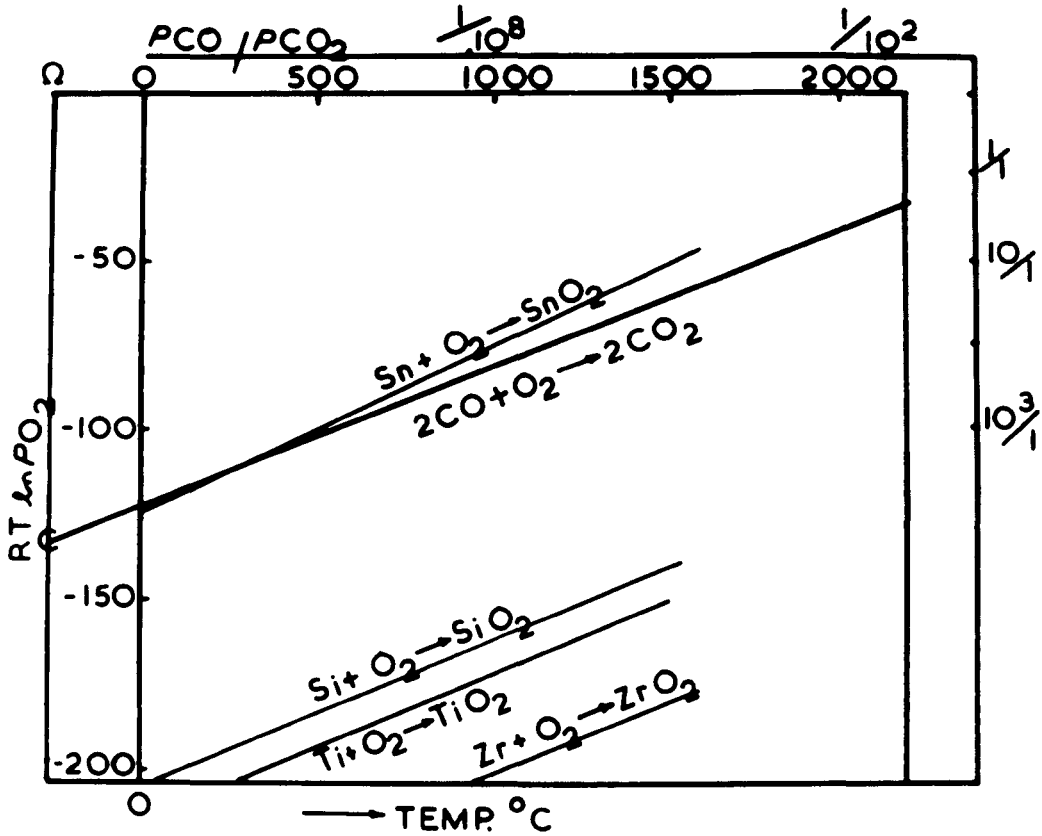
PCO / PCO2
1/10^8
1/10^2
Ω
0
500
1000
1500
2000
1/1
10/1
10^3/1
-50
-100
-150
-200
RT ln PO2
Sn + O2 → SnO2
2CO + O2 → 2CO2
Si + O2 → SiO2
Ti + O2 → TiO2
Zr + O2 → ZrO2
0
TEMP. °C

FIGURE 54a: Scanning electron micrograph of 1:1 mole $BaCO_3(s):SiO_2$ II
Magnification x 5,200

FIGURE 54b: Scanning electron micrograph of 1:1 mole mixture containing a precipitated silica
Magnification x 1,000

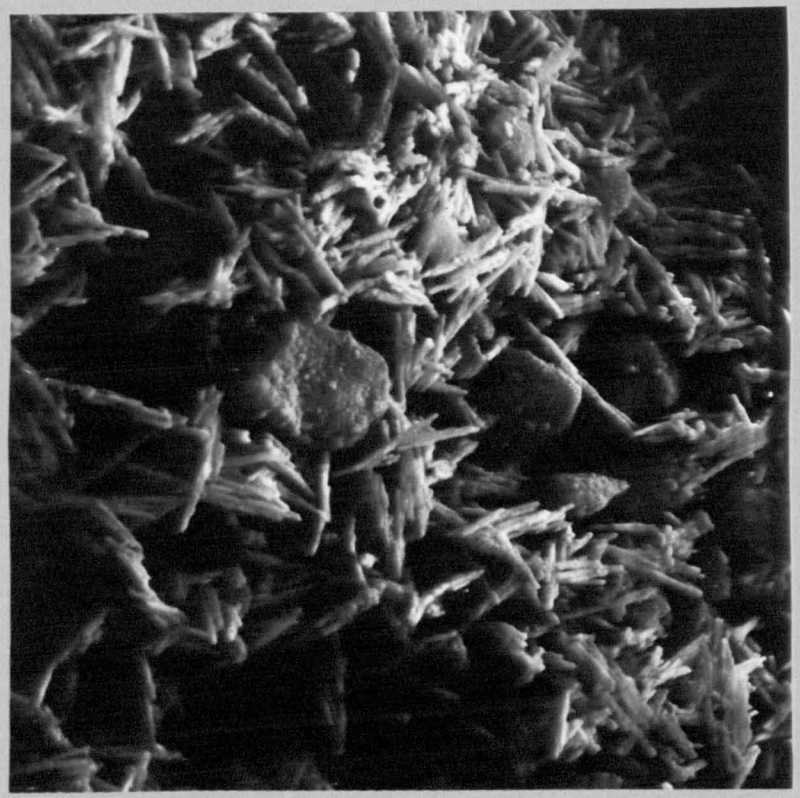

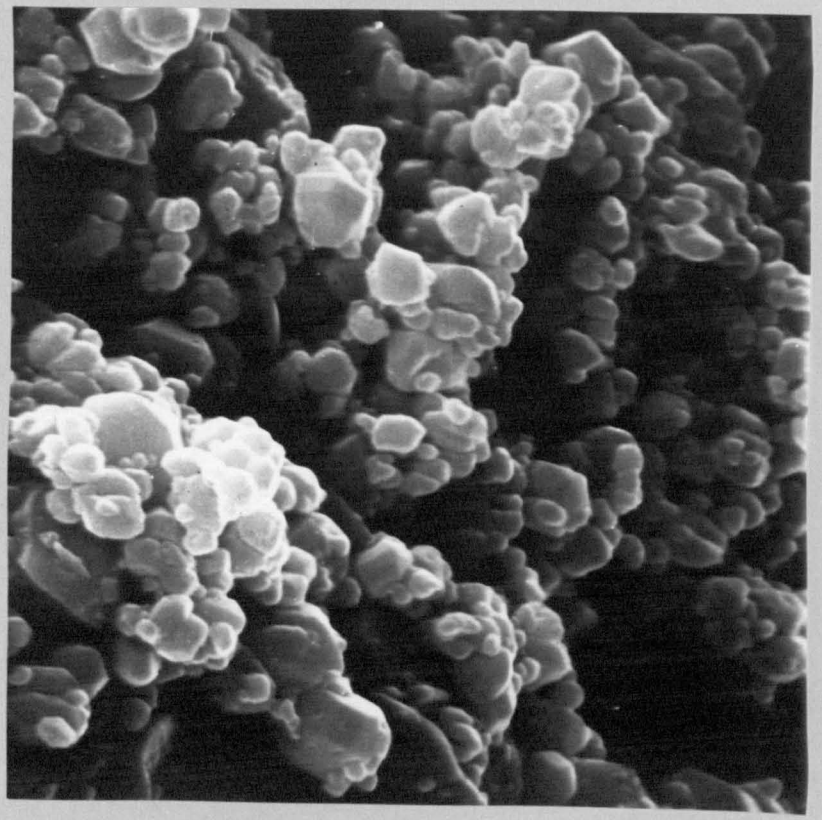

CHAPTER 14

Discussion

The kinetics of many solid state decompositions have been studied by dynamic thermal methods such as TG and DTA. This approach has been criticised since the constantly increasing temperature inevitably results in temperature gradients within the sample. Heat is evolved or taken in by the sample during reaction, so that the temperature gradient within the sample changes in a complex and variable manner. The kinetics of solid state reactions can only be investigated when the temperature gradient is sufficiently small that heat transfer effects within the sample can be neglected, and this requires the use of very small samples. More recently, it has been realised that heat transfer effects may control the kinetics of a reaction studied under isothermal conditions. Hills[11] has suggested that the decomposition of calcium carbonate can be related to a heat-mass transfer model, and is not controlled by a chemical step at the reaction interface. It seems certain that transfer of heat to the interface, and mass transfer away from the interface, governed the kinetic behaviour observed by Hills for ~2g samples and half lives of ~40 minutes. Vallet and Richer[30] have suggested that the decomposition of calcium carbonate is controlled by heat conduction to and within the sample.

On the other hand, heat and mass transfer should cease to be gross effects with extremely small samples, and a chemical step may then control the reaction. In many previous investigations, sample weights of ~ 1g have been used, yet it has been assumed that heat transfer effects are negligible, and that a chemical step controls the reaction.

It has been widely recognised that small samples and slow reaction rates should be used in isothermal kinetic studies to reduce self cooling effects within the sample, and so minimise departures from isothermal conditions. The extent of self cooling will depend on several factors, e.g. the heat of reaction, the sample size, the rate of reaction, but may be considered in terms of the absolute reaction rate measured in mg. of CO_2 evolved/minute. Thus the temperature of a small sample, reacting at a fast rate, may drop more than that of a large sample reacting slowly, although the total loss of carbon dioxide and the amount of heat required are greater for the larger sample. Hills observed a maximum temperature drop of ~ 40°C in the decomposition of 2g samples of calcium carbonate at a rate having a half life of ~40 minutes. A rough calculation suggests that a maximum temperature drop of ~ 2°C would be likely to occur in a 100mg sample reacting at a comparable rate. By using very

small samples and slow reaction rates, the self cooling effect should be reduced still further, and some data for calcium carbonate is shown in Table 23.

TABLE 23: Self Cooling in the Decomposition of Calcium Carbonate (using isothermal DTA, Tinsley[31]).

Sample Weight mg	Temperature °C	ΔT °C	Time for complete reaction minute
100	700	0.2	270
200	700	0.2	400
300	700	0.2	520
900	810	10	70
300	860	10	20

However, in this investigation, even when precautions were taken, self cooling was thought to have exceeded the limits of the isothermal enclosure ($\sim \pm$ 2°C). The temperature drop of the samples in this investigation could not be measured, due to practical difficulties in incorporating a thermocouple within the sample, but self cooling effects were thought to be indicated by the curvature of the Arrhenius plots at the fast reaction rates. Bed pressure effects can also lead to non-linear Arrhenius plots, but this investigation has indicated that bed pressure effects result in a displacement of the Arrhenius plots, similar to the results obtained

by Tinsley[29] in the decomposition of calcium carbonate under different P_{CO_2} atmospheres. Self cooling effects are also indicated by the apparent phase transformation temperatures of barium carbonate samples in nitrogen. A change to zero order kinetics is indicative of the phase transformation, and the temperature of transformation as recorded on the Stanton thermobalance is always higher than the literature values; the temperature is the same for 100 and 200mg. samples (~981°C), but is higher for 50mg samples (~993°C), possibly indicating a larger temperature drop, due to self cooling of 50mg samples, than occurs for 100 and 200mg samples.

It has often been suggested that reactions involving the evolution of a gaseous product should be investigated in an atmosphere of the same gas. However, liquid formation and the resultant zero order kinetics, which occurs even at low carbon dioxide pressures, prohibit meaningful kinetic mechanism studies of barium carbonate over a wide temperature range, and vacuum conditions must be used to prevent liquid formation during the reaction. The results obtained for the decomposition of powder samples of barium carbonate in nitrogen are similar to those obtained for the decomposition of calcium carbonate[28], where small samples follow a zero order model, larger samples follow an $R_2\alpha$ model, and even larger samples (~300mg)

tend to follow an $R_3\alpha$ model. The decomposition data for 100mg samples of barium carbonate in vacuo are difficult to interpret, even when self cooling effects are thought to be minimal. A constant induction period was observed for the decomposition of 25mg samples of $BaCO_3(s)$ and $BaCO_3(\ell)$ (washed in water), whilst the untreated $BaCO_3(\ell)$ showed a progressive increase in the induction period as the temperature was lowered. This is the only system in which induction periods were observed, and unfortunately the vacuum thermobalance is not suitable for absolute measurements of the decomposition of 25mg samples, since the total weight loss is only $\sim$ 5mg.

The experimental results for the systems at reaction rates at which self cooling effects are not apparent, show that the observed activation energy is comparable with the heat of formation of the reaction product. (Table 22). The barium carbonate-titania system is of particular interest, since the observed activation energy is independent of the composition of the mixture, and similar to the heat of formation of Ba_2TiO_4. Similarly, the observed activation energies for 1:1 mole mixtures of barium carbonate-germania and barium carbonate-silica, are comparable with the heats of formation of Ba_2GeO_4 and Ba_2SiO_4 respectively. The free energy data for the barium carbonate-titania

system indicates that $BaTiO_3$ should be the first compound formed in the decomposition of barium carbonate-titania mixtures, and it seems reasonable to conclude that a similar argument will apply to the other carbonate-oxide systems. However, a 1:1 compound was not observed as the initial reaction product in the decomposition of any of the barium carbonate-metal oxide mixtures, and the 2:1 compound was always found as the reaction product of all the systems during the decomposition of the barium carbonate. The close correspondence of the experimental activation energy with the heat of reaction for a variety of endothermic reactions, has been noted by Fishbeck and Snaidt[32] as long ago as 1932. Garner[3] has suggested that the close correspondence of the two energies occurs when the rate-of-decomposition studies are conducted under reversible conditions. Both the forward and reverse reactions would be involved, and the magnitude of the change in rate, with change in temperature, would be controlled by the magnitude of the heat of reaction, rather than by either, the activation energy of only the forward reaction or only the reverse reaction. Hills[11] has shown that a heat-mass transfer model for the decomposition of calcium carbonate indicates that the activation energy will be virtually equal to the heat of reaction, since the rate of movement of the interface

($CaO/CaCO_3$) is almost entirely controlled by the decomposition partial pressure.

The x-ray analysis investigation (Chapter 6) has shown that the 2:1 compound was the major reaction product during the decomposition of barium carbonate, regardless of the composition of the carbonate-metal oxide mixture. The reactivity of a mixture was found to depend, not only on the chemical nature of the metal oxide, but also on the particle morphology of both components, and in particular, on the state of aggregation of the oxide. The geometry of a mixture, in particular the number of particle-particle contacts, has been recognised as a major factor in determining the reactivity of a mixture, but direct observation of its effect has been lacking.

Transmission electron microscopy is not a suitable technique for direct observation of the mixing geometry of two phase samples because the sample has to be dispersed in a liquid before examination. In SEM the sample does not have to be dispersed before examination, but merely coated to provide a conducting surface. Therefore the effect of different mixing media, used in the preparation of the sample, on the mixing geometry, and in particular, the aggregation of the oxide, can be observed. This investigation includes one of the first applications of SEM to the geometry of reaction mixtures of two solid phases prior to kinetic mechanism studies.

Kamatsu and other workers have suggested that kinetic studies of two phase reactions should only be attempted when the system corresponds to the ideal case of particles of one component embedded in a continuous matrix of the second component, and therefore the composition of the mixture is controlled by the relative particle sizes and molecular weights of the two components. Compositions of interest to the ceramist are frequently equimolecular with particle sizes such that the ideal geometry is not realised; for barium carbonate-metal oxide systems, the composition of the mixture has to be adjusted to the oxide rich side to comply with the ideal model. When equimolecular compositions are used, SEM is an invaluable aid in deciding whether meaningful kinetic model data can be obtained with the particular mixing geometry of the sample.

A new approach to the analysis of kinetic data combining a nuclei growth analysis with reduced time data has been proposed. The use of this LnLn analysis has proved to be particularly successful in interpreting kinetic data when the mechanism cannot be directly related to a theoretical model. The isokinetic concept, widely used by metallurgists in studies of phase transformations, has been shown to be very useful for observing the temperature dependence of a process and changes in reaction mechanism with temperature. It is somewhat surprising that this technique, or a

similar method, is not in common use in chemical kinetic studies, since changes in reaction mechanism can be shown without the plotting of Arrhenius functions.

Since heat transfer effects have been shown to have widespread significance, it is worth considering the purpose of kinetic studies. There are two approaches; firstly, to obtain information for the sake of scientific knowledge on the reaction mechanisms of ideal systems, and secondly, to obtain practical data on technologically important non-ideal systems. This investigation has shown that it is very difficult to arrange for ideal systems and future investigations might be directed towards the use of large samples and the application of chemical engineering techniques, rather than conventional kinetic thermal analysis to determine reaction mechanisms. The system would be designed so that simple heat transfer models could be derived and tested experimentally, as in the work of Hills on the decomposition of calcium carbonate. Conventional kinetic thermal analysis could still be used to investigate the factors effecting the reactivity of technologically important systems, but without attempting to relate the data to theoretical models.

TABLE 22: A Comparison of Observed Activation Energies and Heats of Formation

System	Activation Energy Kcal/mole	Temperature Range °K	Compound	ΔH_{1100}
$BaCO_3$ (Nitrogen)	60 ± 4	1200-1300	BaO	55
$BaCO_3$ (Vac)	63 ± 5	970-1080	BaO	55
$BaCO_3:TiO_2$	69 ± 4	930-1070	B_2T	64
$BaCO_3:2TiO_2$	69 ± 4	"	B_2T	64
$2BaCO_3:TiO_2$	71 ± 4	"	B_2T	64
$BaCO_3:GeO_2$	66 ± 4	960-1070	B_2G	$\sim 61^{M}$
$BaCO_3:SiO_2$	50 ± 4	920-1080	B_2S	$\sim 49^{M}$

^{M} Estimated using $\Delta H_{1100} = \Delta H_{298} \times \frac{\Delta H_{1100}^{B_2T}}{\Delta H_{298}^{B_2T}}$

BIBLIOGRAPHY

1. Beretka, J. and Ridge, M. J., J. Chem. Soc. (A) 2463-5, 1968.
2. Howard, C. R., "The Influence of the Texture of the Reactants in the Synthesis of Barium Hexaferrite", Doctoral dissertation, Ceramics Department, Sheffield University.
3. Ward, R. and Struthers, J. D., J. Am. Chem. Soc., 59, 1849, 1937.
4. Wanamaker, W. L. and Radieloric, R. "Reactivity of Solids", Ed. C. M. Schwab (Elsevier 1965).
5. Harris, N. H. and Cook, R. L., Phys. Chem., 72, 3326, 1968.
6. Hulbert, S. F. and Popowich, M. J., "Kinetics of Reactions in Ionic Systems", Ed. Gray T. J. and Fréchette V. D. (Plenum 1969).
7. Jander, W., A. Z. Angem. Chem., 49, 875, 1936.
8. Garner, W. E., Ed. "Solid State Chemistry", (Butterworth 1953).
9. Templeton, L. K. and Pask, J. A., "Reactivity of Solids", Ed. de Boer (Amsterdam 1960).
10. Swann, E., Klei en Keramiek, 18, 187, 1968.
11. Hills, A. W. D., Chem. Eng. Sci., 23, 297, 1968.
12. DeVine et al., J. Brit. Ceram. Soc., 6, 179, 1970.
13. Templeton, L. K. and Pask, J. A., Am. Ceram. Soc., 42, 212-6, 1959.
14. White, J., a paper presented at the 13th Annual Brazilian Ceramic Congress (February 1969).

BIBLIOGRAPHY CONTD.

15. Lander, J. J., J. Am. Chem. Soc., 73, 5794-97, 1951.
16. Kelley, K. K. et al., U.S. Bur. Mines. Rept. Invest., No. 5059, 37pp., 1954.
17. Hulbert, S. F., J. Brit. Ceram. Soc., 6, 11, 1969.
18. Ginstling, A. M. and Brounshtein, B. I., J. Appl. Chem., U.S.S.R. 23, 1327-38, 1950.
19. Barrer, R. M., Phil. Mag., 35, 802-11, 1944.
20. Carter, R. E., J. Chem. Phys., 34, 2010-15, 1961.
21. Valensi, G., Compt. Rend., 202, 309-12, 1936.
22. Avrami, M., J. Chem. Phys., 9, 177-84, 1941.
23. Erofe'ev, B. V., Compt. Rend. Acad. Sci. U.S.S.R., 52, 511-14, 1946.
24. Sharp, J. H., Brindley, G. W. and Narahari Achar, B. N., J. Am. Ceram. Soc., 49, 379-82, 1966.
25. Burke, J., "The Kinetics of Phase Transformations in Metals", (Pergamon 1965).
26. Kubaschewski, O and Evans, E. LL. "Metallurgical Thermochemistry", (Pergamon 1958).
27. Hedvall, J. A., "Reactionsfähigkeit fester Stoffe", Leipzig, 1938.
28. Tinsley, D. M., private communication.
29. Tinsley, D. M., private communicttion.
30. Vallet, P.and Richer, A., Compt. Rend. 238, 1020-22, 1954.
31. Tinsley, D. M., unpublished data.
32. Fishbeck and Snaidt, Z. Elektrochem., 38, 199, 1932.